UNIVERSIDADE DE LISBOA
FACULDADE DE CIÊNCIAS
DEPARTAMENTO DE QUÍMICA E BIOQUÍMICA

Theoretical investigation of the energy of olefin- and sila-olefin insertion/β-H elimination reactions of two late transition metals – DFT MO calculations

Rita Leonor Veiga da Silva e Veiga Ferro

Doutoramento em Química
Química Inorgânica
2013

UNIVERSIDADE DE LISBOA
FACULDADE DE CIÊNCIAS
DEPARTAMENTO DE QUÍMICA E BIOQUÍMICA

Theoretical investigation of the energy of olefin- and sila-olefin insertion/β-H elimination reactions of two late transition metals – DFT MO calculations

Rita Leonor Veiga da Silva e Veiga Ferro

Tese submetida nos termos do

n.º 4 do Artigo 39.º do Diário da República,

2.ª série — N.º 65 — 30 de março de 2012

Doutoramento em Química

Química Inorgânica

2013

to my family.

Acknowledgments

I would like to thank my supervisor Prof. Dr. rer nat. Wadepohl from the Ruprecht Karl University of Heidelberg (Germany) for the interesting theme of my investigation and for the good working atmosphere in the department of inorganic chemistry.

A very special thanks to my supervisor Prof. Doutora Maria José Calhorda from the Faculdade de Ciências da Universidade de Lisboa (Portugal) for her support and for the good advice.

I am also grateful to my family for their support, and for the inspiration that comes from Lisbon, the most beautiful city in the world.

And a special thank you to my husband for being there for me, and the interesting and adventurous life we lead together all over the world.

Abstract (Portuguese)

A reacção de inserção/migração de uma olefina e a sua reacção inversa, a eliminação-β foi estudada recorrendo ao método da Teoria do Funcional da Densidade (Density Functional Theory, DFT).O estudo engloba o cálculo dos mínimos locais (intermediários) e dos estados de transição, com o intuito de delinear um perfil energético para a reacção em estudo.

O primeiro passo da reacção envolve a inserção migratória de um hidrogénio numa olefina e resulta na formação de uma estrutura com uma interacção β-agóstica. O segundo passo da reacção refere-se à isomerização da estrutura β-agóstica dando origem a um composto de etilo electronicamente insaturado. Os estados de transição que caracterizam cada passo da reacção são obtidos mediante o uso inicial de coordenadas reaccionais pré-definidas que definirão um perfil, sendo o máximo da curva usado para calcular o estado de transição.

Foi dada especial atenção à influência no perfil energético da reacção de uma gama de substituintes com diversas propriedades electrónicas e estereoquímicas, em compostos organometálicos de dois metais do grupo IX da tabela periódica, o cobalto e o ródio.

Para o capítulo 3, os cálculos envolvem os compostos neutros $[L_3M(C_2H_4)(H)]$ (M=Co, Rh; L=PMe_3, PF_3) com uma estrutura trigonal bipiramidal e com um centro metálico de cobalto(I) ou ródio(I).

As barreiras de energia relativas $\Delta E_{ins}^{\neq}$ para a reacção de migração/inserção do hidrogénio dos complexos olefínicos $[L_3M(C_2H_4)(H)]$ (M=Co, Rh; L=PMe_3, PF_3) são +6.6 kcal/mol (M=Co, L= PF_3), +10.4 kcal/mol (M=Rh, L= PF_3) e +23 kcal/mol (M=Rh, L= PMe_3). Estes cálculos revelam que para ambos os complexos de Co e Rh, $\Delta E_{ins}^{\neq}$ aumenta na mesma ordem que a capacidade dadora de electrões de L. Este resultado sugere que este passo da reacção é criticamente influenciado pelo carácter electrónico do ligando L. Um centro metálico envolvido por ligandos com substituintes aceitadores de electrões é representado por barreiras energéticas $\Delta E_{ins}^{\neq}$ inferiores.

As energias dos compostos com uma interacção β-agóstica situam-se -2.8 kcal/mol para o cobalto (Co) e +0.4 kcal/mol para o ródio (Rh), para L=PF_3. Este estudo permite concluir que a interacção β-agóstica diminui ao longo do grupo na

tabela periódica e a reacção torna-se cineticamente menos favorável. Para os complexos de cobalto, a interacção β-agóstica representa o mínimo global da reacção.

A isomerização do composto β-agóstico no composto de etilo insaturado ocorre através do estado de transição 2 (TS2). A barreira de energia relativa é mais elevada em relação ao primeiro passo da reacção, e tende a aumentar ao longo do grupo do Co na tabela periódica.

A isomerização do composto β-agóstico conduz à formação do composto de etilo com 16 electrões de valência. Os compostos insaturados de etilo têm energias mais elevadas que o complexo de referência (complexo de etileno neutro inicial). Por se tratar de compostos com 16 electrões de valência, foi levado a cabo um estudo para comparar as energias dos estados singuleto e tripleto. Para o estado singuleto a estrutura mais estável obtida corresponde a uma geometria quadrangular plana distorcida para os complexos de ródio. O estado tripleto é mais estável no caso do cobalto quando adopta uma geometria tetraédrica. Este resultado confirma a tendência de que compostos insaturados de metais de transição 3d têm maior propensão para adoptar estados tripletos. O composto insaturado de etilo é estabilizado de acordo com o poder dador de electrões de L.

No capítulo 4, o estudo envolve os complexos catiónicos $[(\eta^5\text{-}C_5R'_5)ML(H)(C_2H_4)]^+$ (R´=H, CH_3; M=Co, Rh; L=PF_3). A reacção de inserção/migração foi calculada com diferentes métodos computacionais com o intuito de avaliar a coerência dos cálculos com resultados obtidos experimentalmente. O método computacional eleito para a discussão de resultados permanece o B3LYP/SDD. Os cálculos efectuados revelam que $\Delta E_{ins}^{\neq}$ se situa +0.03 kcal/mol (M=Co, L= PF_3) e +2.91 kcal/mol (M=Rh e L= PF_3) mais elevadas que o complexo de referência (complexo de etileno neutro inicial). As barreiras energéticas calculadas para complexos análogos são comparáveis com as energias de activação obtidas em estudos experimentais de NMR levados a cabo, que mostram que as barreiras de inserção migratória de hidrogénio $\Delta E_{ins}^{\neq}$ são praticamente insensíveis relativamente a L, mas um pouco maiores para R=H do que para R=Me. Os compostos β-agósticos apresentam energias de -7.39 kcal/mol (Co) e -1.22 kcal/mol (Rh), relativas aos complexos de referência.

O capítulo 5 diz respeito ao estudo da reacção de inserção/migração de uma "sila-olefina" e a reacção inversa, a eliminação β-H. A substituição de C1 ou C2 por

Si na olefina $H_2C1=C2H_2$ vai afectar a energia da reacção de inserção migratória do hidrogénio para os complexos catiónicos $[C_5R'_5ML(H)(SiR_2=CH_2)]^+$ (R´=H, Me; M=Co, Rh; L=PH_3, PF_3, PMe_3), assim como os parâmetros estruturais das espécies envolvidas.

A reacção de inserção migratória do átomo de hidrogénio numa "sila-olefina" resulta na formação dos isómeros com uma ligação η^2-agóstica, "sililo" ([M]-SiR_2-CH_3), quando o átomo C estiver envolvido na inserção migratória do hidrogénio e "etilo" ([M]-CH_2-SiR_2), quando o átomo Si estiver envolvido na reacção.

Para o complexo com uma conformação em que o C da "sila-olefina" está envolvido na inserção migratória do hidrogénio, $\Delta E_{ins}^{\neq}$ apresenta valores +1.3 a +1.6 kcal/mol para L= PH_3, +0.4 a +0.6 kcal/mol para L= PF_3, e +2.0 a 2.7 kcal/mol para L= PMe_3, relativamente à "sila-olefina" de referência correspondente. A barreira de energia relativa $\Delta E_{ins}^{\neq}$ para a inserção migratória do hidrogénio aumenta na mesma sequência do poder dador de electrões de cada ligando. Os substituintes C_5H_5 e C_5Me_5 criam a mesma gama de impacto em $\Delta E_{ins}^{\neq}$ do que L. A $\Delta E_{ins}^{\neq}$ para o complexo L=PF_3 é consideravelmente mais baixa (+0.42 kcal/mol), quando comparada com os compostos olefínicos homólogos (+2.91 kcal/mol).

O mínimo global da reacção exibe uma interacção *β*-agóstica M–H···C. A conformação "sila-olefina" vai ser consideravelmente estabilizada (12-14 kcal/mol para L=PH_3, 13-16 kcal/mol para L=PF_3, 11 kcal/mol para L=PMe_3) aquando da formação da interacção η^2-"sililo-agóstico". A energia calculada para o composto de etileno estudado no capítulo 4 é de -1.22 kcal/mol, relativamente ao composto de referência. O composto "sililo" com 16 electrões de valência só é obtido para os complexos com um centro metálico electronicamente mais rico. Para o composto insaturado de "sililo" com um centro metálico electronicamente mais pobre pode ser originada uma vasta gama de reacções subsequentes, nomeadamente a reacção de 1,2-migração.

Para o complexo com a conformação em que o Si da "sila-olefina" vai estar envolvido na inserção migratória do hidrogénio, a estrutura calculada apresenta uma geometria em que a ligação $H_2C=SiH_2$ da "sila-olefina" está distendida e apresenta um comprimento de ligação entre uma ligação simples e uma ligação dupla. A ligação entre o hidrogénio envolvido na reacção migratória de inserção e o centro metálico Rh está parcialmente distendida. Deste modo não foi possível obter uma barreira

energética de inserção $\Delta E_{ins}^{\neq}$ relativa à isomerização do composto "sila-olefina" e o composto com uma interacção β-agóstica, devido às interacções Si-H···M criadas. O composto insaturado "etilo" é destabilizado energeticamente, deste modo não foi conferida muita atenção ao estudo deste composto.

O composto insaturado "etilo" ([M]-CH_2-SiH_3) apresenta uma energia consideravelmente superior à do seu homólogo "sililo" (10 kcal/mol para L=$C_5R'_5$ e 25 kcal/mol para L=C_5H_5). Este composto com 16 electrões de valência é instável pelo facto da ligação H_2C-SiR_3 ser polarizada, o que vai criar uma atmosfera electrónica mais pobre para o centro metálico.

Palavras chave: Inserção migratória de hydrogénio, interacções agósticas, mecanismos reaccionais, complexos de etileno, complexos de alquilo, DFT.

Abstract

The energetic of the olefin insertion/ β-H elimination processes is going to be studied using density functional theory (B3LYP/SDD, Gaussian 03). The observed trends based on steric and electronic properties of two late transition metals (Co and Rh) and ligands (L) are reproduced.

In a $[L_3M(C_2H_4)(H)]$ (M=Co, Rh; L=PMe_3, PF_3) neutral complex the isomer with a β-agostic metal-H-C interaction becomes stabilized when a rather less electron-donating ligand (*e.g.* PF_3) is involved. Comparison of the activation parameters with those for other complexes suggests an increase of the barrier of migratory insertion with increasing electron richness of the metal center, which destabilizes species with agostic metal –H-C interactions.

The computed energy barriers obtained for the cationic $[C_5R_5ML(H)(C_2H_4)]^+$ (R=H, CH_3; M=Co, Rh; L=PF_3) complexes compare very well with activation energies from previously reported NMR studies and confirm that the activation barriers are insensitive to L, but somewhat higher for R=H than R=Me.

The study was extended to the cationic complexes of the type $[C_5R'_5ML(H)(SiR_2{=}CH_2)]^+$ (M=Co, Rh; L=PH_3, PF_3, PMe_3; R=H, Me), in which either C or Si atoms of the “sila-olefin” are involved in the "sila-olefin" insertion/β-H elimination reaction. The "sila-olefin" conformation in which C is involved in the hydrogen migratory insertion is going to be deeply stabilized upon the formation of the "silyl-agostic" bond and the ΔE_{ins} barrier decreases to a greater extent comparing to the olefin isomer. In the course of these reactivity studies, subsequent rearrangements of the initially formed insertion products gave rise to a large number of different reaction pathways for the unsaturated “silyl” with a facile decomposition, including 1,2-migration to produce silylene.

The study could not be extended the "sila-olefin" conformation in which Si is involved in the hydrogen migratory insertion owing to the role of the Si-H$\cdots$M non classical interactions.

The unsaturated “ethyl” isomers can be stabilized through a 1,3-migration reaction.

Key words: Hydrogen migratory insertion, agostic interactions, reaction mechanisms, ethylene complexes, alkyl complexes, DFT.

Abbreviations

16e	16 valence electrons
6-31G**	Pople basis set
ax	H positioned on the axial plane
B3LYP	Becke-exchange-3-parameter-Lee-Yang-Parr-correlation
BP86	Becke Perdew 86
CCSD (T)	Coupled cluster single double
Cp	C_5H_5
Cp*	C_5Me_5
DFT MO	density functional theory molecular orbital
EH	extended Hückel
eq	H positioned on the equatorial plane
HF	Hartree-Fock
IHI	Interligand hypervalent interactions
IRC	Intrinsic reaction coordinate
Me	methyl
NMR	nuclear magnetic resonance
QM/MM	quantum mechanics/molecular mechanics
ref	reference
RB3LYP	restricted closed-shell wavefunctions
ROB3LYP	restricted open-shell wavefunctions
SDD	Stuttgart/Dresden basis set
SISHA	Secondary interactions between a silicon and a hydrogen atom
SP	distorted square planar
split	split-valence basis set
TH	distorted tetrahedral
TS	transition state
UB3LYP	unrestricted open-shell wavefunctions

Table of Contents

Table of Figures

Chapter 1 Introduction

Introduction

Industrial application of homogenous catalysis plays a major role in chemical industry. The impact of homogenous catalysis on industrial processes has developed to such an extent that organometallic chemistry has expanded into a science.

Acquainted information concerning structure and reactivity of organometallic compounds supported the creation of new catalytic systems. Ziegler-Natta catalysts for ethylene polymerization are good examples, and Wilkinson catalysts for alkene hydrogenation, as well. Improvements on the development of new catalysts will further support advances in industrial chemistry. Thus organometallic compounds with their vast variety of compositions, structures and reactivity present a promising approach.

There are still unresolved questions that require further work, and depend first and foremost on mechanistic insight. There are both new experimental techniques and theoretical approaches still lacking in mechanistic studies due to the intrinsic difficulty of the problem as compared to other areas of organometallic chemistry.

In many cases, extreme conditions or instrumentation are needed to detect short-lived highly reactive intermediates that play a decisive role in important areas of the industry. A greater emphasis should be given to theoretical advances incorporated in mechanistic studies. The understanding of the factors governing activity and selectivity would provide new criteria for the design of catalytic systems.

Many transition metal-catalyzed reactions occur via an alkene π-complex intermediate. Mechanisms involving alkene π-complex intermediates have been postulated for a number of catalytic systems. Thus, developments in alkene complex chemistry have supported the progress in several industrial processes. Furthermore, alkenes play a role as cheap raw materials in quite a lot of industrial processes in which transition metal-containing catalysts are used. Commercially, the most significant of them include polymerization, hydrogenation, or hydroformylation.

Cossee-Arlman Mechanism (direct insertion)

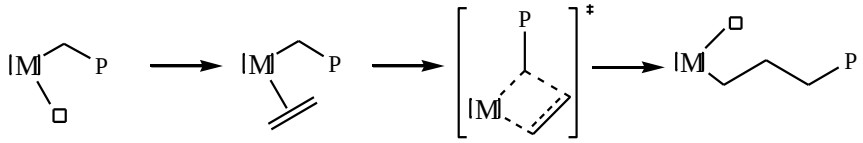

Green-Rooney Mechanism (hydride shift)

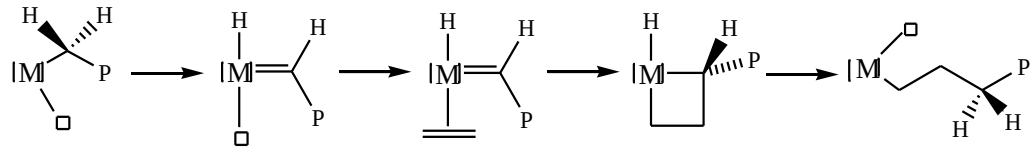

Modified Green-Rooney Mechanism (ground and transition State α-agostic interaction)

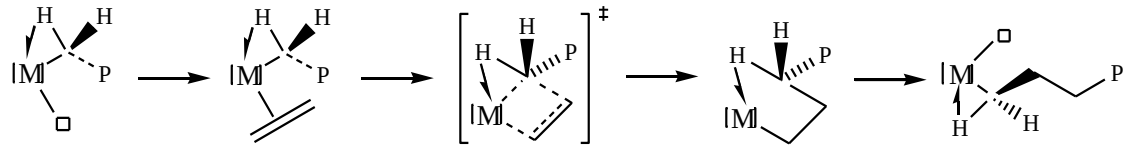

Transition state α-agostic mechanism

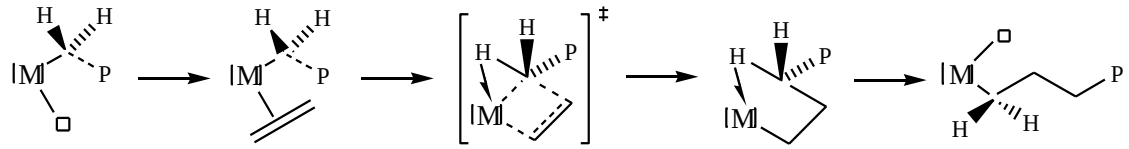

Figure 1: Four general mechanistic proposals for olefin polymerization.

A sizeable amount of research in the last 40 years, since the discovery of transition metal catalysts for olefin polymerization by Ziegler and Natta [1,2], has been directed toward understanding the basic mechanistic steps of this important industrial process. The process of monomer enchainment, which is generally considered to occur through olefin coordination [3-5] followed by insertion into a metal-carbon bond, has regularly been under particular scrutiny. Four general mechanistic proposals for the nature of this insertion became known (figure 1).

The first mechanistic possibility is the alkyl migration to the coordinated olefin [6-10] and is known as the Cossee-Arlman mechanism. Rooney and Green [11,12] proposed the second model that consists of an oxidative 1,2-hydrogen shift (α-elimination) from the α-carbon of the polymer chain, creating a metal-alkylidene hydride. A metallacyclobutane will then be generated through the reaction with an

olefin, and the sequence is completed with a reductive elimination. A mechanism proposed by Green, Rooney and Brookhart [13-15] where a hydrogen atom on the α-carbon of the growing polymer chain interacts with the metal center throughout the catalytic cycle, is seen somewhat as an intermediate to the first two proposals. This three-center, two-electron covalent bond, termed an "agostic interaction" [15,16], happens when the hydrogen atom is simultaneously bonded to a carbon and a metal atom. The fourth is olefin "insertion" where an α-hydrogen interacts with the metal center only during the transition state of the C-C bond forming step. This mechanism is a hybrid of the Cossee-Arlman and modified Green-Rooney mechanisms.

Elimination of a hydrogen atom from an ethyl ligand, usually from the carbon atom β to the metal (*β*-elimination), is the reverse process of "migratory insertion" of an olefin into a metal hydrogen bond.

For example, during olefin polymerization, *β*-H elimination can be a factor that limits the growth of the polymer chain. Efficient olefin polymerization can occur via the sequence shown in figure 2.

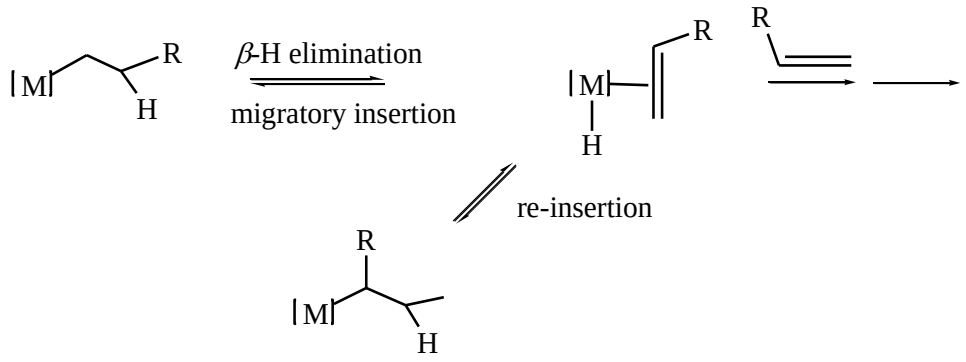

Figure 2: Olefin polymerization mechanism.

Depending on the relative rates of olefin dissociation and re-insertion, further reaction (or decomposition) or isomerisation may occur. With certain catalysts rapid re-insertion leads to "hyperbranched" polymers with unusual physical properties (figure 3).

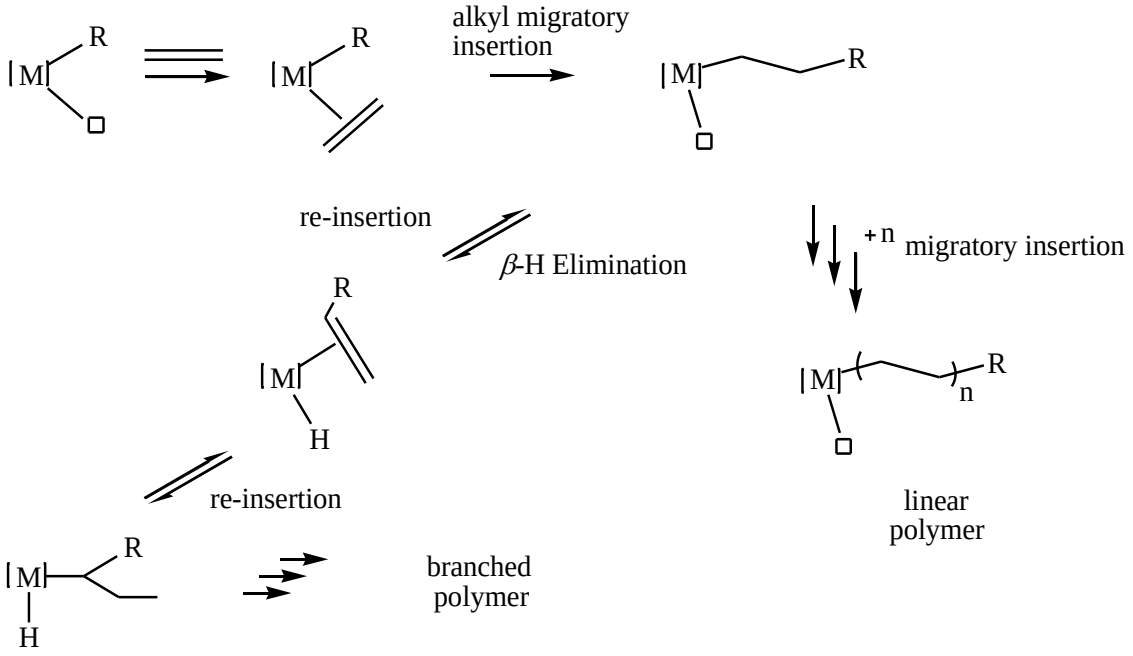

Figure 3: Olefin polymerization leading to "linear" and "hyperbranched" polymers.

Given the importance of β-migratory insertion and β-elimination processes, it is quite understandable that these reactions have been extensively studied. Experimental and theoretical studies have been undertaken by several authors in order to understand these fundamental transformations.

There are now numerous, well-documented cases where alkene-, polyene-, or polyenyl-metal hydride complexes adopt the bridged or agostic structure containing a three-center, two-electron M-H-C bond rather than the classical, terminal hydride structure.

It is worthwhile to briefly review the syntheses and properties of agostic systems, before discussing this aspect.

Agostic interactions are of general significance in organometallic chemistry since they often lead to C-H activation [17,18]. Concerning polymerization catalysts, it has been proposed that an understanding of the factors which control agostic interactions will contribute to a better control of catalyst activity [19] and polymer molecular weights [20-22].

Numerous examples have been documented where agostic complexes are in rapid equilibrium with olefin-hydride and/or the unsaturated 16-electron alkyl species. The metal center should have an empty orbital to receive the two electrons of the C-H

bond, as a minimum prerequisite. This orbital is presumed to be essentially of d character for transition metal compounds. The directionality and energy of this orbital should approach those of the C-H bonding orbitals as much as possible and it should also be a very good acceptor. A metal atom often achieves a maximum coordination number only when all the valence orbitals are occupied. Nonetheless, it is probable from normal considerations of steric restriction that the formation of agostic alkyl groups will be favoured when this bond results in the metal attaining a coordination number of six or less.

The formation of an H_α agostic group is sterically fairly unchallenging. In the absence of steric constraints it is to be expected that agostic H_α-hydrogens will be easily displaced from the metal center by another donor group, requiring only a small distortion. The reactivity patterns of agostic systems are dictated by two general features. Strongly donating ligands can often displace the agostic C-H group, as it is regarded as a weak ligand.

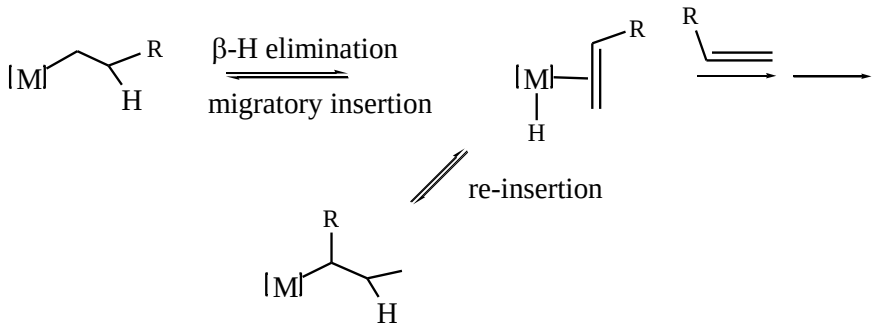

Figure 4: The two general features that dominate the reactivity patterns of agostic systems.

Steric factors can favour the agostic system, considering that the agostic C-H interactions are intramolecular, and there are now numerous examples where the equilibrium illustrated in figure 4 favours the M-H-C system.

A second possibility considers that the C-H group in the M-H-C system is interacting with an essentially electrophilic metal center. The agostic hydrogen becomes acidic and, for example, deprotonation reactions can occur. The pK_a values of agostic C-H hydrogens fluctuate over a wide range, and in some systems strong

bases are needed. Nucleophilic species are created in anionic systems. Reactions with other electrophiles can end in new C_α-electrophile bonds and a net overall electrophilic substitution of H_α.

This expectation raises the question of competition between the formation of a *β*-agostic bond and donation by lone pairs of ligands such as halogen atoms or the oxo ligand. This point is illustrated by [TiMe(dmpe)Cl_3], in which those lone-pair electrons of the three chloride ligands that have suitable symmetry to overlap with the titanium orbitals do not successfully compete with the *β*-agostic C-H electron pair. Finally, the requirement of an unsaturated 16-electron (or fewer) metal center is a necessary but not sufficient condition for the occurrence of a *β*-agostic hydrogen. It is known that the 16-electron compound [Ti(η-C_7H_7)(dmpe)(η^1-Et)] does not fulfill these requisites [23].

By the time a saturated 18-electron species looses a ligand, it yields the unsaturated 16-electron species possessing a low-lying empty orbital. The 16-electron complex is then capable of coordinating a C-H bond (i.e., use the C-H bond as a two-electron donor ligand) to form a bridged species. A small HOMO-LUMO gap is favoured by classical oxidative addition, while *β*-agostic bonding takes place when the metal center is very electrophilic (i.e. very low lying LUMO) and has a large HOMO-LUMO gap.

Invariably, the bridged *β*-agostic species is in rapid equilibrium with the classical hydride and the 16-electron species. It suggests the chance that the structure and dynamics of the hydride system species can parallel that of the alkyl analogues.

M-H-C agostic groups may be classified in line with the position of the carbon atom giving rise to the C-H bond relative to the metal center, such as complexes with α- and β- and γ-agostic alkyl groups.

The titanium compound [Ti(η^2-Me)Cl_3(dmpe)] [24] was the first example in the α-agostic alkyl groups to be fully characterized. It was demonstrated that the methyl group is tilted in such a way that one hydrogen atom approaches the metal leading to a Ti-C-H_α angle of 93.5º. An interesting symmetrical distortion has been suggested to happen in the compound [TiMeCl_3] [25]. The methyl group is apparently flattened.

The α-agostic interaction is of particular interest since it might dramatically lower the activation barrier to olefin insertion [26] and influence the stereochemical outcome of the olefin insertion step [27-30]. Brintzinger has proposed that an α-agostic interaction increases rigidity of the transition state of a C_2-symmetric catalyst undergoing propylene insertion, thereby increasing the isotacticity of the resulting polypropylene [27,28]. Specifically, the α-agostic interaction firmly orients the polymer chain into the open sector of the catalyst structure to minimize interactions between the alkyl substituent of the monomer and the ligand/polymer array during olefin insertion.

The *β*-agostic alkyls can also be viewed as bridged ethylene-hydride complexes and are often in rapid equilibrium with the olefin-terminal hydride and/or the unsaturated alkyl complex, as is clear from dynamic studies summarized below. Those *β*-agostic alkyl complexes that involve early transition metal systems provided evidence to be closer in energy to the 16-electron metal-alkyl formulation ($\Delta G^{\neq}_A < \Delta G^{\neq}_B$). On the other hand, the structure of later transition metal complexes (d^n, n>0) most likely lie closer in energy to the olefin-hydride formulation ($\Delta G^{\neq}_B < \Delta G^{\neq}_A$) (figure 5).

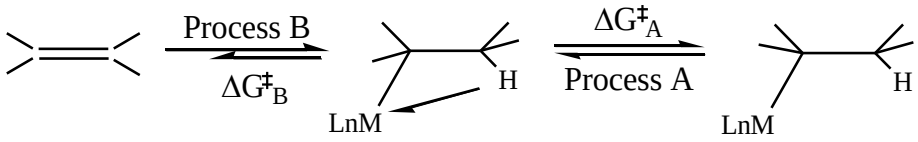

Figure 5: β-agostic alkyl complex in rapid equilibrium with olefin-terminal hydride and/or the unsaturated alkyl complex.

The first unequivocal example of a *β*-agostic ethyl complex, the d^o [Ti(η^2-Et)(dmpe)Cl_3] was reported by Green and co-workers [24]. The X-ray crystal structure confirms a very small distorted Ti-C_α-C_β angle of 86° well-suited to a Ti- H_β-C_β interaction. Schrock [31], Bercaw [32] and their co-workers made similar proposals for agostic interactions in high valent early transition metal-alkyl complexes.

The γ-agostic interaction might serve to stabilize catalytic species (both geometrically and electronically) between the insertion and monomer coordination. Guerra *et al.* has proposed that the high syndiospecificity of Cs-symmetric catalysts [33] for propylene polymerization results from a γ-agostic structure which persists in the catalytic species after olefin insertion. Several theoretical studies suggest that γ-agostic interactions are present following insertion [34, 35] and that these contacts can be relatively long lasting [37-39]. The β-migratory insertion of transition metal olefin hydride complexes is a fundamental transformation of significance in a number of catalytic processes, including olefin hydrogenations, hydroformylations, and isomerizations. The related β-migratory insertion reaction of metal alkyl olefin complexes is the key carbon-carbon bond forming step in metal-catalyzed olefin polymerization reactions and associated oligomerizations and dimerizations [40].

The classical view of the migratory insertion reaction of a metal olefin hydride complex is illustrated in figure 6 with ethylene hydride complex, A, and involves the transformation of this species into a high energy unsaturated ethyl intermediate, C, via a transition state, B, in which hydrogen is half-bridged between the metal and the β-carbon.

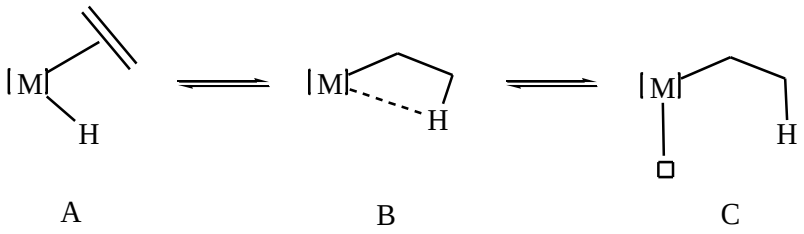

Figure 6: Mechanism of the olefin insertion/β-elimination reaction.

By measuring the rates of hydrogen scrambling between the metal hydride and olefinic sites through either dynamic NMR studies or, on slower time scales, through H/D scrambling reactions [41], the barriers to such migratory insertion were examined.

The bridged *β*-agostic species repeatedly proved to be the most stable form of numerous “olefin hydride” complexes (particularly late metal, first row, electrophilic

species) [15, 16, 42, 43]. Starting from an ethylene hydride complex, the exchange is believed to occur in the course of a classical mechanism involving a coordinatively unsaturated metal ethyl complex, or passing through a β-agostic intermediate.

This undertakes facile "in-place" methyl rotation where the CH_3 group keeps bound to the metal in the transition state for exchange (figure 7).

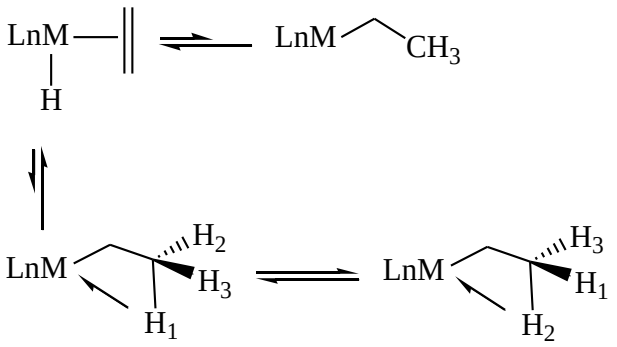

Figure 7: Olefin insertion/β-elimination reaction mechanisms.

There is a strong indication that the scrambling between the *β*-agostic hydrogen and the terminal hydrogen in such species occurs by an "in-place" rotation around C_α-C_β and not by formation of a true unsaturated metal alkyl complex, which displays no β-CH-metal contact [45, 47].

Green and Wong were the first to propose the in-place mechanism by describing the dynamic behaviour of the bis-ethylene hydride complex [Mo(*cis*-$Ph_2PCH{=}CHPPh_2)_2(C_2H_4)H]^+$ [45]. The dynamics of exo-[$Cp_2Nb(CH_2{=}CHCH_3)H$] was investigated by Green, Bercaw *et al.*, who found that the niobium hydride exchanges with the methylene hydrogens ca. twice as fast as it exchanges with the methyl hydrogens [44,47]. It is important to note that the dynamic results are also consistent with a classical mechanism involving non-agostic 16-electron alkyl intermediates [44, 48].

Experimental studies are frequently unsatisfactory in attempts at discerning the classical description from the mechanism in figure 7, and computational studies have been modest in enlightening the delicate features of these processes [50].

Nonetheless, a number of facts were cited to support in-place rotation in a *β*-agostic intermediate (figure 8).

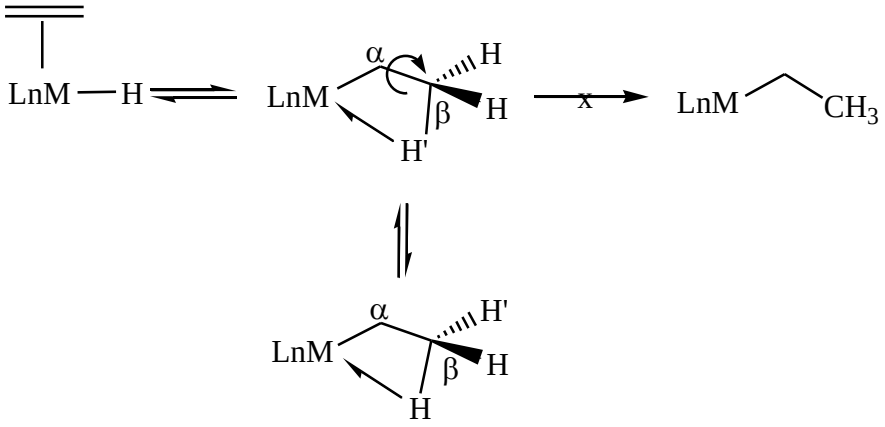

Figure 8: Hydrogen scrambling processes in ethylene hydride complex and the β-ethyl agostic complex.

These facts are certainly exemplified by the structure and dynamics of the cationic Co(III) ethylene hydrides and their Rh(III) congeners [51-53]. These d^6, 18-electron complexes display geometries which are best portrayed as distorted octahedral. The stable form of the cobalt complexes is the *β*-agostic structure [50,51]. Computational studies indicate that scrambling of the *β*-agostic H with the terminal hydrogens takes place by in-place rotation and that the 16-electron species is energetically inaccessible.

The α-agostic species is calculated to be more stable than the unsaturated ethyl complex [45,47].

An analogous situation occurs for the Rh complexes [52]. The global minimum is the olefin hydride species. Computations prove that the scrambling happens via the formation of the *β*-agostic species, followed by in-place rotation.

The Rh 16-electron ethyl complex is calculated to be very high in energy and less stable than the α-agostic isomer [45a] (figure 9).

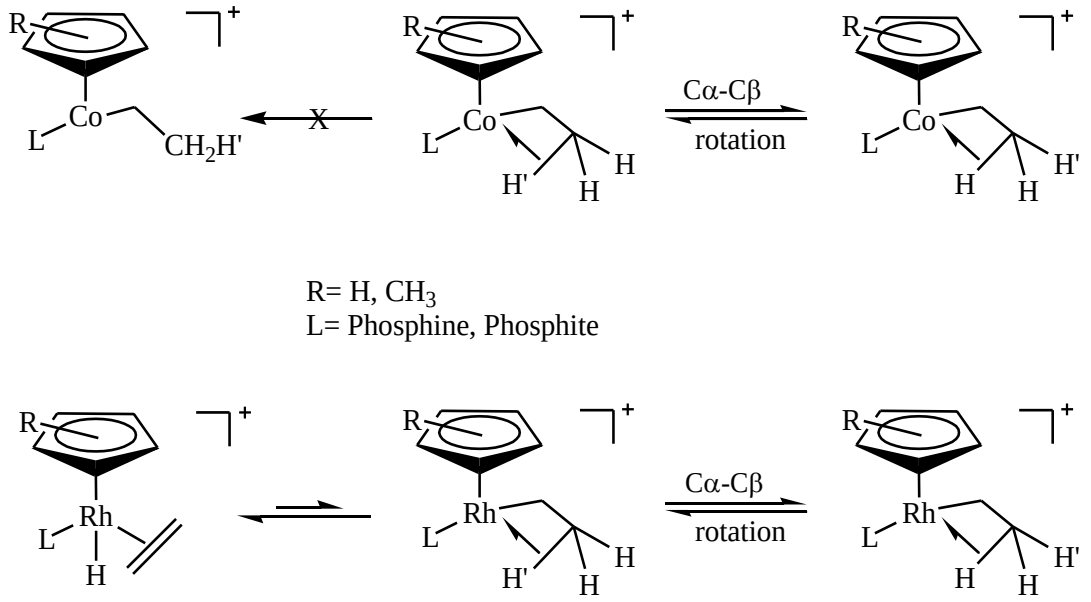

Figure 9: Structure and dynamics of the cationic Co(III) ethylene hydrides and their Rh (III) congeners.

Similarly, experimental [54] and theoretical [55] studies of d^8, 16-electron, square-planar complexes of the type $[(diimine)M\text{-}R]^+$ (M= Ni, Pd, Pt; R= C_nH_{2n+1}, n>1) have shown that *β*-agostic structures are adopted for M=Ni or Pd, while Pt exhibits a classical olefin hydride structure.

Extended Hückel MO calculations have been performed on the reaction profile for the conversion of the 16-electron $[Co(\eta\text{-}C_5H_5)(PH_3)C_2H_5]^+$ to $[Co(\eta\text{-}C_5H_5)(PH_3)(\eta\text{-}C_2H_4)H]^+$. The intermediate structure with a *β*-agostic interaction proved to be more stable than the ethylene-hydride structure [57].

Brookhart *et al.* published NMR data of the methyl-substituted compound $[Co(\eta\text{-}C_5Me_5)(P(OMe)_3)C_2H_5]^+$ that convey the idea of small energy difference between the ethylene-hydride and the *β*-agostic alkyl structures. Model theoretical studies propose $\Delta G^{\neq}_{rot}$ to be considerable (> ~8-10 kcal/mol), so the energy difference between the olefin-hydride and *β*-agostic alkyl structures must be small [56].

Over the past years several *β*-agostic complexes were identified and could offer general insights into migratory insertion reactions and, in particular, the key step of olefin polymerization, the insertion of an olefin into a metal alkyl bond [19].

Since alkyl groups are much poorer bridging groups than hydrogen, the *β*-agostic complex is not expected to be the most stable species among them, and most likely will always represent the transition state in the alkyl migration reaction or an unstable intermediate.

Brookhart *et al.* proposed that there exists a parallel between the structure and dynamics of the hydride complexes and the activation energies for alkyl migration reactions of their alkyl analogues. The barriers for these alkyl migration reactions will be lower in cases where the hydride analogues exist as bridged isomers, rather than terminal hydrides. The same factors that favour a bridging over terminal hydride structure will facilitate alkyl migration [58].

An important generalization consists in that the same features that favour bridging rather than the terminal hydride structure should lower the energy difference between the *β*-agostic and ethyl alkyl complex and thus facilitate alkyl migrations. In other words, the hydride systems can be utilized as a helpful guide in selecting which alkyl systems will experience rapid migratory insertion reactions.

This principle can clearly be relevant to create olefin polymerization catalysts by applying it to simple olefin insertion reactions (figure 10).

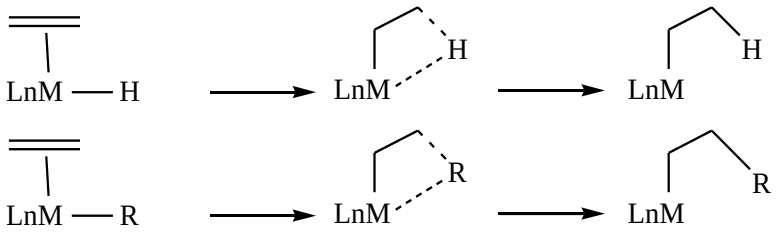

Figure 10: The β-migratory insertion reaction of metal hydride/alkyl olefin complexes.

A quantitative measure of the relative migratory capacity of hydride and alkyl groups in the β-migratory insertion reaction was carried out for the first time in experiments performed by Brookhart *et al.* [58]. The difference in free energies of

activation of the $[Cp^*(P(OMe)_3)Rh(C_2H_4)R]^+$ (R= H, CH_2CH_3) compound ($\Delta G^{\neq}_{Et.\ mig.}$ - $\Delta G^{\neq}_{H\ mig.}$) is 10.3 kcal/mol. This value is somewhat smaller than that observed for the relative rates of –H and $–CH_3$ α-migration in $[Cp^*_2Ta(CH_2)(CH_3)]$ [59]. The divergence in activation barriers for hydride versus alkyl migrations relies on the fact that alkyl migrations are unobserved in ethylene alkyl complexes where the analogous terminal hydride systems involve barriers for migration greater than 17-18 kcal/mol [59,60]. Conversely, relative migratory aptitudes of hydride and alkyl groups may vary significantly from system to system. Several such analogous pairs have been characterized [11,61,71].

In such systems stated above: (a) the hydride analogue has a classical terminal hydride structure; (b) hydride migration can be observed and has $\Delta G^{\neq} > 17$ kcal/mol; (c) migratory insertion reactions cannot be detected in any of the alkyl analogues [62].

Along with the fact such alkyl groups are poorer bridging groups, the barriers to alkyl migrations are expected to be substantially greater than barriers to hydride migrations. The concept proves to be particularly helpful for identifying olefin-alkyl complexes that are expected to experience rapid alkyl migratory insertion reactions.

These classical systems should behave qualitatively according to the free energy diagrams depicted in figures 11 and 12.

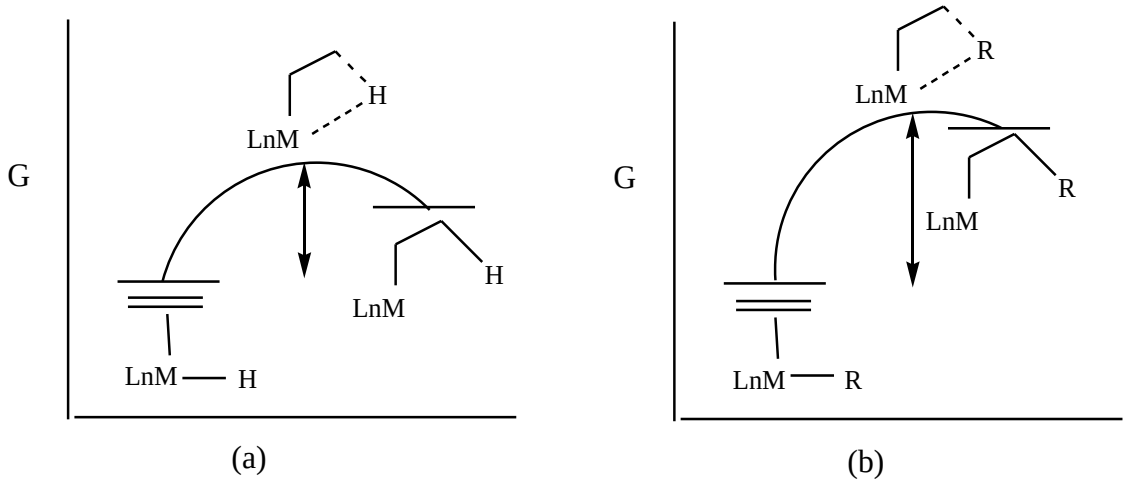

Figure 11: Free energy diagram for systems where the hydride analogue LnM'(H)(C2H4) has a classical terminal hydride structure and $\Delta G_H^{\neq} < \Delta G_R^{\neq}$.

Figure 11 characterizes a classical system with the expected $\Delta G_H^{\neq} < \Delta G_R^{\neq}$. There are numerous cases reported in the literature where $\Delta G_H^{\neq} > \sim 17$ kcal/mol, with the analogous $\Delta G_R^{\neq}$ being too high for the alkyl migration reactions to be kinetically accessible at reasonable temperatures [64,68,70].

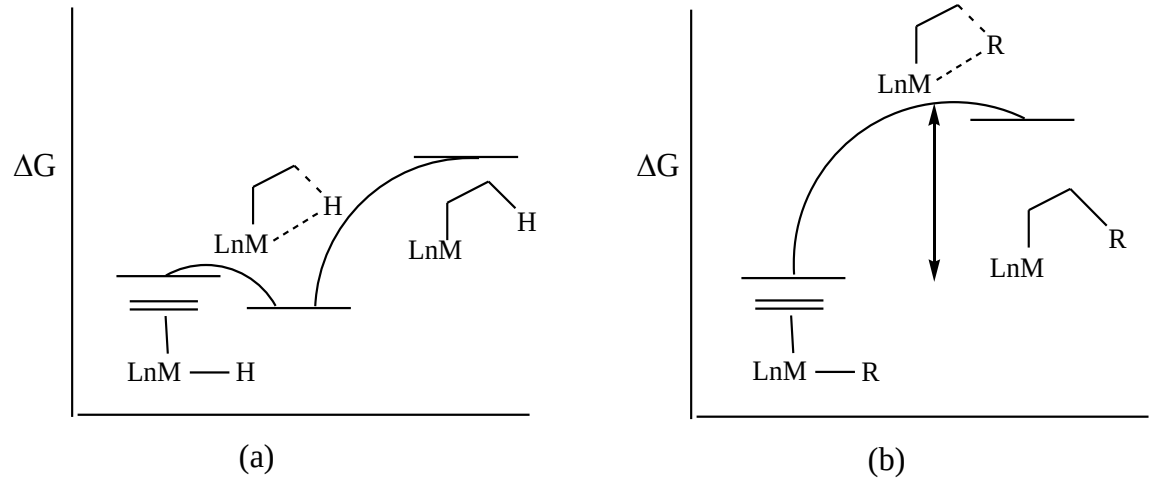

Figure 12: Free energy diagram for systems where the hydride analogue LnM'(H)(C2H4) is β-agostic; $\Delta G_R^{\neq}$ (figure 12) < $\Delta G_R^{\neq}$ (figure 11).

Figure 12 exemplifies the free energy diagram in which the metal center stabilizes the *β*-agostic alkyl structure. In such systems where the *β*-agostic structures happen to be the ground state, it has been suggested that there is a significant decrease in the corresponding $\Delta G^{\neq}$ for the alkyl migration. It is proposed that for systems where the hydride analogue $L_nM'(H)(C_2H_4)$ is *β*-agostic, values for $\Delta G^{\neq}_R$ should be significantly reduced. If metal complexes of the type $LnM'(CH_2{=}CH_2)R$ experience rapid migratory insertion reactions, they may represent good candidates for catalysts of olefin polymerizations, proceeding according to the normal Cossee-Arlman mechanism.

This idea was first demonstrated using the *β*-agostic-alkyl complex $[Co(\eta^5\text{-}C_5Me_5)\{P(OMe)_3\}(\eta^2\text{-}Et)]^+$, which is a catalyst for ethylene polymerization [19,56,65].

If alkyl migration is as rapid as postulated, 1 should catalyze ethylene polymerization by successive migratory insertion reactions.

The key results and the proposed mechanism are summarized in figure 13.

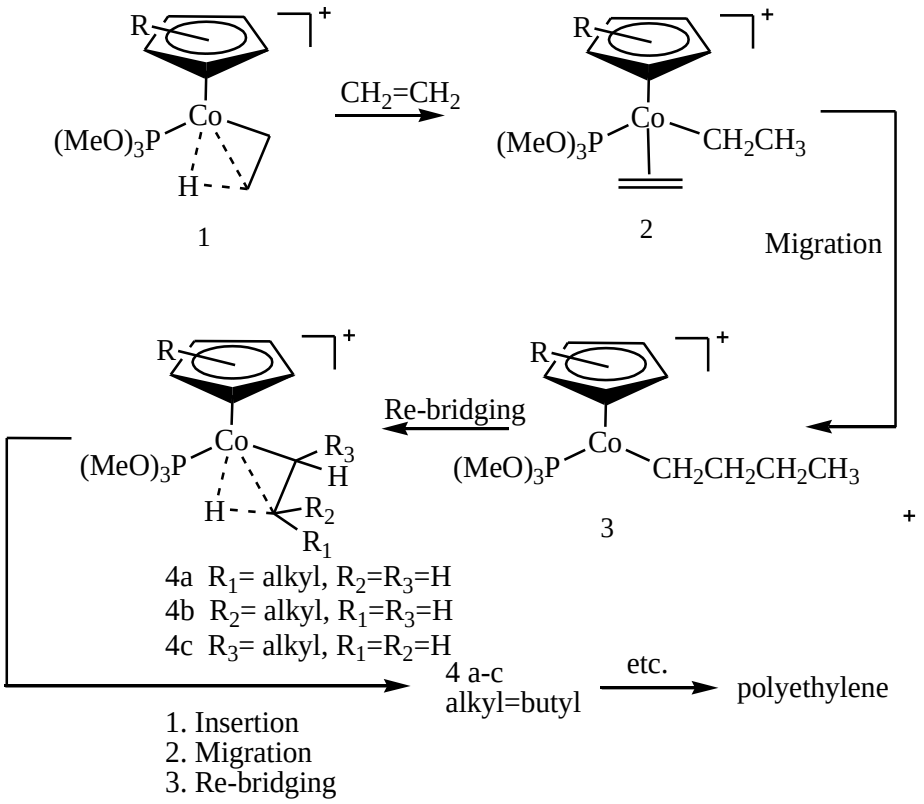

Figure 13: Insertion products detected in ethylene polymerization, monitored by ^{13}C NMR experimental observations, proposed by Brookhart et al. [19].

Indeed, treatment of $[C_5Me_5(P(OMe)_3)Co\text{-}CH_2CH_3]^+$ under ethylene pressure yields linear polyethylene. Following the polymerization by ^{13}C NMR allows detection of first few insertion products [19,56].

A combination of β-agostic complexes 4 a-c is the first observable product in the reaction of the β-agostic complex 1 with ethylene. This reaction is assumed to happen by ethylene coordination to 1 giving rise to the ethylene-ethyl complex 2. Since the equilibrium strongly favours 1, given that the β-agostic structures are the resting state of the catalyst, this complex was never detected. The resting state of the catalyst is not an unsaturated alkyl species such as 3 or an olefin-alkyl complex such as 2, but the β-agostic species 4.

Complex 2 goes through rapid migratory insertion to form the 16-electron *n*-butyl complex 3. The compound 3 then quickly generates a Co-H-C bond to create the more stable *β*-agostic structures 4 a-c, which rapidly interconvert by scrambling of the ethyl group between the C_α and C_β sites. After that, migratory insertion results in 4 a-c with R_1, R_2, R_3 = *n*-butyl when a second ethylene molecule coordinates to 4 a-c (R_1, R_2, R_3 = Et). The alkyl chain continues to grow in this fashion.

Only linear polyethylene is formed so only n-alkyl ethylene complexes ultimately undergo migratory insertion even though branched alkyl substituents could arise by reaction of 4 with ethylene followed by insertion. No α-olefins (from β-elimination) can be detected by NMR spectroscopy; *β*-agostic structures 4 are stable under conditions for polymerization. Propylene is not polymerized under similar conditions.

A few general remarks should be made concerning the factors which favour the *β*-agostic structure over the classical terminal hydride structures. In general, a highly electrophilic metal center seems to be required [15]. Most *β*-agostic species are first row species containing π-acid ligands and are often cationic. Third row examples are known, but they are cationic complexes with metals in high oxidation states containing π-acid ligands. In this regard, several series of complexes, with possible interest in olefin polymerization, were studied (figure 14). All are octahedral d^6 cyclopentadienyl complexes containing a phosphine, ethylene and hydride as the remaining three ligands.

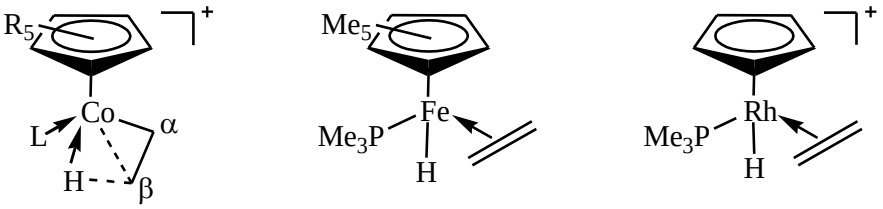

R=Me
L=PPh_3, PMe_3, $P(OMe)_3$

Figure 14: Series of complexes studied, with possible importance in olefin polymerization.

Green and Wong showed that the neutral iron(II) species is a classical, terminal hydride and does not polymerize ethylene [66,67] and the data reported by Werner and Feser [68] suggests that second row Rh(III) complexes are classical terminal hydrides and although treatment with ethylene generates an ethyl ethylene complex no further insertions occur to generate polyethylene. Only the first-row cationic cobalt(III) system is *β*-agostic (the smallest and most electrophilic metal center) and polymerizes ethylene below 0°C. This series supports the previously made observations and further suggest that first-row systems will favour *β*-agostic structures relative to their second- and third-row analogues. The observations of Bennett et al. [69] with regard to values of second- and third-row analogues, Rh and Ir, reinforce this view.

DFT calculations done by Bittner *et al.* clearly show [73] that species (transition states and intermediates) with *β*-agostic M-H-C interactions are destabilized with an electron rich metal center. Although experimental and theoretical data are still not enough to confirm these predictions, it is proposed that the barrier of the insertion reaction increases in this manner in case of an electron richer (more nucleophile) metal. This happens for $[(PMe_3)_3Co(H)(C_2H_4)]$ [73].

Further examples of electron-rich complexes suggest the ethylene-hydride as the most stable structures, from data obtained by NMR experiments, in $[W(\eta\text{-}C_5H_5)_2(\eta\text{-}C_2H_4)H]^+$ [64], $[Ta(\eta\text{-}C_5H_5)_2(\eta\text{-}C_2CHR)H]$ [70,74], $[Nb(\eta\text{-}C_5H_5)_2(\eta\text{-}C_2H_4)H]$ [71], $[Nb(\eta\text{-}C_5H_5)_2(\eta\text{-}C_2CHR)H]$ [75], $[Ru(\eta\text{-}C_6H_6)(PMe_3)(\eta\text{-}C_2H_4)H]^+$ [76] and $[Co(PMe_3)_3(\eta\text{-}C_2H_4)H]$ [77].

Table 1: Experimental activation parameters ($\Delta H^{\ddagger}$ and $\Delta G^{\ddagger}$ in kcal/mol, $\Delta S^{\ddagger}$ in cal.mol^{-1} K^{-1}) for β-migratory insertion.

complex	$\Delta H^{\ddagger}$	$\Delta S^{\ddagger}$	$\Delta G^{\ddagger}(T)$	*T*	*ref*
$[(C_5R_5)_2Nb(H)(C_2H_4)]$					
R=H			17(1)	318	[48]
R=Me	15(1)	-11(3)			[49a]
$[(C_5R_5)_2W(H)(C_3H_6)]^+$	23.7(7)	+12(2)			[53]
$[(C_5R_5)\{P(OMe)_3\}Rh(H)(C_2H_4)]^+$					
R=H	15.0(1)	0.2(3)			[51]
R=Me			12	229	[51]
$[(C_5R_5)(PMe_3)Rh(H)(C_2H_4)]^+$					
R=H	15.0(1)	0.0(3)			[51]
R=Me			12	224	[51]
$[(C_5R_5)(P(OMe)_3)Co(\eta^2\text{-}C_2H_5)]^+$			6-8		[51]
$[(PMe_3)_3Co(H)(C_2H_4)]$	16.4(6)	+8(2)			[72]

By comparing experimental activation parameters for β-migratory insertion with reference to different systems (see table 1), it has been shown that the activation barrier for the neutral cobalt complex $[(PMe_3)_3Co(H)(C_2H_4)]$, the neutral niobium complex $[(C_5R_5)_2Nb(H)(C_2H_4)]$ and the cationic rhodium complex are similar, and considerably higher than in case of the cationic cobalt complex $[(C_5R_5)(L)Co(\eta^2\text{-}C_2H_5)]^+$.

A few theoretical calculations have been carried out to examine the energetic and dynamic of the β-hydrogen elimination. Bittner *et al.* [72] investigated, in a previously study, two complexes $[(C_5H_5)(PH_3)M(H)(C_2H_4)]^+$ (M=Co, Rh) by DFT calculations. Their theoretical results are in good agreement with the corresponding experimental findings. The β-agostic structure proved to be the global minimum of the β-hydrogen elimination reaction in the cobalt complex. On the other hand, the Rh analogue confirmed the trend of the second row transition metal, and the ethylene structure represents the global minimum of the reaction.

Bittner *et al.* [73] further investigated the neutral, greatly electron rich complex $[(PMe_3)_3Co(H)(C_2H_4)]$. The selection of this complex symbolizes an extreme representation of an antagonism of the electronic requirements expressed to define a good catalyst, and stands for a good model to discuss these predictions.

Their results are a piece of evidence that there are insertion/β-elimination reactions where the β-agostic structure is not an intermediate.

In the present work emphasis will be given to theoretical approaches based on mechanistic studies of experimental techniques, playing a role in catalytic processes. The understanding of the factors governing activity and selectivity will provide new criteria for the design of catalytic systems.

Chapter 2 Theoretical Methods in Organometallic Chemistry

Theoretical Methods in Organometallic Chemistry

The intention of the present chapter is to describe briefly the main features of the theoretical methods that are currently in use for the study of organometallic compounds, taking special emphasis in those methods used in this thesis.

Qualitative molecular orbital (MO) theory based on extended Hückel (EH) calculations marked the early stages of computational organometallic chemistry. Qualitative methods are not capable of presenting accurate results, like sophisticated modern methods, but their simplicity makes them suitable for the qualitative interpretation of orbital interactions. These studies, although of a qualitative nature, founded the theoretical basis of organometallic chemistry.

The use of ab initio quantum chemistry methods, either based on the Hartree-Fock (HF) theory or on density functional theory (DFT) were instigated soon after semi-quantitative results. Ab initio molecular orbital theory aims at predicting the properties of atomic and molecular systems and stands on the fundamental laws of quantum mechanics. More advanced HF based methods suitable for systems with simplified ligands, such as Møller-Plesset perturbation theory, configuration interaction, or coupled cluster theory, became available. Another major impact in computational chemistry came from the widespread acceptance of density functional theory methods, which yield reliable structures and energies with simpler computations.

The use of hybrid quantum mechanics/ molecular mechanics (QM/MM) methods to replicate steric effects of bulky ligands began to be more popular. A number of QM/MM methods have been reported in the literature [78]. In the hybrid QM/MM methods the molecular system is divided in different regions, and each of them is treated at different computational level. In transition metal complexes, an accurate quantum mechanics (QM) method will treat the metal centre (the active region), and the remnants of the system (bulk of the ligands) can be obtained with a much more affordable molecular mechanics (MM) approach.

2.1 Density Functional Theory

Density functional theory [79] based methods ultimately derive from quantum mechanics research from the 1920's, especially the Thomas-Fermi-Dirac model, and from Slater's fundamental work in quantum chemistry in the 1950's.

The DFT method relies in modelling electron correlation using general functionals of the electron density. No attempt is made to solve directly the Schrödinger equation, contrasting to ab initio methods. The energy is expressed as a functional of the electron density (ρ) instead of being associated with the wave function (ψ). These methods sustain their origin on the Hohenberg-Kohn theorem [80], published in 1964, which demonstrated the existence of a unique functional that determines the ground state energy and density exactly. With reference to the work done by Kohn and Sham [81], the approximate functionals employed by current DFT methods divide the electronic energy into several terms,

$$E_{DFT}(\rho)= E^{T}(\rho)+E^{V}(\rho)+E^{J}(\rho)+E^{XC}(\rho)$$

where E^{T} is the kinetic energy term coming up from the motion of the electrons, E^{V} expresses the potential energy of the nuclear-electron attraction and of the repulsion among pairs of nuclei, E^{J} label the electron-electron repulsion term (it is also described as the Coulomb self-interaction of the electron density), and E^{XC} delineates the exchange correlation term that comprises the remaining part of the electron-electron interactions. The electron correlation is defined as the difference in energy between the HF and the exact energy, but the HF approximation does not account for it [82].

Density functional methods turned out to become very popular since the 1990s. The foremost attraction comes from their capability to deal with even rather large molecular systems with comparable accuracy but faster, and thus less computational demanding, than by standard wave function based methods.

The so-called hybrid functional deviates somewhat from pure DFT methods, however it has proved to be a rather successful approach. Hybrid methods combine the standard Kohn-Sham form of the exchange energy with the Hartree-Fock exchange (non-local single-determinant exchange). In many aspects, hybrid methods are definitely believed to be currently the most accurate DFT procedures accessible for most applications. The most popular hybrid method at the present is the semi-

empirical B3LYP scheme (Becke-exchange-3-parameter-Lee-Yang-Parr-correlation). It owes its origins to a proposal by Becke [83] for a parameterized hybrid approximation involving the Perdew correlation functional [84], which was subsequently was replaced by the LYP correlation functional [85].

2.2 Open Shell Methods

For open shell systems, an unrestricted method capable of treating unpaired electrons, is required. The alpha and beta electrons are in different orbitals, resulting in two sets of molecular orbital expansion coefficients. The two sets of coefficients end in two sets of Fock matrices (and their associated density matrices), and finally to a solution producing two sets of orbitals. These separate orbitals create proper dissociation to separate atoms, correct delocalized orbitals for resonant systems, and other attributes.

2.3 Technical Details

A standard DFT method (B3LYP) with the Stuttgart-Dresden basis set (SDD) [87] is employd to locate the stationary points and transition states involved in the hydrogen migratory insertion with the purpose of shaping an energy profile for the reaction. The Stuttgart-Dresden basis set (SDD) is used for the metal center and all the ligands of the complexes studied, following a prior work done by Bittner *et al.*. Bittner *et al.* determined the structural and energetic parameters concerning the hydride olefin migration/*ß-H* elimination reaction of the $[CpRh(PH_3)(C_2H_4)(H)]^+$, by DFT MO electronic structure calculations [72]. In their research they applied several methods and basis set with the purpose to evaluate their consistency for the current system. This B3LYP/SDD combination has proven to be reliable by high accuracy CCSD(T) calculations for the same system [88,89]. This method/basis set combination was used by them in a subsequent theoretical study of the olefin insertion/*β*-H elimination reaction in an electron-rich neutral cobalt $[(PMe_3)_3Co(H)(C_2H_4)]$ complex, providing again evidence of being an adequate method/basis set combination to apply to these systems [73].

The calculations of the 16e-ethyl isomers in chapters 3 and 4 are going to be carried out with different methods/basis sets: the B3LYP and BP86 methods as well as the SDD and split basis sets. The "split" basis introduce more polarized functions (6-31G**) in the three active H of the reaction (i.e., the migrating hydrogen atom and the ones bonded to the terminal ethylenic atom C2 involved in the migration/insertion reaction). The polarized 6-31G*basis set [151] is going to be employd for the calculations involving the PF_3 ligands. The split basis set was already tested in PMe_3, in a complete prior study accomplished by Bittner *et al.* [72]. Regarding the open shell calculations that involve the unsaturated ethyl isomers, the singlet states are determined by means of a RB3LYP (restricted closed-shell wavefunctions) DFT MO method. The triplet states are calculated with a UB3LYP method (unrestricted open-shell wavefunctions) and the obtained single point with a restricted open-shell method ROB3LYP (restricted open-shell wavefunctions).

The optimization of the geometries and the computation of the energies of the reactants, products, all relevant intermediates and transition states of the olefin insertion/*β*-H-elimination reaction in the present work are based on their model, as described next.

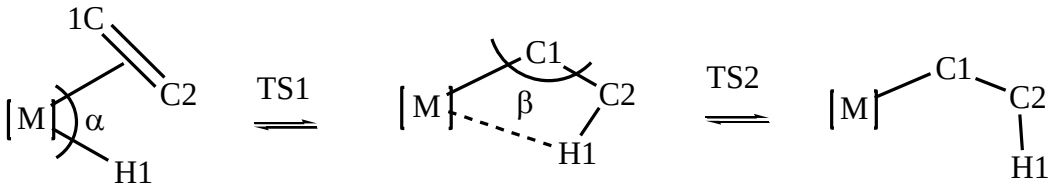

Figure 15: Angles chosen as approximate reaction coordinates.

Beginning with the ethylene-"starting structures" and the *β*-agostic calculated geometries, they chose two angles α and β as reaction coordinates to localize saddle points and possible intermediates, as depicted in figure 15.

The first "scan" runs as a progressive decrease of the angle α of the reaction coordinate (C2-M-H1) so to approximate H to C2 of the olefin and form the η^2-agostic bond. This step will "convert" the ethylene-"starting structure", through a

transition state (TS1), into the η^2-agostic structure. The second "scan" runs as a progressive increase of the angle β of the reaction coordinate (M-C1-C2) and will "convert" η^2-agostic structure, through a transition state (TS2), into the 16-electron ethyl complex.

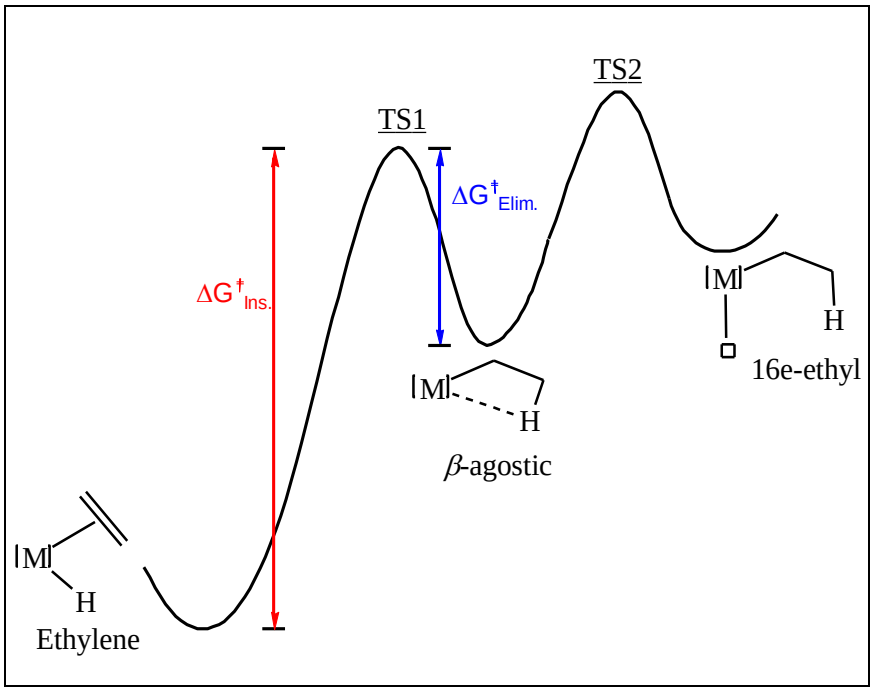

Figure 16: Energy profile of the hydride olefin migration /β-H-elimination reaction.

The "scan" obtained gives rise to an energy profile resembling the one depicted in figure 16.

The characterization of the stationary points involves the differentiation between the local minima (intermediates, reactants, products) and the saddle points (transition states). In cases that all the eigenvalues in the Hessian matrix are positive, it is a precise evidence of finding a local minimum. On the other hand, in saddle points there is one and only one negative eigenvalue, indicating the energy is a minimum in all directions but one. The negative eigenvalue of a transition state corresponds to an imaginary vibrational frequency, whose normal mode should be examined in order to check whether the transition state connects the right reactant and the right product. In some instances, it may not be straightforward whether the appropriate transition state has been determined and the intrinsic reaction coordinate

(IRC) should be calculated [86]. The IRC follows the reaction path from the transition state to the connected local minima. The *Gaussian 03* [90] program package was used for all calculations.

Chapter 3 Theoretical investigation of the energy of the olefin insertion/β-H-elimination in $[L_3M(C_2H_4)(H)]$, M=Co; L=PF_3 and M=Rh; L=PF_3, PMe_3 complexes

Theoretical investigation of the energy of the olefin insertion/β-H-elimination in $[L_3M(C_2H_4)(H)]$, M=Co; L=PF_3 and M=Rh; L=PF_3, PMe_3 complexes

3.1 Introduction

The kinetics of the β-elimination and migratory insertion processes have been studied in the past for quite a few cases. However, little generalization can be obtained from the available data except from the rather vague statement of elimination being slower with the late transition metals [91] (i.e. possibly at the more electron rich metal centers). It had been accepted already for more than 20 years [92], that the catalytic polymerization of ethylene by late-transition-metal complexes is presumed to be severely limited by rapid β-hydrogen elimination. More lately, the use of specially tailored catalysts, usually with bulky ligands, showed that the chain transfer processes caused by β-hydrogen elimination [93] can be prevented and that the facile elimination process can even be utilized to generate novel varieties of "hyperbranched" polymers with high molecular weight [94, 54b, 92c-e]. The molecular weight and structure of the polymers is then the result of the interplay between alkyl migration (chain growth) and β-hydrogen elimination/reinsertion. Little generalization can be drawn from the available data that permits a comparison of the energy barrier for the migratory insertion between the lighter and heavier metals within a group in the transition metal series. A more detailed experimental study of a series of complexes of cobalt and rhodium seems to point out a lower barrier ($\Delta H^{\neq}$) for cobalt [51] than for rhodium [53]. However, owing to the fact that the β-agostic is the ground state for the cobalt systems, the relevant activation barrier could only be estimated with considerable uncertainty.

Some nickel and palladium complexes, where the activation parameters ($\Delta H^{\neq}$ and/or $\Delta G^{\neq}$) for the β-hydrogen elimination/reinsertion process have been reported, gave evidence of showing the same problem [95, 97, 98].

It is interesting to note that most of the available kinetic data were obtained with cationic systems, such as the above mentioned polymerization catalysts. For the neutral, electron rich cobalt ethylene hydride complex $[(PMe_3)_3Co(H)(C_2H_4)]$, Bittner *et al.* reported experimental kinetic data for the migratory insertion (i.e. the hydride migration process). Theoretical calculations served to obtain an energy profile for the reaction and establish intermediates and transition states [73].

Bittner *et al.* examined the two trigonal bipyramid structures of $[L_3M(C_2H_4)(H)]$, M=Co und L=PMe_3 illustrated in figure 17 as potential Ethylene-"starting points". The nomenclature followed refers "ax" to H in the axial position and "eq" to H in the equatorial site.

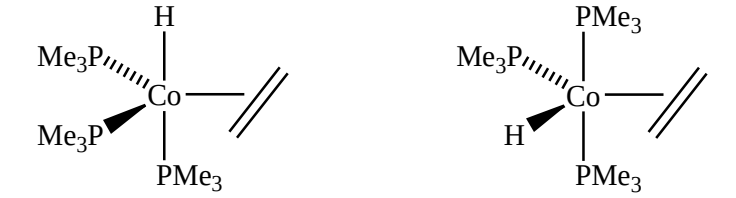

$(PMe_3)_3Co(C_2H_4)H]$_Hax $(PMe_3)_3Co(C_2H_4)H]$_Heq

Figure 17: Trigonal bipyramidal structures proposed by Bittner et al. [73].

Klein *et al.* suggested, in their original paper, a structure based on a trigonal bipyramid for the pentacoordinated complex, with an axial hydrido ligand and the ethylene in the equatorial position [100]. The axial position of the hydride could not be deduced directly from the NMR spectra, so the $[(PMe_3)_3Co(C_2H_4)(H)]$ structure was built in analogy to that of $[(PMe_3)_3Co(C_2H_4)(CH_3)]$ [100], which in turn was based on a comparison of the spectra with those of $[(PMe_3)_4Co(CH_3)]$ [101].

In their famous paper on pentacoordination, Rossi and Hoffmann [102] showed that the most likely candidate is indeed the structure with the hydride in the axial position. However, preliminary DFT MO calculations indicate Heq to be of comparable energy.

Bittner *et al.* ruled out several alternatives based on the observed coupling pattern of the hydride NMR resonance at low temperature [73], namely the structure with both the hydride and ethylene ligands in axial sites, the structure with ethylene in

the axial and hydride in the equatorial position and most of the possible structures based on the tetragonal pyramid. They further reduced the number of possible structures taking into account the temperature dependence of the resonances of the ethylene ligand. This was only consistent with one of the remaining two likely candidates, namely Hax but not with Heq. Preliminary DFT MO calculations also favoured Hax with respect to Heq. However, the assignment of the ground-state structure is of limited value for the comparatively high energy dynamic process (i.e. migratory insertion) pertinent the study, considering the low energy barriers between the many possible conformations of these systems.

For a pentacoordinated complex, the dynamic behaviour is not surprising. The dynamic behaviour of $[(PMe_3)_3Co(C_2H_4)(H)]$ in solution was described by Bittner *et al.* in terms of three different processes.

Process I is the scrambling of the ligands over all the sites in the five-coordinated complexes (figure 18). The most likely rearrangement mechanism for five coordinate complexes, including trigonal bipyramidal molecules, is assumed to be a Berry pseudorotation [103] and is also likely active in process I.

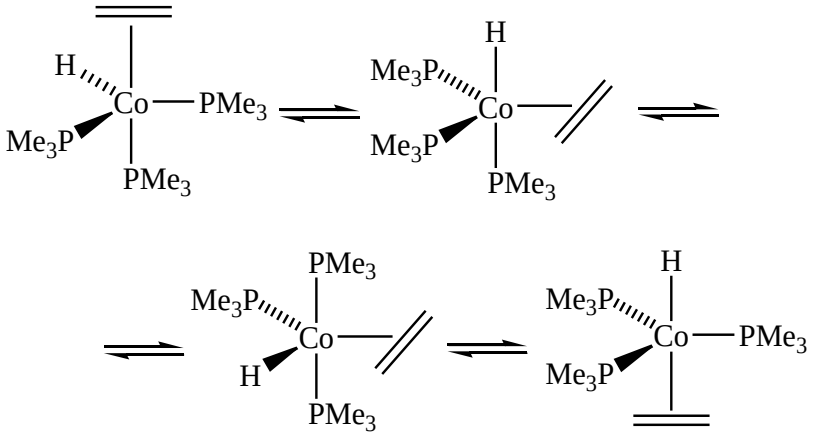

Figure 18: Scrambling of the ligands over all the sites in the five-coordinated complexes. Process I of the dynamic behaviour of the $[(PMe_3)_3Co(C_2H_4)(H)]$ complex in solution.

Process II is the rotation of the ethylene which exchanges the two CH_2 termini of this ligand (figure 19). It can take place in any of the various conformational isomers occurring in process I.

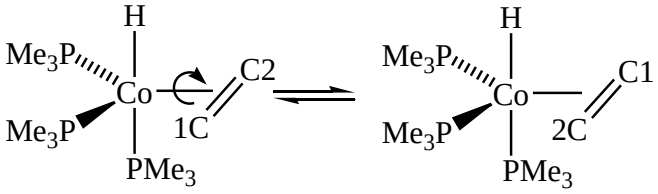

Figure 19: Rotation of the ethylene which exchanges the two CH_2 termini of this ligand. Process II of the dynamic behaviour of $[(PMe_3)_3Co(C_2H_4)(H)]$ in solution.

The hydride migration process III is the slowest step of the dynamic behaviour (figure 20).

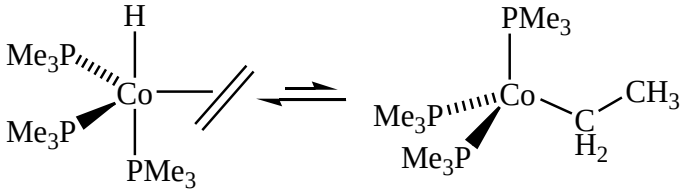

Figure 20: Hydride migration. Process III of the dynamic behaviour of $[(PMe_3)_3Co(C_2H_4)(H)]$ in solution.

The equilibrium concentrations of the "olefin inserted" products (with a β-agostic and/or free ethyl group, respectively) are too small to be observed by NMR spectroscopy. Klein *et al.* observed in a deuteration experiment that Process I and II in fact occur [100].

After locating both ethylene minima, a "scan" going from the Ethylene-"starting geometries", through defined coordinates (figure 15, Chapter 2) gave rise to an energy profile capable of locating two more minima and the transition states in-between (figure 21).

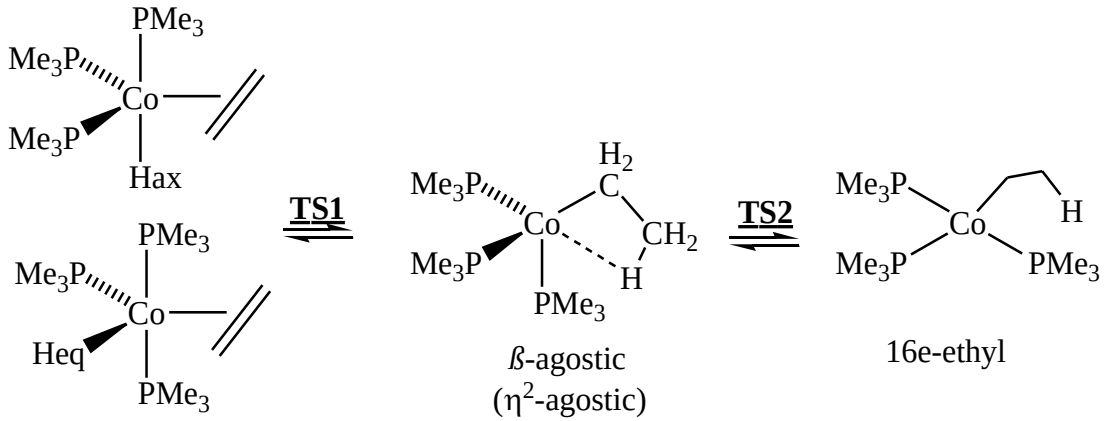

Ethylene-"starting structures"

Figure 21: Key structures of the hydride migration of $[L_3M(C_2H_4)(H)]$, M=Co and $L=PMe_3$ complexes [73], as well as the reverse β-hydrogen elimination reaction, by Bittner et al..

The determination of the activation parameters was carried out in toluene solution using ^1H magnetization transfer methods. The structural and energetic parameters were established by means of DFT electronic structure calculations.

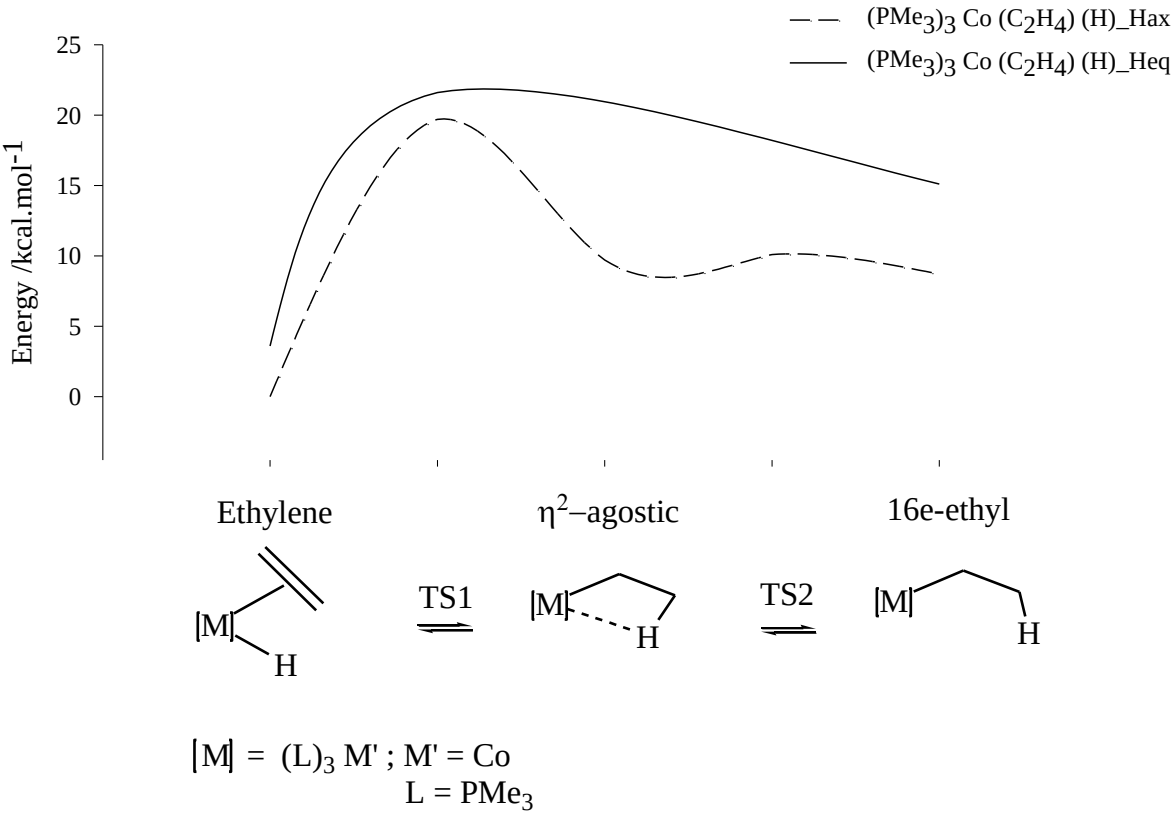

Figure 22: Energies ΔE of the stationary points (B3LYP/SDD) pertaining to $[(PMe_3)_3Co(C_2H_4)H]$_ Hax [73] and reaction path for the β-migratory insertion of ethylene into the metal hydrogen bond.

The global minimum thus obtained is in agreement with the experimental findings. The same holds true for the activation energies for migratory insertion as well as for β-elimination. Two reaction channels of the hydrogen migratory insertion reaction were examined, one for $[(PMe_3)_3Co(C_2H_4)H]$_Hax and one for $[(PMe_3)_3Co(C_2H_4)H]$_ Heq. The relative energies of the various states are shown in the energy scheme in figure 22 and table 2. The global minimum achieved agrees with the experimental results. $[(PMe_3)_3Co(C_2H_4)H]$_ Hax is the global minimum and $[(PMe_3)_3Co(C_2H_4)H]$_ Heq lies 3.6 kcal/mol above. A local energy minimum was found following the predefined reaction coordinates between the ethylene $[(PMe_3)_3Co(C_2H_4)H]$_ Hax and the fully inserted coordinative unsaturated ethyl complex. It shows the important characteristics of a β-agostic interaction. The

activation energies for migratory insertion as well as for β-elimination are in good agreement, as well.

Table 2: Relative energies of the species involved in the hydride migration, (B3LYP/SDD) in kcal/mol (relative to $[(PMe_3)_3Co(C_2H_4)H]$_Hax ethylene minimum), by Bittner et al. [73].

Initial structure	*Ethylene*	*TS1*	*β-agostic*	*TS2*	*16e-ethyl*
$[(PMe_3)_3Co(C_2H_4)H]$_Hax	0	19.7	9.7	10.1	8.7
$[(PMe_3)_3Co(C_2H_4)H]$_Heq	3.6	21.6	-[a]	-[a]	15.1

Comparison of the activation parameters with those for other complexes suggests an increase of the barrier of migratory insertion with increasing electron richness of the metal center, which destabilizes species with β-agostic metal-H-C interactions. It is proposed that there may even be cases where a β-agostic structure is not an intermediate.

The selection of $[(PMe_3)_3Co(H)(C_2H_4)]$, which is a neutral, very electron rich complex symbolizes an extreme representation of the electronic requirements expressed to define a good catalyst, and stands for a good model to discuss these predictions.

This chapter will focus on the association between the electron richness of the metal center and the energy of the hydride migratory insertion reaction, as well as the correlation on going down a group in the periodic table. This work evaluates two late transition metals (Co und Rh) in combination with more (*e.g.* PMe_3) and rather less electron-donating ligands (*e.g.* PF_3). It is proposed that species with a η^2-agostic metal-H-C interaction become stabilized when the very electron poor $(PF_3)_3Co$ moiety is involved, and a raise of the barrier of hydrogen migratory insertion reaction occurs on going down a group in the periodic table.

3.2 DFT MO calculations of the Olefin insertion/β-elimination reaction in $[L_3M(C_2H_4)(H)]$, M=Co; L=PF_3 and M=Rh; L=PF_3, PMe_3 complexes

The energy of the hydrogen migratory insertion reaction, the structural parameters and the variation of the coordinates of the stationary points are going to be investigated for the $[L_3M(C_2H_4)(H)]$, M=Co (L= PF_3) and M=Rh (L= PF_3, PMe_3) complexes. The influence of the electronic configuration around the metal center and the ligands, with different steric and electronic properties, on the energetic of the olefin insertion process is discussed. Full geometry optimizations are performed starting from the two most likely trigonal-bipyramidal candidates for the $[PMe_3Co(C_2H_4)(H)]$ ground state, proposed by Bittner *et al.* [73] (see figure 17).

Starting from the ethylene-"starting structures" and the β-agostic optimized geometries, the two angles chosen as reaction coordinates to localize saddle points and possible intermediates are employed (see figure 15, Chapter 2). The reaction pathway of the hydride migration then runs as follows: after the migration of the hydride to ethylene the reaction path leads to a structure with a pronounced M···H-C elongation, the η^2-agostic, which is also isolated as a minimum, confirmed by frequency calculations. These two isomers are connected through a transition state (TS1). Then, it will be studied the isomerisation of the η^2-agostic structure through a transition state (TS2) that leads to the 16-electron with a vacant coordination site ethyl structure.

The objective is to estimate the energies of the olefin hydrido, β-agostic species and 16e-ethyl complexes. In addition, attention will be given to barriers of activation for the two processes and the nature of the transition states TS1 and TS2. Finally the study of the two members of the cobalt triad allows us to probe periodic trends in the relative migratory aptitude (see figure 22).

The following icons (1ax and 1eq, TS1, 2, TS2, 3) are employed to describe the structures studied in this chapter (see figure 23).

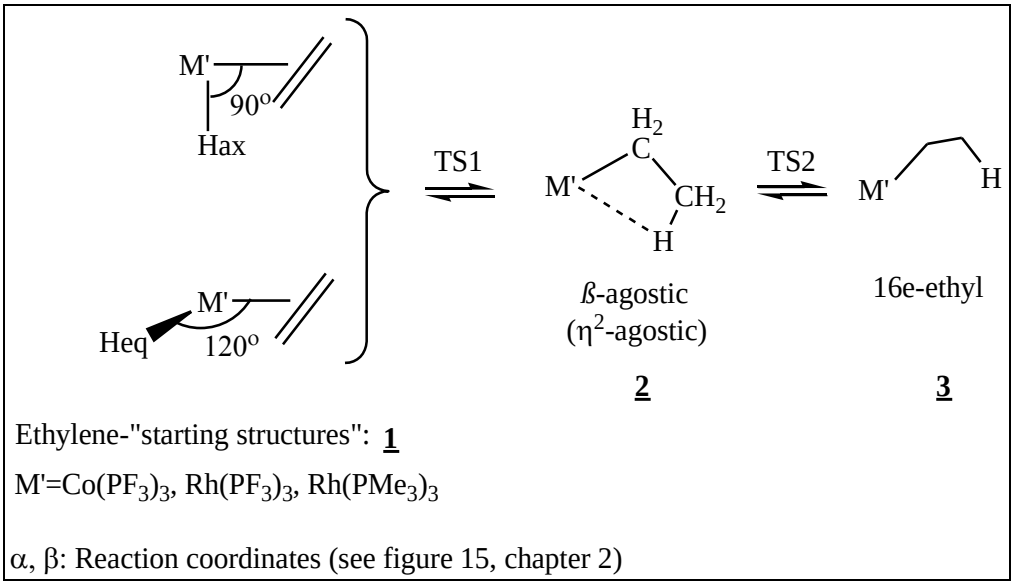

Figure 23: Key structures of the hydride migration of the $[L_3M(C_2H_4)(H)]$, M=Co; L=PF_3 and M=Rh; L=PF_3, PMe_3 complexes.

3.2.1 Structural parameters of the stationary points

The analysis of the substitutional preferences of the ligands on the trigonal-bipyramidal geometry, based on electronic effects and steric properties, is carried out in this section. The prime consideration is whether a given donor or acceptor interacts with molecular orbitals of the ML_5 geometry more or less at a given position. For a ligand with acceptor properties, the site with maximum interaction will be stabilizing, for a donor the interaction may be stabilizing or destabilizing. The choice between substitution sites is a resultant of preferences set by both the σ- and π-donating capabilities of the ligand in question. In a paper from Hoffmann *et al.* [102] arguments based on symmetry and overlap allow some predictions.

The optimization of the ethylene-"starting structures" 1ax and 1eq depicted in figure 23 as key structures, gave rise to the geometries showed below (see figure 24).

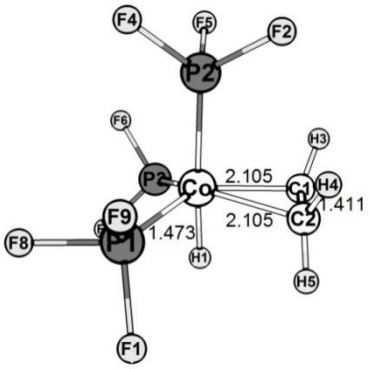

0

(1ax; M=Co, L=PF_3)

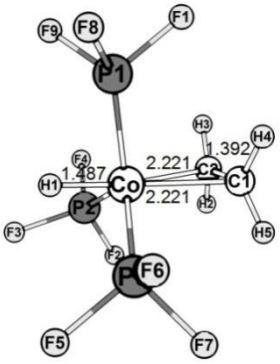

+0.9

(1eq; M=Co, L=PF_3)

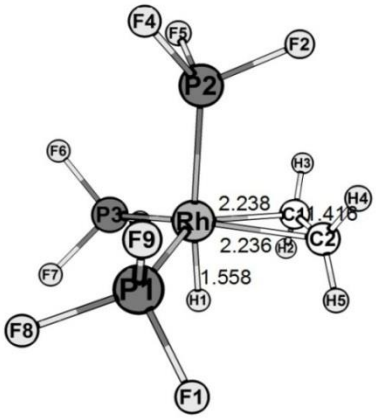

0

1ax (M=Rh; L=PF_3)

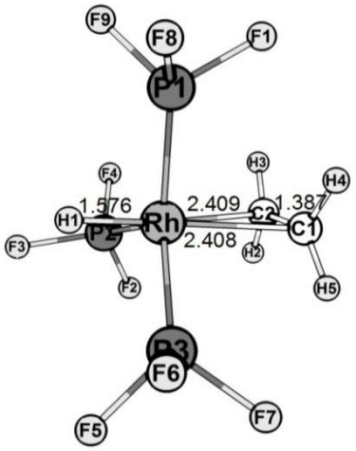

+1.2

1eq (M=Rh; L=PF_3)

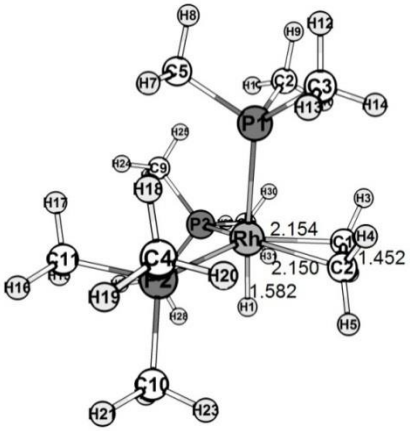

0

(1ax, M=Rh; L=PMe_3)

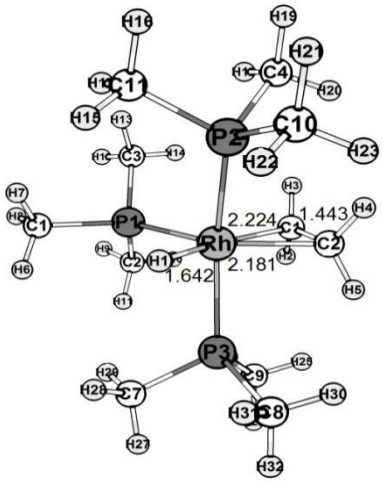

8.1

(1eq, M=Rh; L=PMe_3)

Figure 24: Optimized structures and relative energies (kcal/mol) of the ethylene complexes (relative to 1ax).

Key parameters of the calculated geometries are given in table 3.

Table 3: Relevant distances (Å) and angles (°) of the $[L_3M(C_2H_4)(H)]$, M=Co, Rh and L=PF_3, PMe_3[1] ethylene complexes.

	$[(PF_3)_3Co(C_2H_4)(H)]$		*$[(PF_3)_3Rh(C_2H_4)(H)]$*		*$[(PMe_3)_3Rh(C_2H_4)(H)]$*	
	1ax	1eq	1ax	1eq	1ax	1eq
d(M-C1)	2.104	2.22	2.236	2.408	2.150	2.224
d(M-H1)	1.472	1.487	1.558	1.576	1.582	1.642
d(C1-C2)	1.411	1.392	1.416	1.386	1.452	1.443
α(M-C1-C2)	70.41	71.76	71.64	73.20	70.16	69.25
β(H1-M-C2)	81.48	159.37	80.63	161.25	83.48	132.26
φ(P-M-P)	113.95, 101.52, 101.69	120.54, 116.24, 115.06	111.43, 101.30, 100.55	122.72, 116.46, 115.94	106.45, 98.64, 98.82	151.14, 100.96, 100.94

[1] Preliminary DFT MO calculations of the $[(PMe_3)_3Co(C_2H_4)(H)]$ ethylene complex were published by Bittner *et al.* [73].

For the M=Co and L=$(PF_3)_3$ complex, the 1eq isomer lies +0.9 kcal/mol above 1ax. Pertaining to Rh, the 1eq M=Rh and L=$(PF_3)_3$ isomer is +1.2 kcal/mol and the energy of 1eq M=Rh and L=$(PMe_3)_3$ lies +8.1 kcal/mol, above each correspondent 1ax isomer.

The 1ax (M=Co, Rh) ethylene rearranges to a slightly distorted trigonal bipyramidal structure (see structural parameters in table 3). The 1eq complex also converts into a minimum, but the geometry reorganizes in a more pronounced way. The H and CH_2=CH_2 in the equatorial position are now occupying the axial position, in case of L= PF_3 but not for L= PMe_3 (β(H1-M-C2)=159.37° for M=Co and L=$(PF_3)_3$ complex, β(H1-M-C2)=161.25° for M=Rh and L=$(PF_3)_3$, but β(H1-M-C2)=132.26° for M=Rh and L=$(PMe_3)_3$).

Since the xy and x^2-y^2 orbitals in a d^8 ML_5 trigonal bipyramidal are filled in a low spin complex, more electron density develops in the equatorial plane and the strong electronegative PF_3 ligands rather occupy the equatorial positions [102].

Consequently, it is found that a higher electron density in the equatorial plane created by the metal center and the donor properties of the ligands provides a larger π-backdonation and consequently d(M-C1) decreases and d(C1-C2) increases. The π-backdonation degree increases in the order Co<Rh for the metal and PF_3<PMe_3 for the ligand.

For the 1eq M=Rh and L=PMe_3 isomer both ethylene and hydrogen occupy the equatorial plane (β(H1-M-C2)=132.26º). Steric effects are extremely important for structures with phosphorus ligands. Increasing the size of substituents on P will tend to favour isomers which are less crowded [104]. The carbon-carbon distance of the olefin ligand M=Rh L=PMe_3 1ax and 1eq ethylene structures is rather long (1.452 Å and 1.443 Å) but agrees reasonably well with the experimental value 1.43(1) Å of the similar complex $[(PMe_3)_3Co(Ph)(C_2H_4)]$ [32]. The considerable increase with respect to the main value (1.39 Å) taken from other published crystal structures of ethylene complexes [105] reflects the strong π-backbonding from the very electron rich metal centre. The C1-C2 bond is longer in favour of 1ax owing to an increased π-backdonation created by this geometry configuration.

Optimized structures of the Co- and Rh-complexes η^2-agostic minima are illustrated in figure 25.

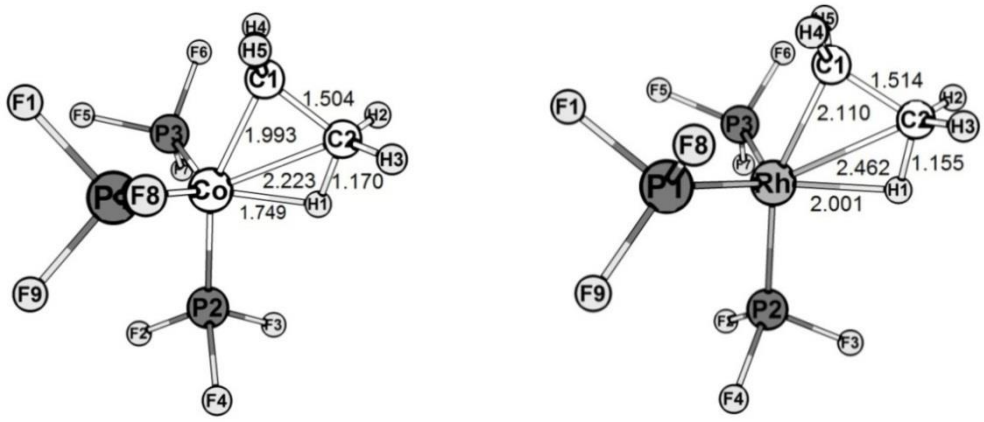

-2.8 (M= Co; L= PF_3)

+0.4 (M= Rh; L= PF_3)

Figure 25: Optimized structures and relative energies (kcal/mol) of the η^2-agostic complexes (relative to 1ax).

The M=Rh and L=PMe_3 η^2-agostic minimum could not be located. Both Co ethylene complexes (1ax and 1eq for L=PF_3) converged to a structure with very close structural parameters, as well as both rhodium ethylene structures (1ax and 1eq for L=PF_3). The cobalt η^2-agostic minima, 2, lies -2.8 kcal/mol and -2.7 kcal/mol below 1, ax und eq respectively. The rhodium η^2-agostic minima, 2, are +0.4 kcal/mol and -0.7 kcal/mol relative to 1, ax und eq, respectively.

The η^2-agostic interaction for the three-center two-electron M···H-C bond is marked clearly by elongated C2-H1 distances of 1.170 and 1.155 Å for Co and Rh, respectively. The C1-C2 bonds with distances of 1.504 Å (Co) and 1.514 Å (Rh) show clearly an elongation upon the formation of the η^2-agostic bond and are characteristic of a C-C single bond. These distances are 0.1 Å longer than the corresponding C1-C2 double bonds of the olefin hydride reactants (1.411 and 1.416 Å for Co and Rh, respectively). The β-agostic products have M-H1 distances 1.749 (Co) and 2.001 Å (Rh). They are substantially longer than the M-H1 bonds of the olefin hydride reactants with 1.473 and 1.558 Å, for Co and Rh, respectively. The C2-H1 bond of η^2-agostic is more stretched in case of cobalt (1.170 Å) than of Rh (1.155 Å) (table 4).

Table 4: Relevant distances (Å) and angles (°) of the $[L_3M(C_2H_4)(H)]$, M=Co, Rh and L=PF_3, PMe_3[1] η^2-agostic complexes.

	Co		*Rh*	
d(C2-H1)	1.170		1.155	
d(M-H1)	1.749		2.001	
d(C1-C2)	1.504		1.514	
α(M-C1-C2)	77.55		83.83	
β(H1-M-C2)	31.48		27.61	
φ(P-M-P)	114.34, 101.44	101.12,	118.56, 100.65	101.42,

[1] For 2 (M=Rh; L=PMe_3) a η^2-agostic minimum could not be located.

This agrees well with the results published by Ziegler *et al.* that give evidence for Co being the 3d member of the triad that forms the strongest β-agostic bonds within the C-H linkage [37].

The complex with a β-agostic M···H-C bond rearranges to a 16e-ethyl species. In a d^8-ML_4 complex, it will be expected it adopts a square planar structure.

Following the reaction coordinates described before (see figure 15 in Technical Details, Chapter 2), the located ethyl complexes resulted in the following geometries, as in figure 26 and table 5.

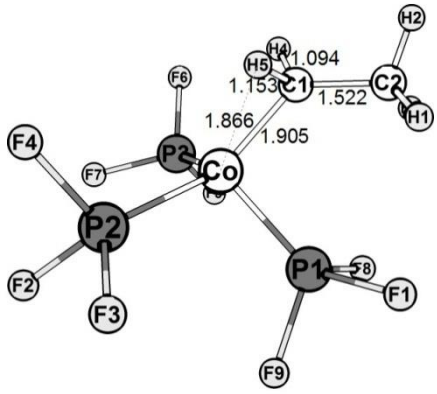

+7.7

(M=Co, L=PF_3)

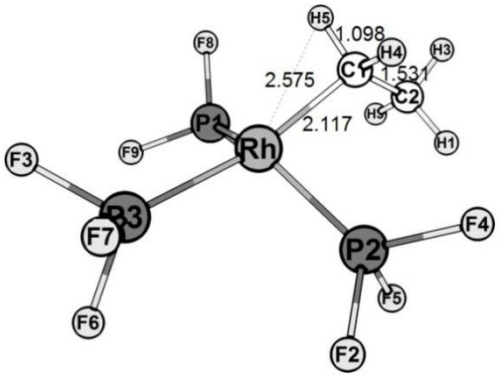

+5.7

(M=Rh,L=PF_3)

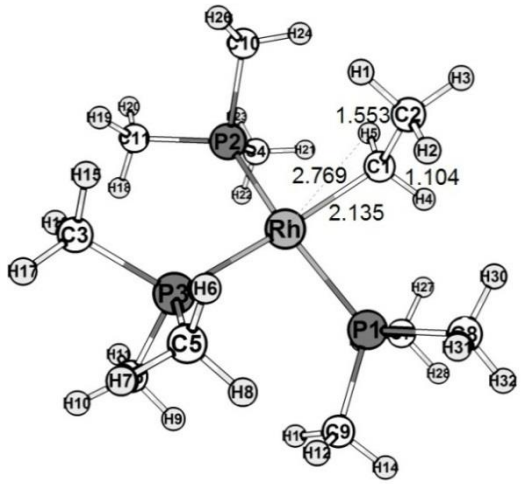

+1.5

(M=Rh; L=PMe_3)

Figure 26: Optimized structures and relative energies (kcal/mol) of the 16e-ethyl complexes (relative to 1ax).

Table 5: Relevant distances (Å) and angles (°) of the $[L_3M(C_2H_4)(H)]$, M=Co, Rh and L=PF_3, PMe_3[1] 16e-ethyl complexes.

	$[(PF_3)_3Co(C_2H_4)(H)]$	*$[(PF_3)_3Rh(C_2H_4)(H)]$*	*$[(PMe_3)_3Rh(C_2H_4)(H)]$*
d(M-C1)	1.905	2.117	2.135
d(C1-C2)	1.522	1.531	1.553
d(C1-H4/5)	1.094, 1.153	1.101,1.098	1.104, 1.04
d(C2-H1/2/3)	1.095, 1.098, 1.101	1.096, 1.101, 1.096	1.099, 1.106, 1.098
π(P-M-P)	116.62, 101.36, 102.46	132.22, 98.71, 99.40	96.64, 100.09, 153.11

The 16e-ethyl minima demonstrate a distortion from the idealised square planar structure. The d^8-ML_4 ethyl minima adopt a structure fairly balanced between a square planar and the tetrahedric geometry, as expected, based on an analogy with the compounds described by *Hoffmann et al.* in their paper [102]. The M=Co and L=PF_3 η^2-agostic complex rearranges to a 16e-ethyl species stabilized by an α-H agostic interaction. This α-H agostic bond is characterized by a stretched C1-H5 link (1.153 Å). This geometrical arrangement is now justified in a way that the acceptor ability of the dz^2+pz will be improved upon pyramidalization. As a consequence, an important degree of pyramidalization is to be expected when the metal atom acts as an acceptor through its pz orbital. Judging from the relative C-H bond elongations in the cobalt η^2-agostic and α-H agostic complexes, it seems clear that the former has a stronger β-agostic interaction M···H-C between the C-H bond and the metal center. This is also supported by the assessment of the M-H distances.

3.2.2 Kinetics

An energy profile of the olefin insertion/β-elimination reaction is presented und discussed next. An attempt will be made to discern a trend concerning the influence of the electronic and steric properties of the metal center and the ligands in the energetic of the reaction.

The reaction pathway of the olefin insertion/migration runs as described in figure 15 (Chapter 2). The hydride migratory insertion reaction to the olefin isomer leads to a structure with a pronounced M···H-C elongation, the η^2-agostic. These two isomers are connected through a transition state (TS1). Then, the point of isomerisation of the η^2-agostic structure, through a transition state (TS2), to the 16-electron with a vacant coordination site structure will be determined. The transition states are calculated through optimizations of the maxima located in the reaction pathway.

The energy of the stationary- and the tied saddle points are then depicted graphically and evaluated.

$[(PF_3)_3Co(H)(C_2H_4)]$: Ethylene "Starting-structures" 1ax and 1eq

An energy scan scheme over approximated reaction coordinates, α and β (see Technical Details, Chapter 2), for the M=Co and L=PF_3 complex is represented in figure 27. The energy profile of the hydride migratory insertion reaction is illustrated below (see figure 28). It gives an overview of the olefin insertion/β-H-elimination reaction for the $[(PF_3)_3Co(C_2H_4)H]$ complex.

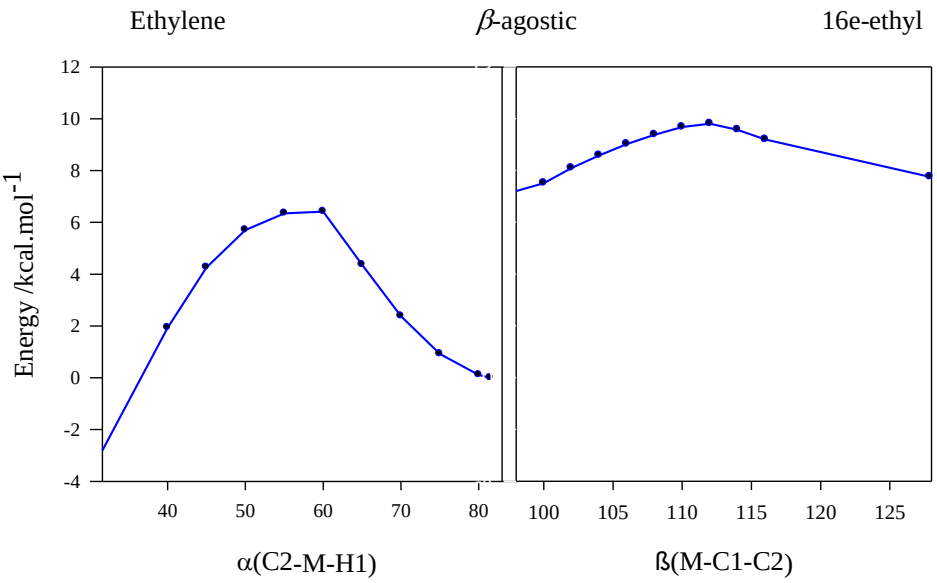

Figure 27: Energy scan scheme over approximated reaction coordinates (α and β), pertaining to 1eq.

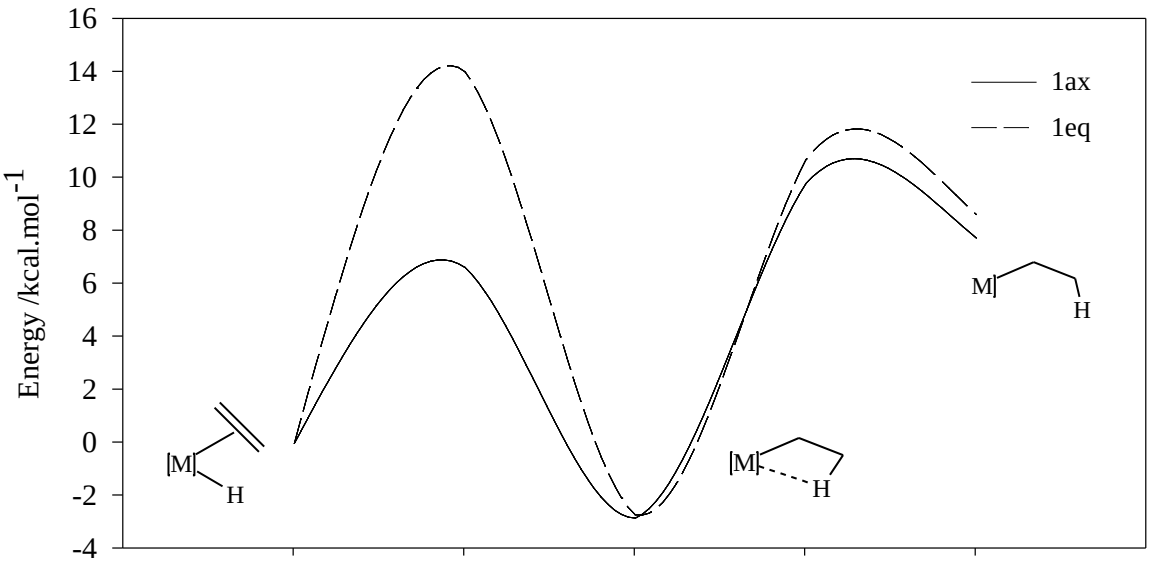

Figure 28: Energy profile of the hydrogen migratory insertion reaction pathway, with reference to 1ax and 1eq (in kcal.mol^{-1}).

Table 6: Relative energies of the species involved in the hydride migratory insertion reaction. The energies ΔE of the subsequent stationary and saddle points (B3LYP/SDD) are calculated relative to each preceding ethylene initial structure, in kcal/mol.

Initial structure	*Ethylene*		*TS1*		*β-agostic*		*TS2*		*16e-ethyl*
1ax	0	TS1	6.6	2	-2.8	TS2	9.8	3	7.7
1eq	0	TS1	14.0	2	-2.7	TS2	10.7	3	8.6

The energy scheme of the olefin insertion/*β*-H elimination reaction of 1ax and 1eq $[(PF_3)_3Co(C_2H_4)H]$ isomers clearly elects the η^2-agostic structures 2 as global minima of the reaction studied, being nearly 3 kcal/mol more stable than the ethylene structures 1 (table 6). This is in line with the qualitative reasoning that depletion of electron density from the metal center by the electronegative PF_3 ligands is partially compensated by electron donation from the C-H bond via the 3c/2e *β*-agostic interaction.

The geometries and key parameters of the transition states are given below (figure 29 and table 7). The optimization of the transition states was confirmed by frequency calculations. An imaginary frequency that matches the scan progress of the reaction coordinate α(C2-Co-H1) was obtained for both isomers.

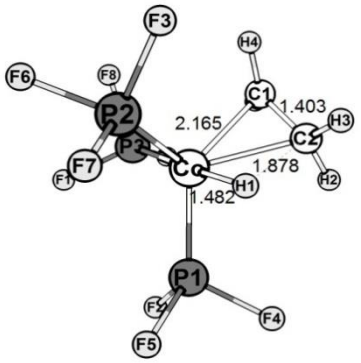

+6.6

(from 1ax)

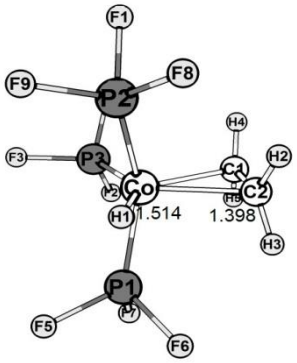

+14.0

(from 1eq)

Figure 29: Optimized structures and relative energies (kcal/mol) of the transition state 1 (TS1) complexes.

Table 7: Relevant distances (Å) and angles (º) of TS1.

	from 1ax	*from 1eq*
d(M-C1)	2.164	2.189
d(M-H1)	1.482	1.514
d(C1-C2)	1.403	1.398
α(M-C1-C2)	71.99	70.30
β(H1-M-C2)	57.89	92.88
φ(P-M-P)	116.13, 101.28, 102.42	141.38, 100.12, 100.14

The calculated barriers for the hydrogen migratory insertion reaction are +6.6 (1ax) and +14 kcal/mol (1eq). To balance this disparity with the minute energy difference between the two isomeric ethylene complexes, this variation is quite large. There are many factors that must be considered to explain this divergence. In what concerns the reaction path of H1 moving toward C2, the H1 equatorial has a longer pathway to reach C2 (β(H1-M-C2)=120º), comparing to H1 in the axial position (β(H1-M-C2)=90º). Besides, as the H1 on the 1eq isomer starts to approach C2, steric hindrance will be created with the PF_3 groups in the axial position, φ(P-Co-P)= 141º. Additionally, in case of 1eq, H1 points already to C2, while for the 1ax isomer the ethylene group still has to rotate so that the H1 can reach C2.

The 1ax TS1 complex is a reactant-like. The M-H1 bond distance (1.482 Å) is close to the value found in the terminal hydride complex (1.472 Å). Both d(M-H1) and d(C1-C2) coordinates do not vary much in the insertion reaction step (see figure 27).

Regarding 1eq, β(H1-Co-C2) decreases from 156º to 92.9º upon the formation of the transition state. This angle reduces further to 31.4º when it converges to the η^2-agostic structure. The M-H1 distance in TS1 (d(M-H1)=1.514 Å) does not alter much comparing to the ethylene isomer (d(M-H1)= 1.487 Å), by 3.6%, but shows a greater discrepancy relative to the η^2-agostic geometry, d(M-H1)= 1.749 Å (see table 8).

The *β*-agostic isomer rearranges to a 16-electron ethyl isomer, which is stabilized by an α-H agostic interaction (+7.7 kcal/mol). The barrier between the η^2-agostic isomer and the 16e-ethyl structure is 9.8 kcal/mol.

Further, the d(M-H) reaches a maximum by TS2 and decreases upon the formation of the α-bond in 1ax (figure 30).

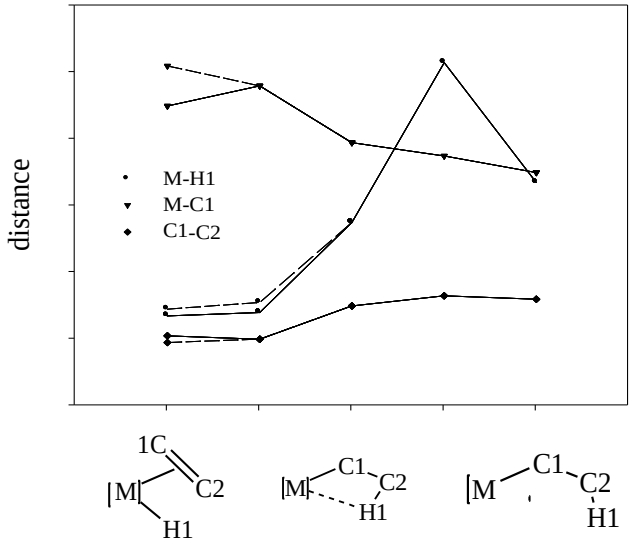

Figure 30: Variation of the relevant distances along the hydrogen migratory insertion pathway, with reference to 1ax (solid line) and 1eq (dashed line) (d (Å)).

Table 8: Variation of the relevant distances along the pathway of the hydrogen migratory insertion reaction, relating to 1ax (in Å).

distance	*Ethylene*	*Δd*	*TS1*	*Δd*	*β-agostic*	*Σ [Å]*
M-H1	1.47	+3.6%	1.48	+96.4%	1.75	+0.28
M-C1	2.10	+54.5%	2.16	-154.5%	1.99	-0.11
C1-C2	1.41	-11%	1.4	+111%	1.5	+0.09

$[(PF_3)_3Rh(C_2H_4)(H)]$: Ethylene "Starting-structures" 1ax and 1eq

Figure 31 and table 9 point out the relative energies (in kcal/mol) of the 1ax and 1eq rhodium species involved in the hydride migratory insertion. The 1ax ethylene isomer lies -1.2 kcal/mol relative to 1 eq, as enlightened before (see section

3.2.1 Structural parameters of the stationary points). The energies ΔE of the subsequent stationary and saddle points are calculated relative to each preceding ethylene structure. Regarding 1ax, the ethylene structure is the ground state of the reaction, being 0.4 kcal/mol more stable than the η^2-agostic isomer obtained. The η^2-agostic isomer is the ground state for 1eq, lying 0.7 kcal/mol below the ethylene starting structure. Weighting up against the findings of the cobalt complex, the energies of the ethylene and η^2-agostic complexes for M=Rh are here approximately in the same range.

The energy of the rhodium 16e-ethyl complex lies 5 kcal/mol above the energy of the ethylene isomer, measured up with the +9 kcal/mol for cobalt.

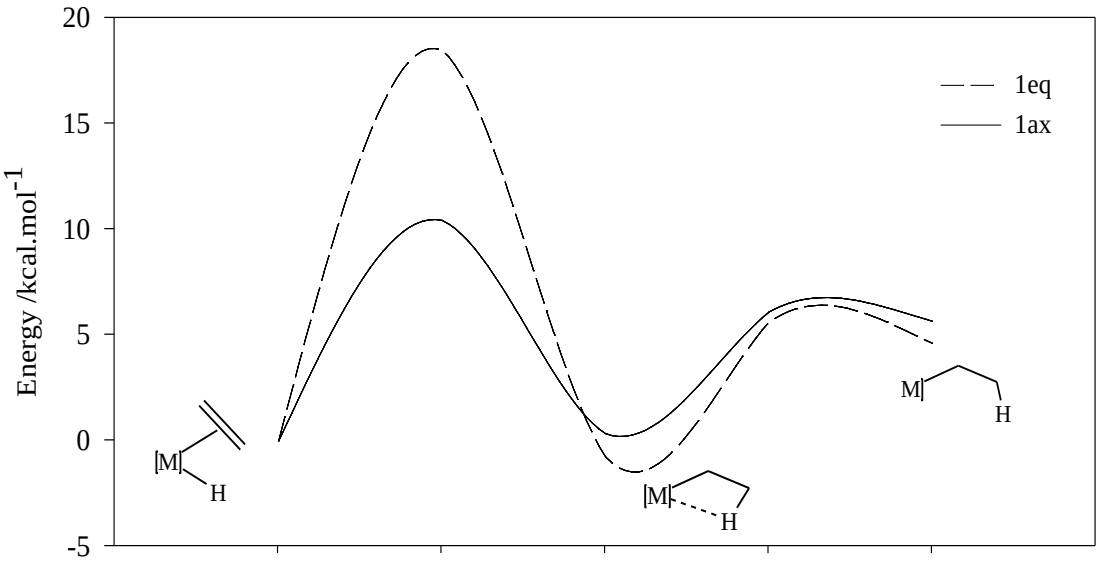

Figure 31: Energy profile of the hydrogen migratory insertion pathway, with reference to 1ax and 1eq (in kcal.mol^{-1}).

Table 9: Relative energies of the species involved in the hydride migratory insertion reaction. The energies ΔE of the subsequent stationary and saddle points are calculated relative to each preceding ethylene initial structure, in kcal/mol.

Initial structure	*Ethylene*		*TS1*		*β-agostic*		*TS2*		*16e-ethyl*
1ax	0	TS1	10.4	2	0.4	TS2	6.1	3	5.7
1eq	0	TS1	18.5	2	-0.7	TS2	5.6	3	4.6

The achievement of the transition states was confirmed by frequency calculations. An imaginary frequency that matches the scan progress of the reaction coordinate α(C2-Co-H1) is obtained in both cases. The 1ax and 1eq TS1 geometries are shown below (see figure 32) and the structural parameters are given in table 10. The energy barrier of insertion ΔE_{ins} is +10.4 (1ax) and +18.5 kcal/mol (1eq), relative to 1ax ethylene isomer.

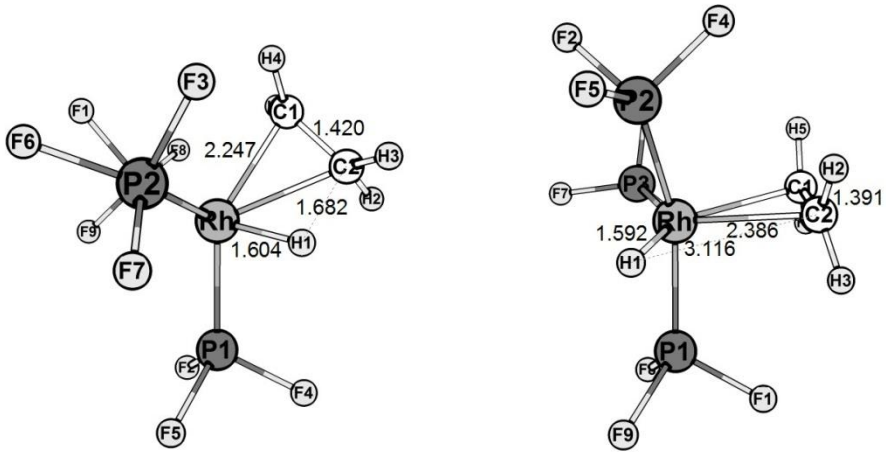

+10.4 (from 1ax) +18.5 (from 1eq)

Figure 32: Optimized structures and relative energies (kcal/mol) of the transition state 1 (TS1) complexes.

Table 10: Relevant distances (Å) and angles (º) of TS1.

	from 1ax	*from 1eq*
d(M-C1)	2.247	2.416
d(M-H1)	1.604	1.592
d(C1-C2)	1.420	1.391
α(M-C1-C2)	75.77	71.99
β(H1-M-C2)	45.84	101.28
φ(P-M-P)	112.28, 104.70, 101.14	153.17, 98.49, 98.23

The 1ax and 1eq TS1 are reactant-like isomers.

Regarding 1ax, the M-H1 and C1-C2 bond distances resemble those found in the terminal hydride complex, being +9% and 0% respectively (figure 33 and table 11). The β-agostic isomer rearranges to a 16-electron ethyl complex (+5.7 kcal/mol) through an energy barrier of 6.1 kcal/mol, balanced with the energy of the ethylene isomer.

Pertaining to 1eq, β(H1-M-C2) must decrease from 161.26º to 101.28º in order to be able to overwhelm the energy barrier of the insertion reaction and reach the transition state 1. This angle diminishes additionally to 27.61º when it reaches the η^2-agostic structure. The M-H distance (d(M-H1)= 1.592 Å) does not alter much comparing to the ethylene isomer, d(M-H1)= 1.576 Å, but demonstrates a larger deviation from the η^2-agostic geometry, d(M-H1)= 2.001 Å.

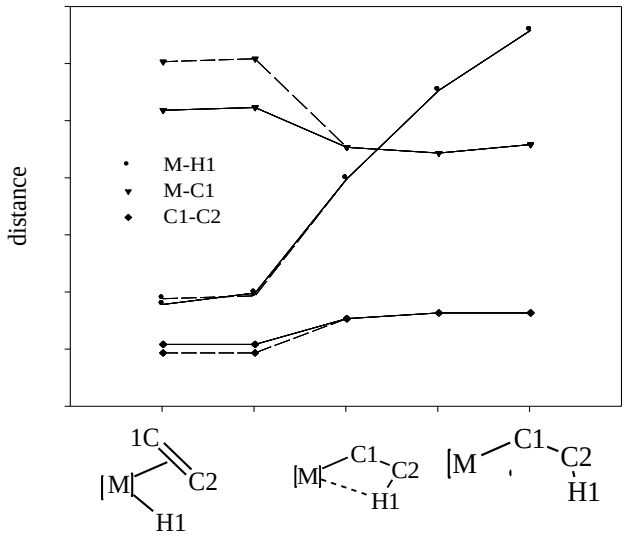

Figure 33: Variation of the relevant distances along the hydrogen migratory insertion pathway, with reference to 1ax (solid line) and 1eq (dashed line)(d (Å)).

Table 11: Variation of the relevant distances along the hydrogen migratory insertion pathway, relating to 1ax (Å).

distance		*Ethylene*	*Δd*	*TS1*	*Δd*	*β-agostic*	*Σ [Å]*
M-H1	Å	1.56	+9%	1.6	+91%	2	+0.44
M-C1	Å	2.24	+7.7%	2.25	-107.7%	2.11	-0.13
C1-C2	Å	1.42	0%	1.42	+100%	1.51	+0.09

$[(PMe_3)_3Rh(C_2H_4)H]$: Ethylene "Starting-structures" 1ax and 1eq

The energy profile of the hydride migratory insertion reaction of the M=Rh and L=PMe_3 neutral complex is depicted in figure 34. Table 12 shows the relative energies of the species involved in the reaction. A scan following selected reaction coordinates described in Chapter 2 was carried out and the 16e-ethyl isomer is obtained directly from the ethylene structure, through an energy barrier of 23 kcal/mol. The η^2-agostic structure could not be located as a minimum, contrasting to

the cobalt homolog studied previously by Bittner *et al.* [73]. The ethylene structure is the ground state being 1.5 kcal/mol more stable than the related 16e-ethyl isomer. The ethylene isomer was the only stationary point located for 1eq, being 8 kcal/mol higher in energy than 1ax (see section 3.2.1).

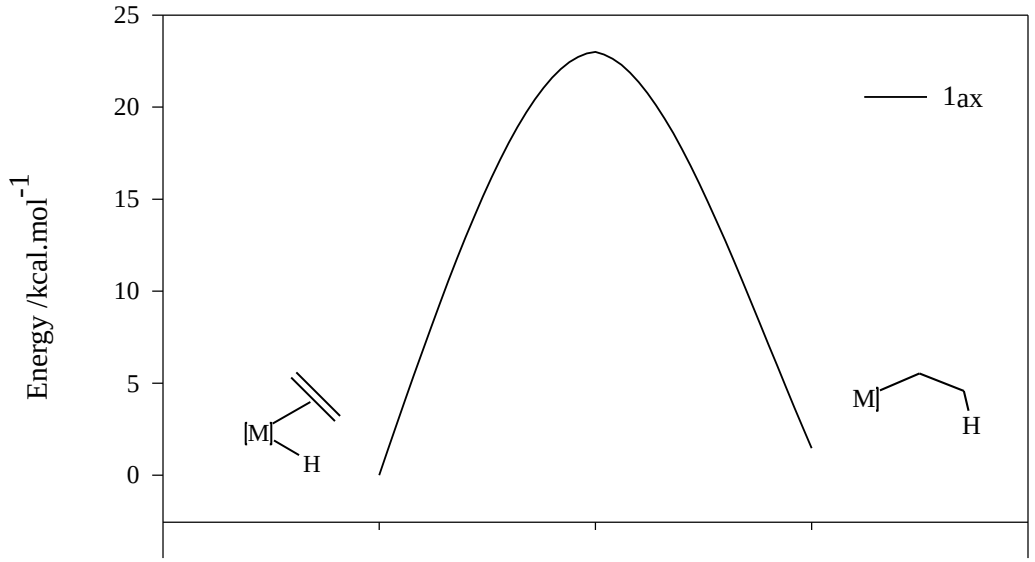

Figure 34: Energy profile of the hydrogen migratory insertion pathway, with reference to 1ax ethylene isomer (in kcal.mol^{-1}).

Table 12: Relative energies of the species involved in the hydride migratory insertion reaction. The energies ΔE of the subsequent stationary points (B3LYP/SDD) are calculated relative to the preceding ethylene initial structure, in kcal/mol.

Initial structure	*Ethylene*		*TS1*		*16e-ethyl*
1ax	0	TS1	23	3	1.5

The 1ax transition state (TS1) calculated is presented in figure 35, and its nature was confirmed by frequency calculations. An imaginary frequency that matches the reaction coordinate α(C2-Co-H1) is obtained.

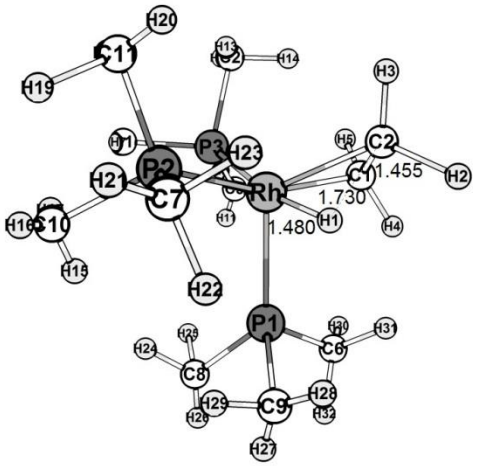

+23

from 1ax (M=Rh; L=PMe_3)

Figure 35: Optimized structure and relative energy (kcal/mol) of the transition state 1 (TS1) complexes.

The 1ax TS1 geometry is similar to the ethylene isomer structure. TS1 is a so-called reactant-like isomer (see the variation of the stationary points distances depicted in figure 36).

The M-H1 bond distance of ethylene (1.582 Å) is more stretched than in the TS1 structure (table 13).

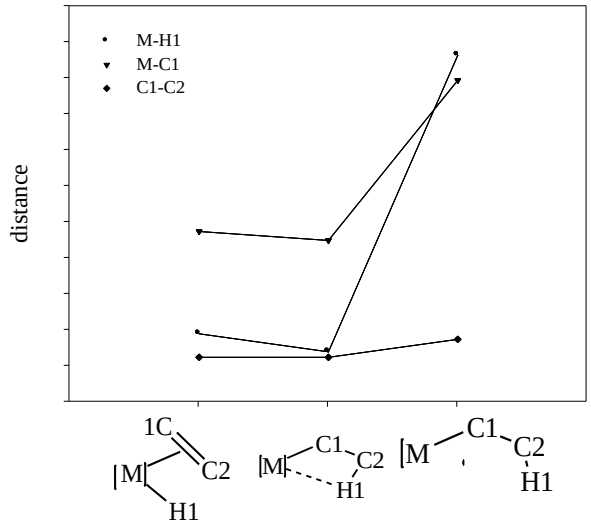

Figure 36: Variation of the relevant distances along the hydrogen migratory insertion pathway, with reference to 1ax (d (Å)).

Table 13: Relevant distances (Å) and angles (º) of TS1.

	from 1ax
d(M-C1)	2.102
d(M-H1)	1.480
d(C1-C2)	1.455
α(M-C1-C2)	75.75
β(H1-M-C2)	50.46
φ(P-M-P)	98.29; 102.69; 108.11

As H1 leaves the axial plane and approaches the olefin ligand is no longer influenced by the electron rich group in its trans position, thus adjusting its bond length. The H moving in the olefin direction does not influence the position of the PMe_3 groups. The φ(P-Rh-P) angles are similar in both the geometries. At this stage, the olefin group has already rotated ca. 45º.

3.3 16-electron Singlet and Triplet States of the ethyl minima

a) Structural parameters and energies

Complexes with a d^8 configuration are expected to have a square planar structure when M is a 4d or 5d metal centre and for 3d metals when ligands are strong. This is the typical situation where the square planar coordination geometry is expected. A distorted square planar structure (SP) is indeed obtained from the hydrogen migratory insertion reaction pathway. Following the reaction coordinates described in figure 15 (Chapter 2), the complex with a β-agostic M···H-C bond rearranges to a 16e-ethyl species with a distorted tetrahedral structure (TH), as reported also by Bittner *et al.* [73]. This structure was then isolated and optimized and attested to have energy comparable and just a few kcal/mol above of the expected square planar structure obtained from the reaction pathway.

In order to get a more complete picture of the formally unsaturated 16e-ethyl complexes, these isomers were also analysed for the triplet state (t). For open shell systems, an unrestricted method capable of treating unpaired electrons is needed. In this case, α and β electrons are in different orbitals, resulting in two sets of molecular orbital expansion coefficients. The two sets of coefficients result in two sets of Fock matrices (and their associated density matrices), and ultimately to a solution producing two sets of orbitals. These separate orbitals produce proper dissociation to separate atoms, correct delocalized orbitals for resonant systems, and other attributes.

Electronically unsaturated, open-shell configurations tend to be more common for higher oxidation states and for lighter (3d) transition metals. The combination of metal size (3d< 4d~ 5d) and the metal-ligand bond strength seems particularly effective at rationalizing these trends. Metal atoms of the 3d series have a smaller covalent radius than the corresponding 4d and 5d atoms and the length of the metal-ligand bonds is correspondingly shorter for the 3d metals. Therefore, there is a greater repulsive interaction between the ligands in a 3d metal complex than in the corresponding complexes of the heavier congeners. The greater bond strength for 4d and 5d relative to 3d metals is in agreement with the greater tendency of systems with these metals to reach a more saturated configuration, which justifies the energy.

The discussion will focus on the geometrical aspects and the relative energies between the different structures.

The RB3LYP (closed-shell restricted wavefunctions) DFT MO methods were employed to determine the singlet states. The triplet states calculations were carried out making use of a UB3LYP method (unrestricted open-shell wavefunctions) and the single point calcualtion with a restricted open-shell method ROB3LYP (restricted open-shell wavefunctions).

Distorted square planar (SP) and tetrahedral (TH) singlet (s) and triplet (t) structures of the $[(PF_3)_3CoC_2H_5]$

The energies of the two singlet state 16e-ethyl isomers obtained are in close proximity and both provide evidence of being minima by frequency calculations.

The calculation of the 16e-ethyl distorted square planar (SP) and tetrahedral (TH) singlet (s) and triplet (t) structures of $[(PF_3)_3CoC_2H_5]$ afforded the following singlet and triplet configurations, as in figure 37.

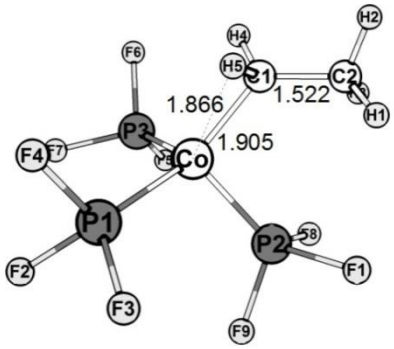

SPs= +7.7

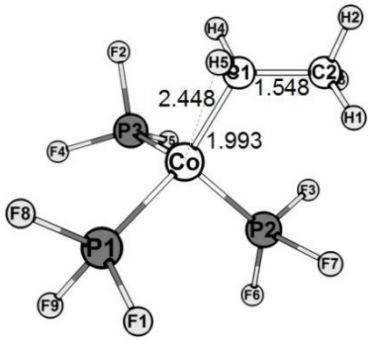

SPt= +2.58

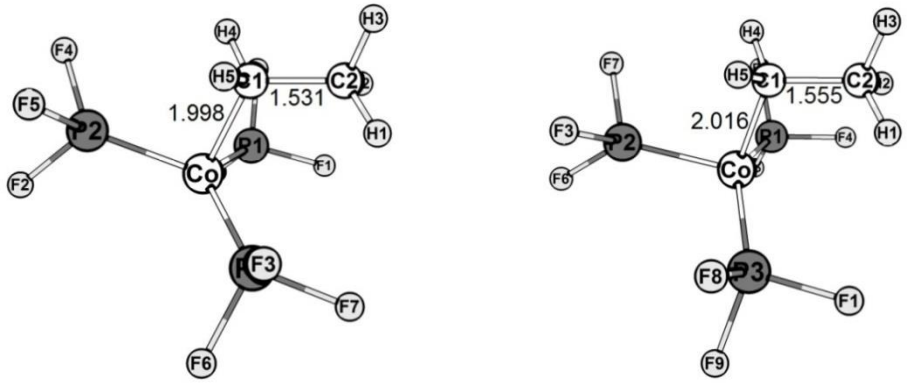

THs= +10.8 THt= +10.65

Figure 37: Optimized structures and relative energies (kcal/mol) of $[(PF_3)_3CoC_2H_5]$ distorted square planar (SP) and tetrahedral (TH) singlet (s) and b) triplet (t) structures (relative to the ethylene isomer).

The -SPs minimum exhibits a misrepresentation of the ordinary square planar structure. The sum of π(P-Co-P)=116.62^o and its perpendicular angle δ(P-Co-C1)= 146.45^o is 262^o, which would be 360^o for a perfect square planar case. On a paper from Hoffmann *et al.* [102], the energy levels of an $M(CO)_4$ fragment of D_{2d} symmetry show d^{10} will prefer a tetrahedron, while d^8 will be fairly balanced between square planar and tetrahedral extremes. Being aware of the similar properties between a CO and a PF_3 ligand, this conclusion can also be applied to this system. Of course, on the tetrahedral side a high spin situation is created for d^8. Another important feature of the conformation adopted by the SPs isomer is the formation of an α-agostic bond. This idea is pointed out based on the values of a shorter d(Co-C1)= 1.905 Å, d(Co-H1)= 1.866 Å and longer d(C1-H1)= 1.153 Å (d(C1-H2)= 1.094 Å), than expected, and π(P-Co-P)= 116.62^o and δ(P-Co-C1)= 146.35^o (table 14).

Table 14: Relevant distances (Å) and angles (°) of $[(PF_3)_3CoC_2H_5]$ distorted square planar (SP) and tetrahedral (TH) singlet (s) and triplet (t) structures.

16e-ethyl	*-SPs*	*-SPt*	*-THs*	*-THt*
d(Co-C1)	1.905	1.993	1.998	2.016
d(C1-C2)	1.522	1.548	1.531	1.555
d(Co-H1/H2)	1.866, 2.583	2.448, 2.558	2.518, 2.516	2.600, 2.601
d(P-Co)	trans: 2.174 eq: 2.108, 2.117	trans: 2.274 eq: 2.281, 2.284	2.146, 2.152, 2.153	2.257, 2.227, 2.258
π(P-Co-P)	116.62, 101.36, 102.46	100.32, 102.15, 102.33	122.90, 118.35, 118.12	142.20, 105.31, 105.34
δ(P-Co-C1)	146.35	134.09	90.69, 93.72, 93.54	95.08, 99.44, 99.32

The -THs shows a distortion from the idealized tetrahedral geometry. For the triplet state isomer π(P-Co-P) alters to a larger extent comparing to the singlet isomer. The δ(P-Co-C1) angle rises from 90.69°, 93.72° and 93.54° in the singlet state (s) to 95.08°, 99.4° and 99.32° (for t), respectively. The P-Co distance is ca. 0.1 Å longer than the singlet state isomer. The different orbital occupancy reflects on the M-C1 distance, being also 0.1 Å longer (t) than the singlet state isomer (s).

Table 15: Relative energies of the 16e-ethyl singlet and triplet species obtained from the reaction pathway of the ehydrogen migratory insertion reaction. The energy ΔE is calculated relative to the ethylene isomer, in kcal.mol$^{-1.}$

16e-ethyl $[(PF_3)_3CoC_2H_5]$	*Energy /kcal.mol^{-1}*
-SPs	+7.7
-SPt	+2.58
-THs	+10.8
-THt	+10.65

The 16e-ethyl singlet isomer adopts two ground state geometries with similar energies, a distorted square planar (SPs) and a distorted tetrahedral (THs) geometries.

The SPs and SPt distorted square planar isomers are +7.7 and +2.58 kcal/mol higher in energy than the ethylene isomer. The SPt isomer is 5.12 lower in energy than the 16e-ethyl singlet isomer (SPs), which is additionally stabilized with a α-bond. The THs and THt isomers are +10 kcal/mol higher in energy, relative to the ethylene isomer.

Distorted square planar (SP) and tetrahedral (TH) singlet (s) and triplet (t) structures of the $[(PMe_3)_3CoC_2H_5]$

The two singlet state 16e-ethyl isomers obtained have close energy values. The THs is 7.08 kcal/mol higher in energy, and both prove to be minima by frequency calculations (figure 38). The triplet state is by far the more stable structure adopted. Measured up with L= PF_3, the $[(PMe_3)_3CoC_2H_5]$ triplet state structure ends in a more distorted geometry, resembling a perfect tetrahedral geometry.

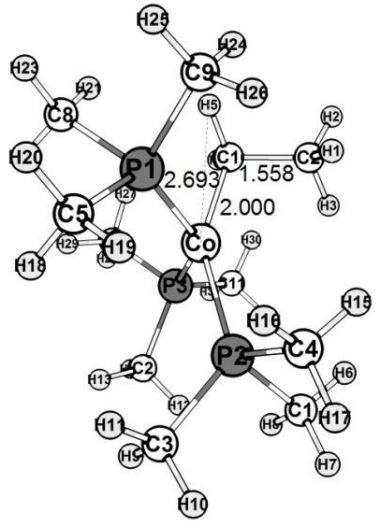

SPs=+8.74

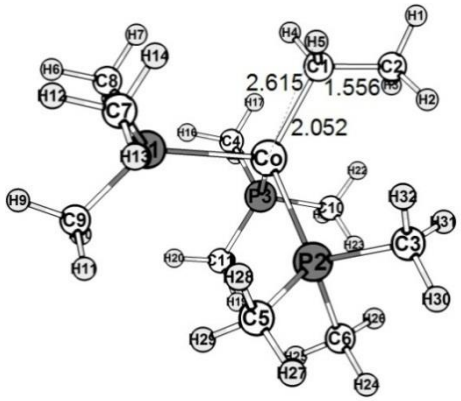

SPt=-12.86

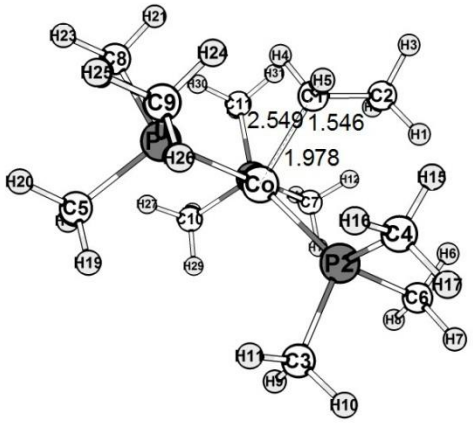

THs=+0.94

Figure 38: Optimized structures and relative energies (relative to the ethylene isomer in kcal/mol) of $[(PMe_3)_3CoC_2H_5]$ distorted square planar (SP) and tetrahedral (TH) singlet (s) and triplet (t) structures.

The SPs minimum exhibits an alteration from the model square planar structure, but not so outsized as in case of L=PF_3. The π(P-Co-P) and δ(P-Co-C1) angles still indicate a deformation from the classic geometry (table 16). The same applies for the -THs singlet state minimum. This structure with L=PMe_3 has a shorter Co-C1 distance, since this donor ligand is not in a trans position. The P-Co-P angles (123.77^o, 116.47^o, 116.62^o) resemble the standard 120^o angles.

Table 16: Relevant distances (Å) and angles (^{o}) of $[(PMe_3)_3CoC_2H_5]$ distorted square planar (SP) and tetrahedral (TH) singlet (s) and triplet (t) structures.

16e-ethyl	*-SPs*	*-THs*	*-t*
d(Co-C1)	2.000	1.978	2.052
d(C1-C2)	1.558	1.546	1.556
d(Co-H1/H2)	2.691, 2.693	2.549, 2.546	2.617, 2.615
d(P-Co)	trans: 2.306	trans: 2.277	2.426,
	eq: 2.240, 2.239	eq: 2.296, 2.296	2.414, 2.414
π(P-Co-P)	138.9, 100.12,	123.77, 116.47,	102.91, 102.88,
	100.18	116.62	102.63
δ(P-Co-C1)	150.50	91.81	111.69, 118.32,
			116.42

The $[Co(PMe_3)_3C_2H_5]$ triplet state complex is by far more stable than the singlet states. The triplet state structure is obtained starting from –SPs and -THs, and it adopts a tetrahedral conformation as expected for a d^8-ML_4 triplet state.

An increase in the δ(P-Co-C1) angle reduces the antibonding interaction in the equatorial plane and reduces the steric hinderance between the ligands, which will mirror a stabilization of this isomer. This complex is 12.86 kcal/mol more stable than the ethylene isomer and becomes the global minimum of the hydrogen migratory insertion reaction (see table 17). The THs is the global minimum of the energy profile that ends in this 16e-ethyl isomer.

Table 17: Relative energies of the 16e-ethyl singlet and triplet species obtained from the reaction pathway of the migratory insertion reaction. The energy ΔE is calculated relative to the ethylene isomer, in kcal.mol^{-1}

16e-ethyl $[(PMe_3)_3CoC_2H_5]$	*Energy /kcal.mol^{-1}*
-SPs	+8.74
-SPt	-12.86
-THs	-0.94

Distorted square planar (SP) and tetrahedral (TH) singlet (s) and triplet (t) structures of the $[(PF_3)_3RhC_2H_5]$

The 16e-ethyl minima achieved for M=Rh and L= PF_3 have similar energies and are minima, authenticated by frequency calculations. The triplet states exhibit a much higher energy. The calculation of the geometries furnished the following singlet and triplet arrangements (figure 39).

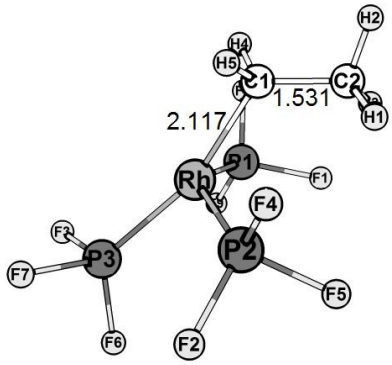

SPs=+5.7

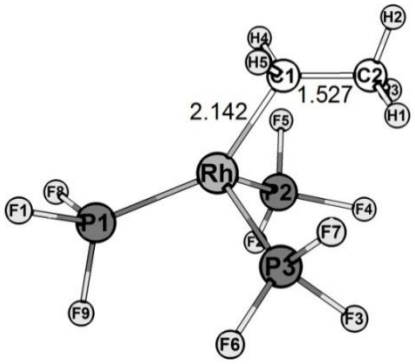

SPt=+31.57

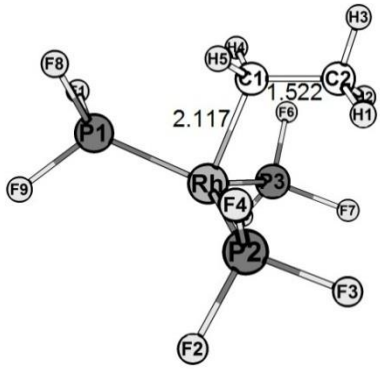

THs=+5.83

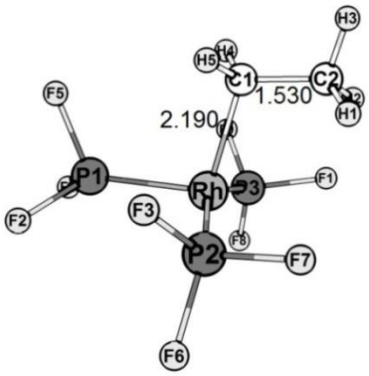

THt=+31.97

Figure 39: Optimized structures and relative energies (relative to the ethylene isomer in kcal/mol) of $[(PF_3)_3RhC_2H_5]$ distorted square planar (SP) and tetrahedral (TH) singlet (s) and triplet (t) structures.

The geometry adopted in case of –SPs shows a visible alteration from the model inferred to a d^8-ML_4 square planar geometry, being δ(P-Rh-C1)=163.35º and the π(P-Rh-P)=132.22º, for L-M-L trans. This distortion is not so determinant for rhodium as for the cobalt complex (δ(P-Co-C1)=146.35º and the π(P-Co-P)=116.62º) and it can be attributed to the formation of the α-bond in -SPs.

The triplet state structure (-SPt) lies 25.87 kcal/mol above the singlet state. In comparison with the singlet state, the δ(P-Rh-C1)=163.35º decreases to 146.31º and the π(P-Co-P)=132.22º to 99.31º giving evidence of a conformation closer to a perfect tetrahedral geometry.

The d(Rh-P) is more stretched in the triplet state, as expected.

The π(P-Rh-P) and δ(P-Rh-C1) for –THs and -THt minima show the same trend as in the cobalt complex. The –THs lies 25.24 kcal/mol below the singlet isomer.

Table 18: Relevant distances (Å) and angles (°) of $[(PF_3)_3RhC_2H_5]$ distorted square planar (SP) and tetrahedral (TH) singlet (s) and triplet (t) structures.

16e-ethyl	*-SPs*	*-SPt*	*-THs*	*-THt*
d(Rh-C1)	2.117	2.142	2.117	2.190
d(C1-C2)	1.531	1.527	1.522	1.530
d(Co-H1/H2)	2.574, 2.522	2.555, 2.531	2.600, 2.602	2.690, 2.691
d(Rh-P)	trans: 2.375	trans: 2.396	trans: 2.306	trans: 2.331
	eq: 2.272, 2.271	eq: 2.358, 2.358	eq: 2.312, 2.314	eq: 2.341, 2.341
π(P-Rh-P)	132.22, 98.71,	105.89, 104.67,	123.18, 118.34,	149.24, 100.62,
	99.40	99.31	118.29	100.62
δ(P-Rh-C1)	163.35	146.31	89.73	101.89

Table 19: Relative energies of the 16e-ethyl singlet and triplet species obtained from the reaction pathway of the migratory insertion reaction. The energy ΔE is calculated relative to the ethylene isomer, in kcal.mol^{-1}

16e-ethyl $[(PF_3)_3RhC_2H_5]$	*Energy /kcal.mol^{-1}*
-SPs	+5.7
-SPt	+31.57
-THs	+5.83
-THt	+31.97

The -THs is only 0.13 kcal/mol higher in energy than –SPs, being significantly closer in energy than in the case of cobalt. The -SPt is found to be +25.87 kcal/mol and -THt to be +26.27 kcal/mol, weighing against the SPs isomer. These energy values show a different trend as for M=Co.

Distorted square planar (SP) and tetrahedral (TH) singlet (s) and triplet (t) structures of the $[(PMe_3)_3RhC_2H_5]$

The SPs and THs 16e-ethyl minima calculated have an energy disparity of 15.01 kcal/mol. Frequency calculations confirmed that both are minima. The triplet states exhibit a much higher energy. The singlet and triplet arrangements obtained are depicted below (figure 40).

The -SPs minimum exhibits a slightly deviation from the standard square planar structure. The δ(P-Rh-C1)=162.97º and the π(P-Rh-P)=153.11º, the L-M-L trans, authenticate the distortion. This distortion is larger for cobalt (δ(P-Rh-C1)=150.5º and the π(P-Rh-P)=138.9º), due to the size of the metal *vs.* steric hindrance of the bulky PMe_3 ligands. The correspondent triplet isomer has longer Rh-P distances, as expected. The π(P-Rh-P)=153.11º angle decreases to 102.84º for the isomer in the triplet state and δ(P-Rh-C1) from 162.97º to 154.56º (table 20).

The THt isomer shows a diminutive distortion from the singlet geometry. On building up the triplet state isomer, the δ(P-Rh-C1) increases from 89.12º to 96.46º and its perpendicular P-Co-P angle from 122.73º to 150.98º, decreasing in this way the steric hindrance between the ligands in the equatorial plane (THt, figure 40).

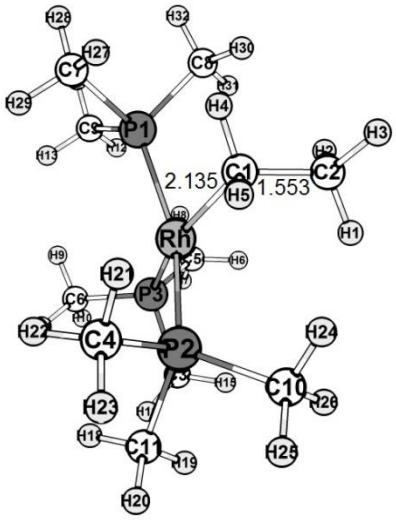

SPs=+1.5

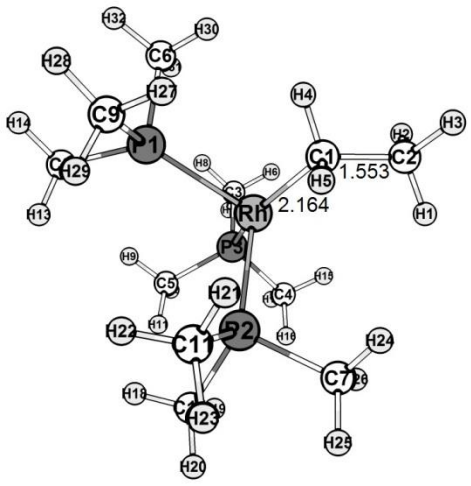

SPt=+25.84

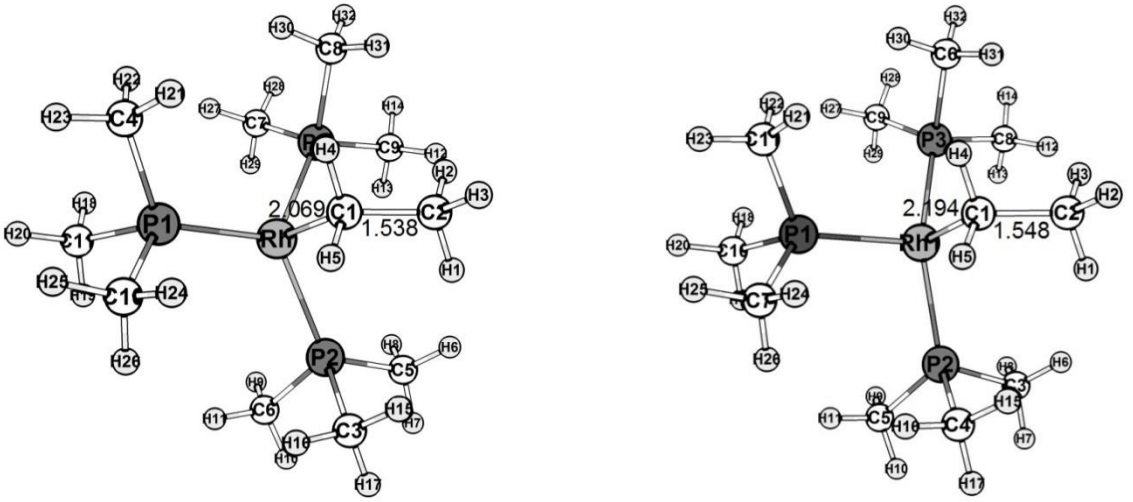

THs=+16.51 THt=+25.55

Figure 40: Optimized structures and relative energies (relative to the ethylene isomer in kcal/mol) of $[(PMe_3)_3RhC_2H_5]$ distorted square planar (SP) and tetrahedral (TH) singlet (s) and triplet (t) structures.

Table 20: Relevant distances (Å) and angles (°) of $[(PMe_3)_3RhC_2H_5]$ distorted square planar (SP) and tetrahedral (TH) singlet (s) and triplet (t) structures.

16e-ethyl	*-SPs*	*-SPt*	*-THs*	*-THt*
d(Rh-C1)	2.135	2.164	2.069	2.194
d(C1-C2)	1.553	1.553	1.538	1.548
d(Co-H1)	2.769, 2.770	2.732, 2.770	2.164, 2.164	2.752, 2.752
d(Rh-P)	trans: 2.428	trans: 2.469	trans: 2.396	trans: 2.436
	eq: 2.370, 2.374	eq: 2.469, 2.469	eq: 2.338, 2.338	eq: 2.422, 2.422
π(P-Rh-P)	96.64, 100.01,	101.88, 102.84,	118.17, 118.17,	101.70, 101.74,
	153.11	103.43	122.73	150.98
δ(P-Rh-C1)	162.97	154.56	89.12	96.46

The THs is found to be +15.01 kcal/mol when compared to SPs. The SPt and THt triplet states energies are +24.34 kcal/mol and +24.05 kcal/mol higher in energy than –SPs, respectively.

Table 21: Relative energies of the 16e-ethyl singlet and triplet species obtained from the reaction pathway of the migratory insertion reaction. The energy ΔE is calculated relative to the ethylene isomer, in kcal.mol^{-1}.

16e-ethyl $[Rh(PMe_3)_3C_2H_5]$	*Energy /kcal.mol-1*
-SPs	+1.5
-SPt	+25.84
-THs	+16.51
-THt	+25.55

b) Orbitals

The frontier orbital regions were investigated for the 16e-ethyl isomers found in previous calculations. The electronic structures of the frontier orbital region of the singlet and triplet states were analysed. The energies shown for the triplet states were obtained at a ROB3LYP level.

The energy of the unsaturated 16 electron ethyl complexes was evaluated for the singlet and the triplet state. The singlet state, a geometry fairly balanced between a square planar and a tetrahedral, is stabilized for the 4d transition metal Rh. The triplet state is stabilized for the 3d transition metal Co. The unsaturated 16e-ethyl complexes are stabilized by increasing the donor strength of L.

For a square planar structure, the x^2-y^2 orbital high in energy explains why a singlet d^8-complex is stable. At the tetrahedral side a d^8 system will have four electrons in t_2. Consequently, a high spin (triplet) situation is required for a stable species. Notice that for the tetrahedral geometry the three members of t_2 have M-L antibonding character. At the square planar geometry only dz^2 is slightly antibonding. As a result it will be expected weaker, and therefore longer M-L distances for high spin d^8 compounds compared to their low spin, square planar equivalent [99].

$[(PF_3)_3CoC_2H_5]$ distorted square planar (SP) singlet (s) and triplet (t)

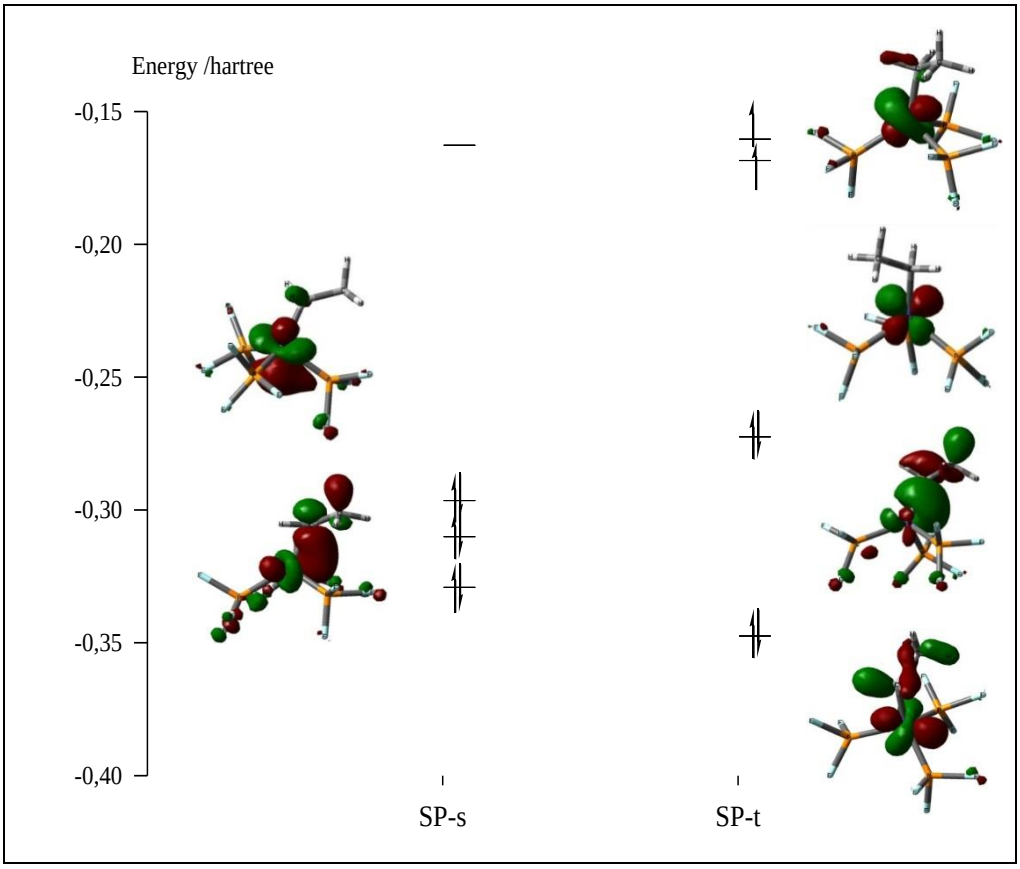

Figure 41: Electronic structure (frontier orbital region) of the singlet (images: HOMO-1 and HOMO-2) and triplet (images: HOMO, HOMO-1, HOMO-2, HOMO-3) distorted square planar $[Co(PF_3)_3C_2H_5]$ ethyl isomers.

The frontier orbital regions were looked over for the distorted square planar (SP) singlet (s) and triplet (t) states found (figure 41). The calculations reveal that SPs and SPt have energies of 7.7 kcal/mol and 2.58 kcal/mol above the corresponding ethylene minima.

This 16e-ethyl singlet isomer (SPs) adopts a conformation with an α-agostic bond (d(Co-H1)=1.866 Å). The acceptor ability of the dz^2+p_z improves upon pyramidalization, which justifies the existence of the α-agostic bond. As a consequence, an important degree of pyramidalization is to be expected when the metal atom acts as an acceptor through its p_z orbital. A theoretical study of the axial

bonding capabilities of square planar d^8-ML_4 complexes were carried out some years ago by Alvarez et al [36]. A β-agostic ethyl ligand bond can occur in a compound with an unsaturated metal with suitable empty orbitals. The minimal requirement is that the metal centre should have an empty orbital to receive the two electrons of the C1-H5 bond. It is to be presumed that this orbital will be essentially of d-character for transition metal compounds. The orbital should be a very good acceptor and the energy and disposition should approach that of the C-H bonding electrons as far as possible. A series of complexes are known in which a C-H bond interacts with a square planar d^8 metal in the axial (±z) direction [102]. The square planar complexes of d^8 transition metal ions comply with the 16 electron rule and can generally be isolated as stable species. These compounds have two nonbonding valence orbitals in the exposed region perpendicular to the molecular plane: the occupied dz^2 and the empty p_z orbitals. In 16-electron d^8-ML_4 square planar species, however, both β-agostic and hydrogen bond interactions are in principle possible, because the metal has available both a lone pair and an empty orbital. Given the existence of an empty p_z orbital at the metal atom, the bonding molecular orbital (essentially dz^2) is hybridized toward the M···C-H interatomic region, whereas the antibonding combination (essentially p_z) is hybridized away from that bond.

In the $[(PF_3)_3CoC_2H_5]$ this interaction exists (see figure 42).

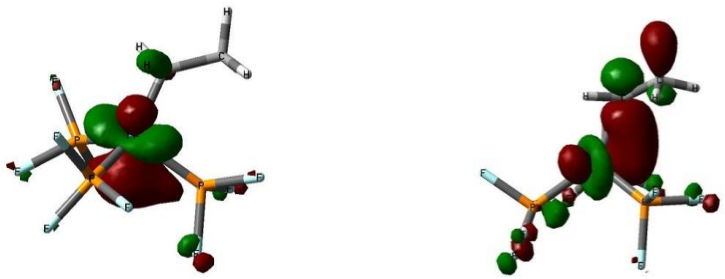

Figure 42: Co-H5 α-bond in $[(PF_3)_3CoC_2H_5]$-SPs (image: HOMO-1 and HOMO-2).

The Co-C1 distance is 0.1 Å longer for SPt than for the singlet state. The H5, now 2.45Å distant from the cobalt atom, does not build an α-agostic bond anymore. This is also supported by the fact that the Co-C1 distance is more stretched (1.992 Å) and the C1 and H5 atoms being closer (1.11 Å).

$[(PF_3)_3CoC_2H_5]$ distorted tetrahedral (TH) singlet (s) and triplet (t)

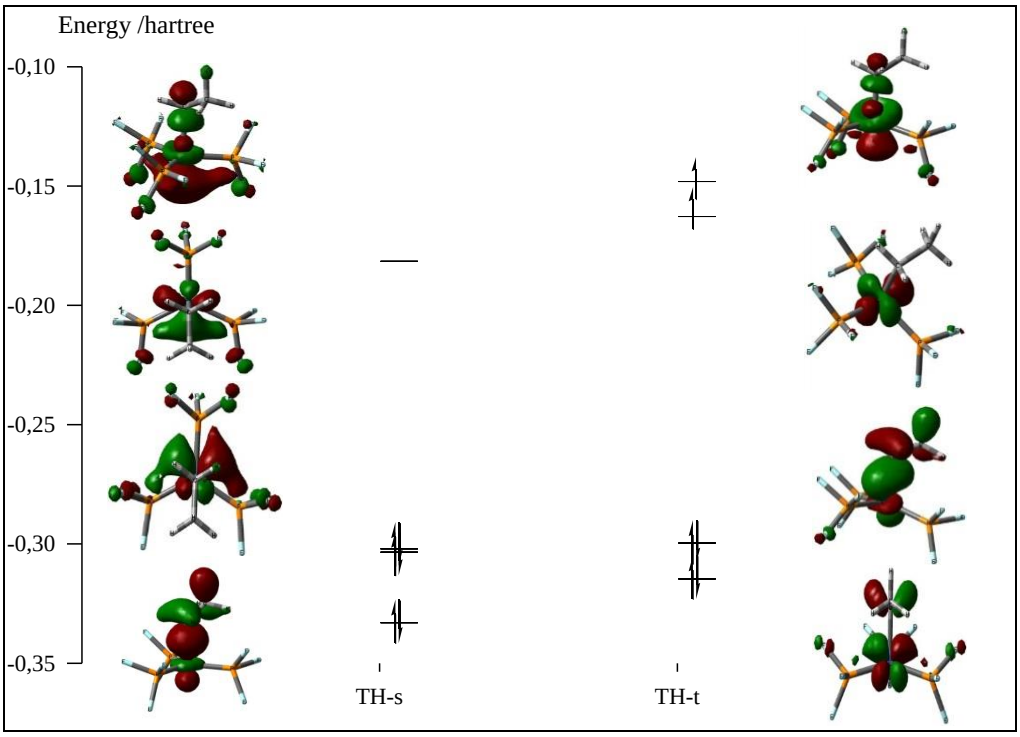

Figure 43: Electronic structure (frontier orbital region) of the singlet (images: LUMO, HOMO, HOMO-1 and HOMO-2) and triplet (images: HOMO, HOMO-1, HOMO-2, HOMO-3) distorted tetrahedral $[Co(PF_3)_3C_2H_5]$ ethyl isomers. The energies shown for the triplet states were obtained at the ROB3LYP level.

The frontier orbital regions were looked over for the distorted square planar (TH) singlet (s) and triplet (t) states calculated (figure 43). The calculations reveal that THs and THt have energies of 10.8 kcal/mol and 10.65 kcal/mol above the corresponding ethylene minima.

Given the existence of an empty p_z orbital at the metal atom in THs, the bonding molecular orbital (essentially dz^2) is hybridized toward the M···C-H interatomic region, whereas the antibonding combination (essentially p_z) is hybridized away from that bond.

Concerning the triplet state isomer, the P-Co-P angle increases which will reduce the antibonding interaction between d_{xy} and the σ orbitals of the two equatorial

PF_3 ligands. The δ(P-Co-C1) angle rises in an attempt to reduce the antibonding interaction, even weak, in the equatorial plane with the now occupied dz^2 orbital and increasing the overlap with L p-orbitals. The different orbital occupancy reflects on the M-C1 distance. The single occupation of the z^2 orbital, lengthens the M-L distance in 0.2 Å relative to the singlet state. The antibonding interaction with z^2 and the C_2H_5 ligand is reduced by mixing with the p_z metal orbital.

$[(PMe_3)_3CoC_2H_5]$ distorted square planar (SP) singlet (s) and triplet (t)

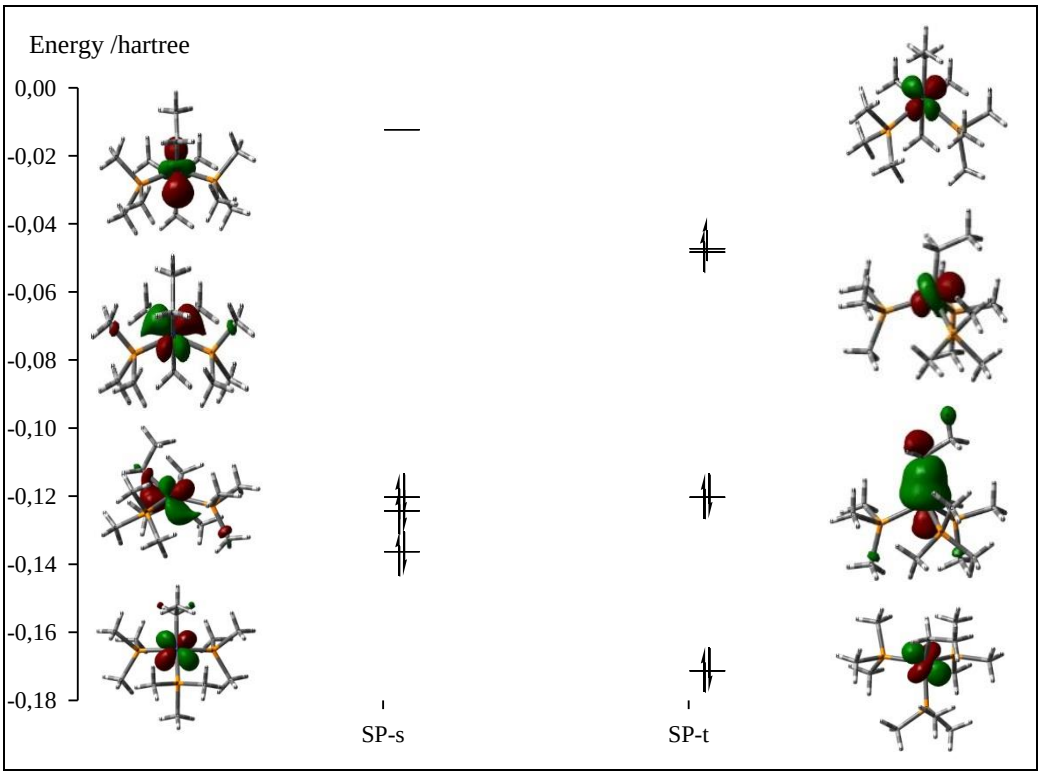

Figure 44: Electronic structure (frontier orbital region) of the singlet (images: LUMO, HOMO, HOMO-1 and HOMO-2) and triplet (images: HOMO, HOMO-1, HOMO-2 and HOMO-3) distorted square planar $[Co(PMe_3)_3C_2H_5]$ ethyl isomers. The energies shown for the triplet states were obtained at the ROB3LYP level.

The frontier orbital regions for the $[(PMe_3)_3CoC_2H_5]$ distorted square planar (SP) singlet (s) and triplet (t) states are illustrated above (figure 44). The calculations reveal that SPs and SPt have energies of +8.74 kcal/mol and -12.86 kcal/mol relative the corresponding ethylene minima.

The triplet state structure adopts a conformation with δ(P-Co-C1)=111.69, 118.32 and 116.42°, that resembles a tetrahedral geometry. This increase of δ(P-Co-C1) reduces the antibonding interaction in the equatorial plane, such as between d_z^2 and the equatorial σ_{PMe3} orbitals and allows in addition the pz orbital to mix in so as to reduce the antibonding interaction between d_z^2 and σ_{C2H5}.

[$(PMe_3)_3CoC_2H_5$] distorted tetrahedral (TH) singlet (s) and triplet (t)

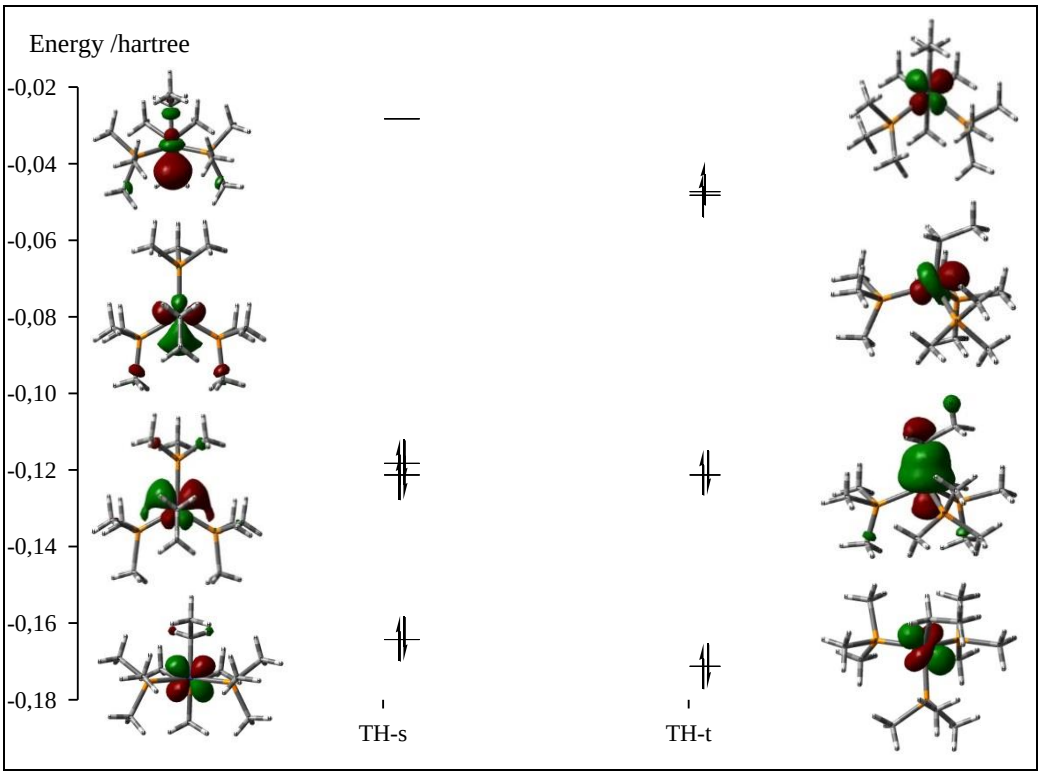

Figure 45: Electronic structure (frontier orbital region) of the singlet (images: LUMO, HOMO, HOMO-1, HOMO-2) and triplet (images: HOMO, HOMO-1, HOMO-2 and HOMO-3) distorted tetrahedral [$Co(PMe_3)_3C_2H_5$] ethyl isomers. The energies shown for the triplet states were obtained at the ROB3LYP level.

The frontier orbital regions were looked over for the distorted tetrahedral (TH) singlet (s) and triplet (t) states found (figure 41). The calculations reveal that THs and THt have energies of 0.94 kcal/mol and 12.86 kcal/mol below the corresponding ethylene minima.

Calculations of the triplet state isomer converge to the conformation obtained for SPt. The geometry adopted represents the global minimum of the reaction.

$[(PF_3)_3RhC_2H_5]$ distorted square planar (SP) singlet (s) and triplet (t)

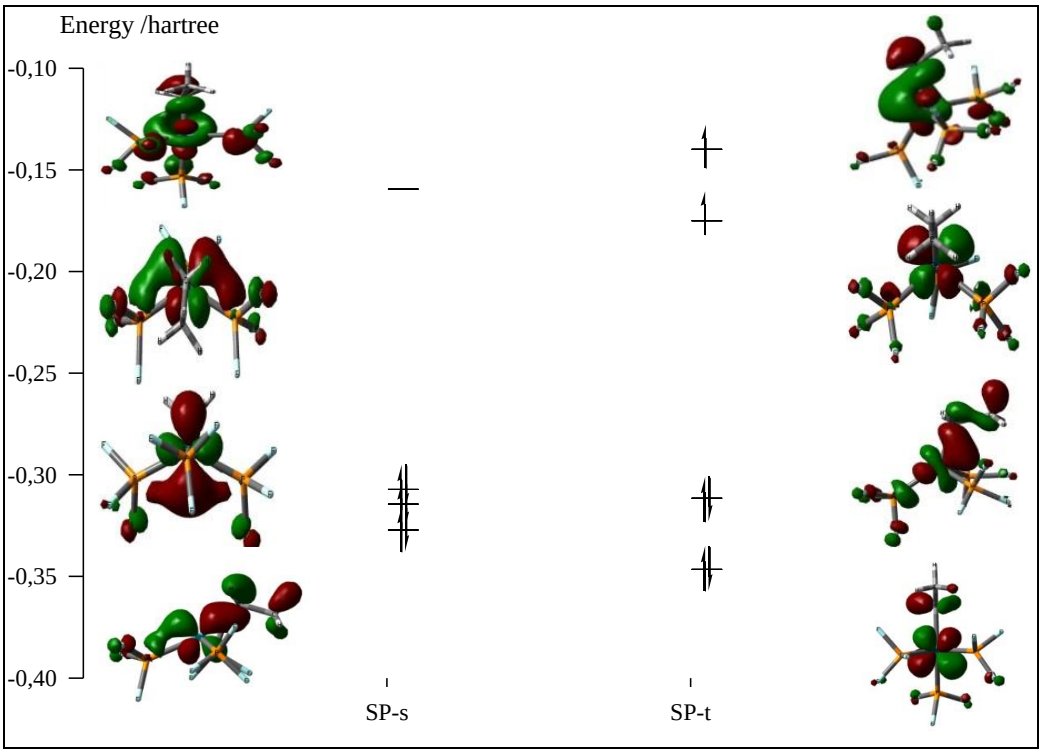

Figure 46: Electronic structure (frontier orbital region) of the singlet (images: LUMO, HOMO, HOMO-1 and HOMO-2) and triplet (images: HOMO, HOMO-1, HOMO-2 and HOMO-3) distorted square planar $[Rh(PF_3)_3C_2H_5]$ ethyl isomers. The energies shown for the triplet states were obtained at the ROB3LYP level.

The frontier orbital regions for the $[(PF_3)_3RhC_2H_5]$ distorted square planar (SP) singlet (s) and triplet (t) states are illustrated in figure 46. The calculations reveal that SPs and SPt have energies of +5.70 kcal/mol and +31.57 kcal/mol above the corresponding ethylene minima.

$[(PF_3)_3RhC_2H_5]$ distorted tetrahedral (TH) singlet (s) and triplet (t)

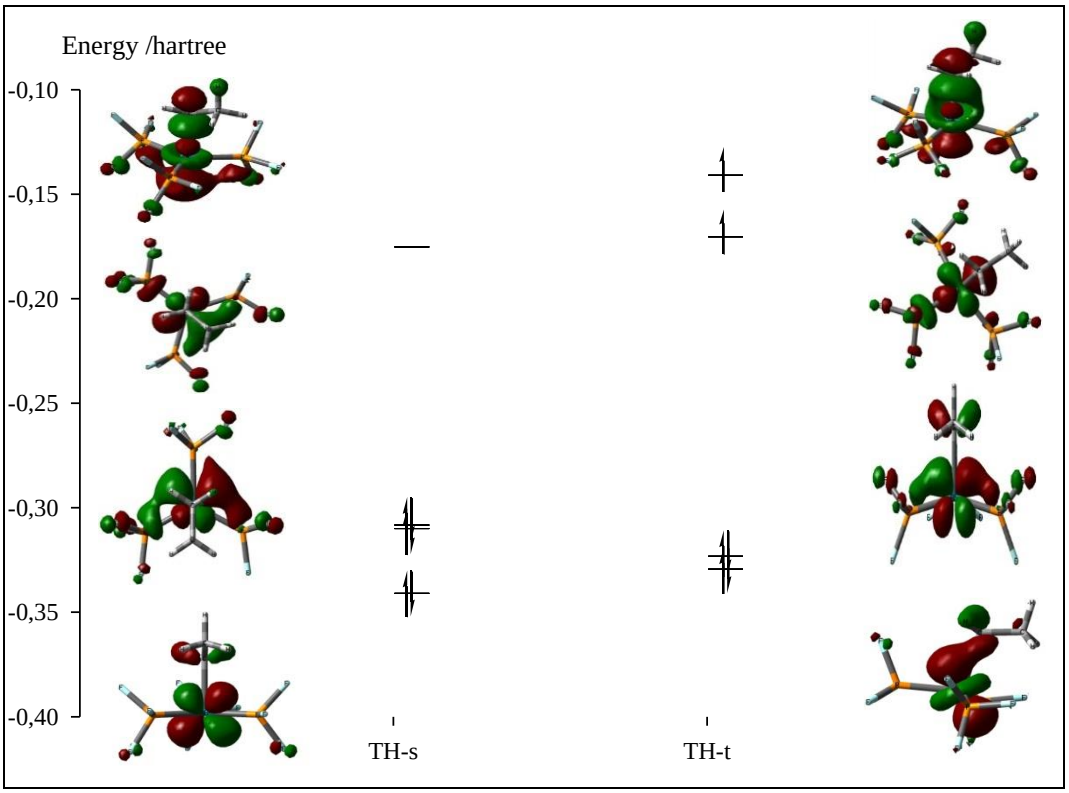

Figure 47: Electronic structure (frontier orbital region) of the singlet (images: LUMO, HOMO, HOMO-1 and HOMO-2) and triplet (images: HOMO, HOMO-1, HOMO-2, HOMO-3) tetrahedral $[(PF_3)_3RhC_2H_5]$ ethyl isomers. The energies shown for the triplet states were obtained at a ROB3LYP level.

The frontier orbital regions were looked over for the distorted tetrahedral (TH) singlet (s) and triplet (t) states found (figure 47). The calculations reveal that THs and THt have energies of 5.83 kcal/mol and 31.97 kcal/mol above the corresponding ethylene minima.

$[(PMe_3)_3RhC_2H_5]$ distorted square planar (SP) singlet (s) and triplet (t)

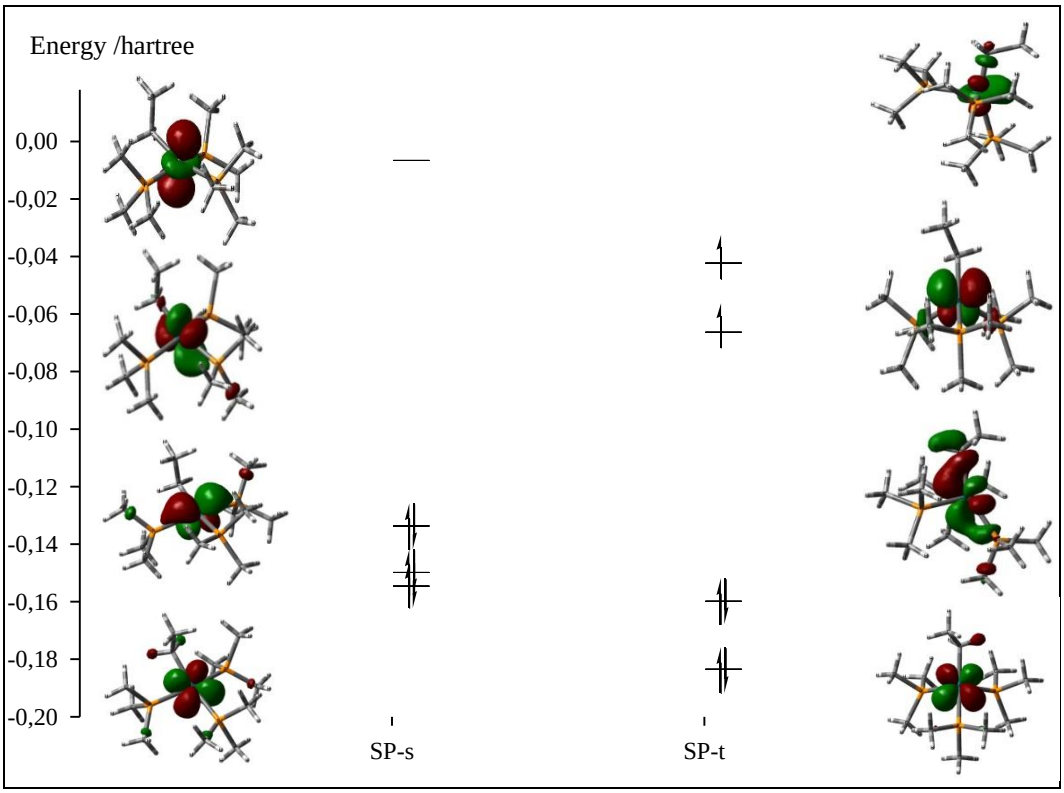

Figure 48: Electronic structure (frontier orbital region) of the singlet (images: HOMO, HOMO-1, HOMO-2 and HOMO-3) and triplet (images: HOMO, HOMO-1, HOMO-2, HOMO-3) distorted square planar $[(PMe_3)_3RhC_2H_5]$ ethyl isomers. The energies shown for the triplet states were obtained at the ROB3LYP level.

The frontier orbital regions were looked over for the distorted tetrahedral (SP) singlet (s) and triplet (t) states found (figure 47). The calculations reveal that SPs and SPt have energies of 1.5 kcal/mol and 25.84 kcal/mol above the corresponding ethylene minima.

$[(PMe_3)_3RhC_2H_5]$ distorted tetrahedral (TH) singlet (s) and triplet (t)

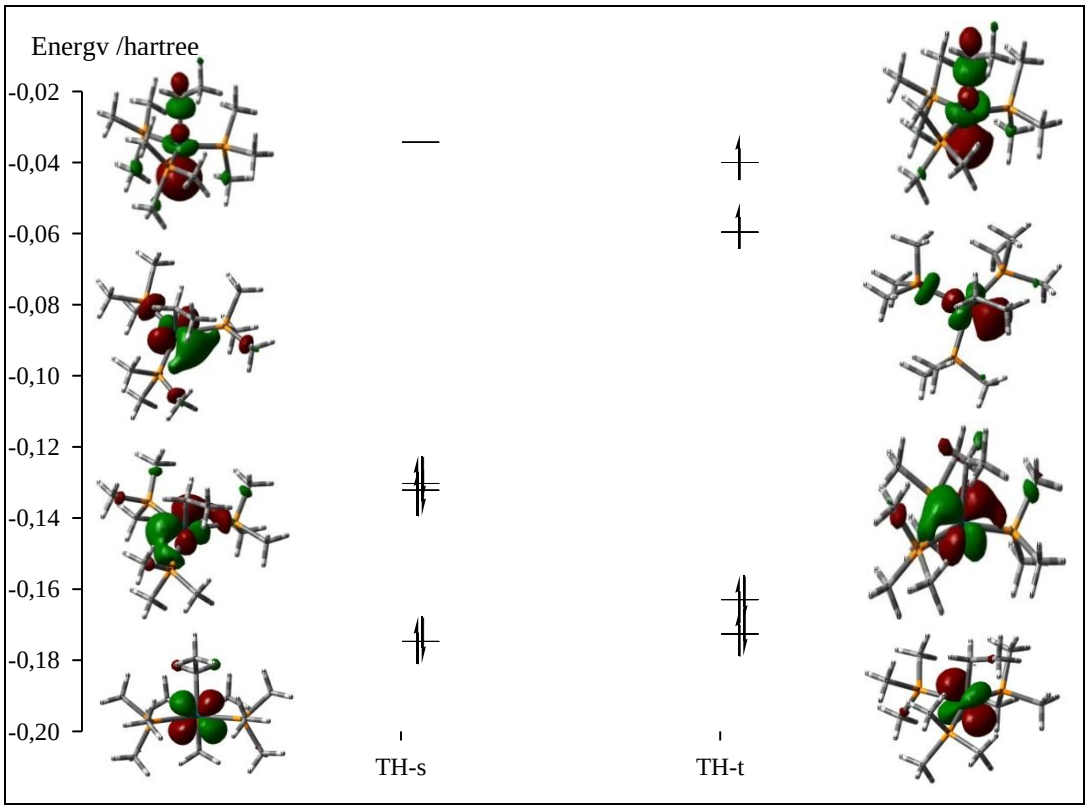

Figure 49: Electronic structure (frontier orbital region) of the singlet (images: LUMO, HOMO, HOMO-1 and HOMO-2) and triplet (images: HOMO, HOMO-1, HOMO-2 and HOMO-3) tetrahedral $[(PMe_3)_3RhC_2H_5]$ 16e-ethyl isomers. The energies shown for the triplet states were obtained at the ROB3LYP level.

The frontier orbital regions were looked over for the distorted tetrahedral (TH) singlet (s) and triplet (t) states found (figure 47). The calculations reveal that THs and THt have energies of 16.51 kcal/mol and 25.55 kcal/mol above the corresponding ethylene minima.

3.3.3 Summary

The structural parameters and the relative energies of the species involved in the hydrogen migration pathway from the ethylene complex to the 16e-ethyl complex were evaluated for $[L_3M(C_2H_4)H]$ (M= Co and L= PF_3, M= Rh and L= PF_3 or PMe_3).

The migratory insertion step of an H to the ethylene ligand results in the formation of the η^2-agostic structure via a transition state TS1. The transition state 1 corresponds to the insertion of an H into the metal-olefin bond. The calculated barriers for the hydrogen migratory insertion reaction are 6.6 (M= Co; L= PF_3), 10.4 (M= Rh; L= PF_3) and 23 kcal/mol (M= Rh; L= PMe_3). For both Co and Rh complexes, the relative energy barrier for the hydrogen migratory insertion reaction step increases in the order L=PF_3<PMe_3, with the electron donor strength of the ligand. This result suggests that the hydrogen migration insertion reaction step is critically influenced by the electronic character of the ligand L. The destabilization caused by the increasing electron donor strength of L is accompanied by higher energetic barriers in the same series. The reaction becomes kinetically less favourable down the triad.

For cobalt and rhodium the transition state is reactant-like with M-H1, M-C1 and C1-C2 bond distances close to that found in the terminal hydride complex.

The η^2-agostic minimum is stabilized by 2.8 kcal/mol in case of cobalt (Co), but is less stable by 0.4 kcal/mol for rhodium, concerning L= PF_3. The β-agostic interaction decreases toward the heavier element in the cobalt triad. The theoretical calculations provide quantitative support to the generally held notion that ethylene complexes are stabilized compared to the β-agostic alkyl isomers toward heavier congeners in a triad of late transition metals.

The second insertion reaction step corresponds to the the isomerisation of the η^2-agostic to a 16-electron ethyl structure via transition state TS2. The relative energy barrier for this reaction step is higher comparing to the first migratory step. For both Co and Rh complexes it increases toward the heavier congeners in a triad of late transition metals.

The isomerisation of the η^2-agostic isomer leads to a 16-electron ethyl structure higher in energy. For d^8 systems in a four coordinate environment, the square planar configuration is usually favoured. The geometry of the ethyl isomer distorts asymmetrically to give a geometry fairly balanced between square planar and tetrahedral extremes.

The energy of the unsaturated 16 electron ethyl complexes was evaluated for the singlet and the triplet states. The singlet state, a geometry fairly balanced between a square planar and a tetrahedral, is stabilized by increasing donor strength of L and for the transition metal Rh. The triplet state is stabilized accompanying the donor

strength of L and for the transition metal Co. The triplet state $[(PMe_3)_3Co(C_2H_5)]$ complex becomes the global minimum of the reaction when it converges to a tetrahedral geometry, the elected geometry for a d^8ML_4 triplet state. This result backs up the trend that electronically unsaturated, open shell configurations tend to be more common for lighter (3d) transition metals.

The α-agostic ethyl M= Co and L= PF_3 complex lies 10.5 kcal/mol above the β-agostic isomer. This difference can be taken as a row estimate (lower bound) for the strength of the β-agostic interaction, assuming that the α-agostic interaction is much weaker. This trend indicates further that the cobalt forms a stronger M-H1 bond than the heavier congeners, in line with the fact that the C2-H1 linkage involved in the M-H1 bond is stretched the most in the case of cobalt.

Chapter 4 Theoretical investigation of the energy of the olefin insertion/β-H-elimination in $[C_5R'_5M(L)(H)(C_2H_4)]^+$, M=Co, Rh, L=$PF_3$, R´=H, CH_3 complexes

Theoretical investigation of the energy of the olefin insertion/β-elimination in $[C_5R_5M(L)(H)(C_2H_4)]^+$, M=Co, Rh, L=$PF_3$, R=H, CH_3 complexes

4.1 Introduction

Catalytic ethylene homo- and copolymerization focused primarily on early transition metal catalysts (mainly based on titanium, zirconium and chromium). However, these catalysts are generally very oxophilic and do not stand for many functionalized olefins. This limitation has impelled significant interest in polymerisation catalysts drawn from late transition metals with assumed greater functional group tolerance. However, in addition to reduced polymerization activities, late metal catalysts generally exhibit a strong propensity to form oligomers, due to β-hydrogen elimination being competitive with chain growth. In recent years, these disadvantages have been beat by a new generation of late transition metal polymerization catalysts, which are capable of producing a wide range of products ranging from oligomers to high polymer and strictly linear to highly branched, giving access to polymers with novel and highly interesting properties [92d]. It is obvious that in these catalysts control of chain termination and chain transfer reactions is of paramount importance.

The isomerisation of a transition metal ethylene hydride to β-agostic and 16e-ethyl complexes via TS1 and TS2 has been the subject of extensive experimental and theoretical work [91]. In several experimental studies attempts were made to deduce the height of the insertion barrier from kinetic data resulting from the scrambling of the metal hydride atom in the ethylene hydride isomer with the olefinic hydrogens, which is often accessible by NMR methods, and kinetic data relevant to a number of scrambling processes are available in the literature [51-53]. Several computational studies of $[(C_5R_5)(L)M(H)(C_2H_4)]^+$ with M=Ir [91], Co [91, 72] and Rh [91, 72] have emerged.

Kinetic studies of the β-migratory insertion reactions of the hydride complexes $[C_5R'_5(L)Rh(C_2H_4)(H)]^+$ (R'=H, CH_3; L=$P(OMe)_3$, PMe_3) were published by

Brookhart *et al*. as well as for Co isomers [92d]. They report spectroscopic detection of an intermediate cobalt hydride ethylene complex during ethylene polymerization by a Co(III) catalyst together with a kinetic study which allows estimation of $\Delta G^{\ddagger}$ for the *β*-migratory insertion reaction. On the basis of low-temperature ^{1}H and ^{13}C NMR studies of the polymerization, the following mechanism was proposed (figure 50).

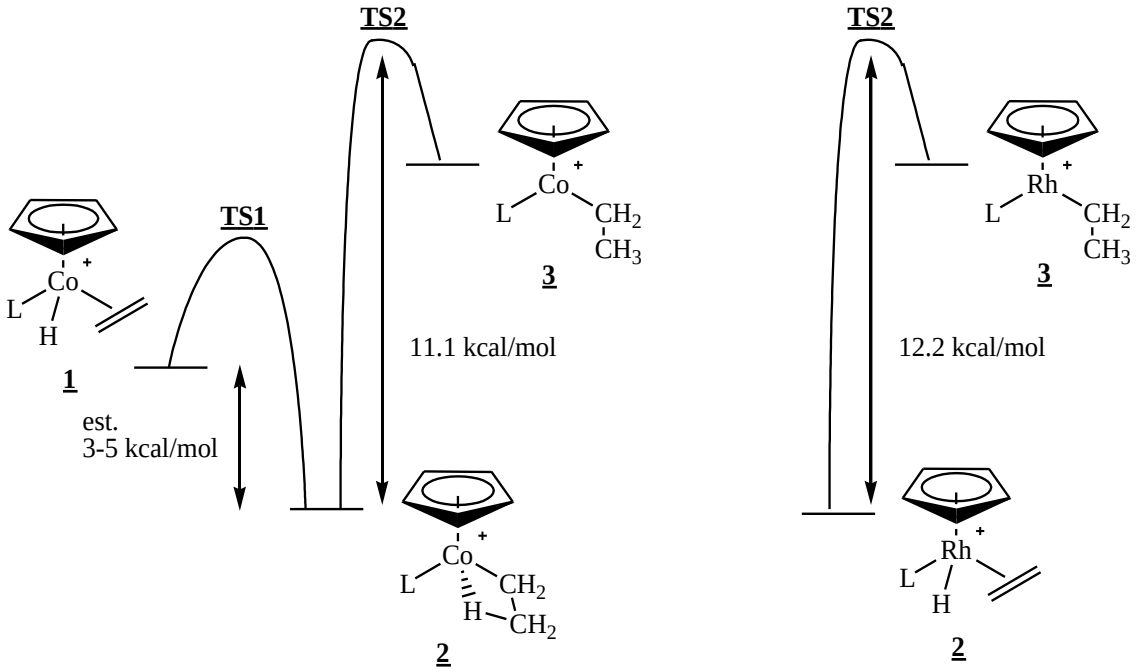

Figure 50: Energy diagram and mechanism illustrating the dynamic behaviour of the $[\eta^5\text{-}C_5H_5LM(C_2H_4)(H)]^+$ (M=Co, Rh; L=$P(OMe)_3$) β-migratory insertion reaction proposed by Brookhart et al. [51].

The *β*-agostic species (**2**) is the "resting state" of the catalyst and were the only species that could be detected spectroscopically. The hydride ethylene complexes, TS1, TS2, were proposed but unobserved intermediates. The variation of the dynamics and structure of these cobalt complexes with ligand and alkene structure is important not only for a fundamental understanding of the energetic relationships between the *β*-agostic species (**2**) and the classical ethylene hydride and 16-electron alkyl forms **1** and **3** but also in making connections between the properties of these *β*-agostic species and their characteristics as olefin polymerization catalysts. It is instructive to compare

the energy of activations for the β-migratory insertion of hydride rhodium analogues to the cobalt system. NMR techniques were used to measure the rates of migratory insertion for $[C_5R'_5(L)Rh(C_2H_4)(H)]^+$ (R'=H, CH_3; L=$P(OMe)_3$, PMe_3) [53]. The barriers to hydride migration are sensitive to Cp vs Cp* ligand substitution, increasing by ca. 3 kcal/mol in substituting Cp for Cp* in both the PMe_3 and $P(OMe)_3$ cases. The barriers are unaffected by the nature of the phosphine ligand (PMe_3 versus $P(OMe)_3$) in both the Cp and Cp* series. Comparison of the energetics of the rhodium systems with the corresponding cobalt systems , the barriers to hydride migration in $Cp^*Rh(P(OMe)_3)(H)(C_2H_4)^+$ (12.2 kcal/mol) and $Cp^*Co(P(OMe)_3)(H)(C_2H_4)^+$ (11.1 kcal/mol) appear unexpectedly close. However the stable form for cobalt hydride is agostic not terminal. To properly compare Rh and Co systems, the energy difference between the terminal cobalt hydride and the transition state for hydride migration must be used. Brookhart *et al*. [51] have been able to estimate the energy difference between the agostic complex and terminal hydride as 3-5 kcal/mol. The same authors observe that the energy difference between 1 and 2 is reduced further (<3 kcal/mol) in the case of rhodium and fairly dependent on the nature of the phosphine or olefin co-ligand. Thus the free energy difference can be estimated as 6-8 kcal/mol, which is significantly less than the corresponding 12.2 kcal/mol difference in the Rh system.

This barrier was also investigated in a theoretical work for a model of phosphines $[CpM(PH_3)(H)(C_2H_4)]^+$ (M=Co, Rh, Ir) [72], evaluated with a combination of several Methods/basis set. They concluded the energy barriers calculated in a B3LYP/SDD level agree well with experimental data, but these values are better representative for cobalt than for rhodium (table 22).

Table 22: Comparison between experimental kinetic studies and DFT MO calculations. The relative energies are given in kcal/mol.

Complex	Method	Basis	TS2-Ethylene	TS2-agostic
$Cp^*Co(P(OMe)_3)(H)(C_2H_4)^+$	Experiment[a]		6-8[b]	11.1
$CpCo(PH_3)(H)(C_2H_4)^+$	B3LYP	SDD	~5.89[c]	~13.35[c]
$CpCo(PH_3)(H)(C_2H_4)^+$	BP86	split2	14.58[c]	18.08[c]
$Cp^*Rh(P(OMe)_3)(H)(C_2H_4)^+$	Experiment[a]		12.2	
$Cp^*Rh(PMe_3)(H)(C_2H_4)^+$			12.1	
$CpRh(P(OMe)_3)(H)(C_2H_4)^+$			15.0	
$CpRh(PMe_3)(H)(C_2H_4)^+$			15.0	
$CpRh(PH_3)(H)(C_2H_4)^+$	B3LYP	SDD	10.69[c]	8.68[c]
$CpRh(PH_3)(H)(C_2H_4)^+$	BP86	split2	16.79[c]	11.48[c]

[a] from Ref. [53]

[b] estimated value from Ref. [51]

[c] from Ref. [72]

More recently, Bittner *et al.* decided to embark on a theoretical study of these exchange processes in eight model complexes $[(C_5R_5)(L)M(H)(C_2H_4)]^+$ (R = H, Me; L = $P(OMe)_3$, PMe_3; M = Co, Rh). Geometry and energy optimizations were performed at the BP86/6-31G**/SDD(Co, Rh) level of theory for all calculated species, and the relative energies were found to be in accordance with experimental observations. For Co complexes the *β*-agostic structure was identified as the global energy minimum, whereas for the rhodium complexes the ethylene hydride structure is invariably more stable. The insertion barriers TS1 are very low for the Co complexes and amount to typically 5-6 kcal/mol for the Rh complexes.

The aim of the present chapter is to demonstrate how effectively theory can guide and inform the experimentalist in the interpretation of kinetic data, e.g. from dynamic NMR measurements. It will touch the facet of a more electron accepting ligand L in the complex $[Cp(L)M(C_2H_4)(H)]^+$, M=Co, Rh, L=PF_3, influencing the energy of the olefin insertion/*β*-H elimination.

4.2 DFT MO calculations of the Olefin insertion/β-elimination reaction in $[C_5R'_5M(L)(H)(C_2H_4)]^+$, M=Co, Rh and L=$PF_3$ and R´=H, CH_3 complexes

4.2.1 Structural parameters of the stationary points

The calculated olefin hydride $[C_5R'_5(L)M(C_2H_4)(H)]^+$, R'=H, Me and M=Co, Rh and L=PF_3, complexes are depicted in figure 51. The relevant distances and angles are given in table 23. There are no significant differences in the geometrical parameters of the C_5H_5 and C_5Me_5 derivatives. Replacing Co for Rh, d(M-H1) and d(M-P) and d(M-C1/C2) increase ca. 7%, but d(C1-C2)=1.40Å in both Co and Rh ethylene minima. By replacing PF_3 with PH_3 d(M-C1/C2) decreases and d(C2-H1) increases.

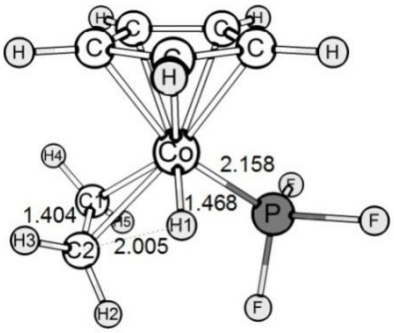

R´=H, M=Co

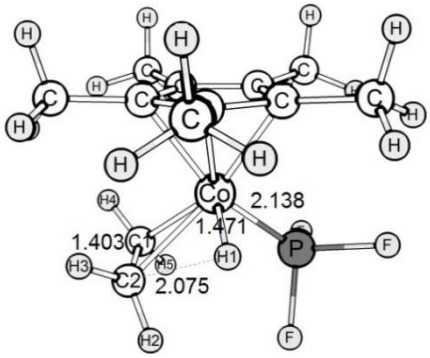

R´=CH_3, M=Co

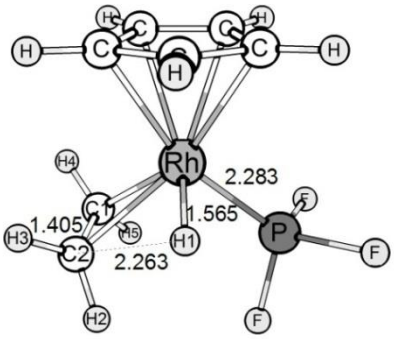

R´=H, M=Rh

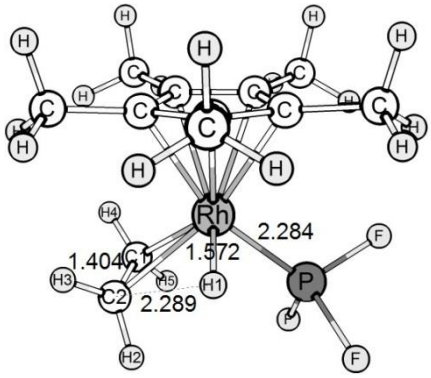

R´=Me, M=Rh

Figure 51: Optimized structures of the $[C_5R'_5(PF_3)M(C_2H_4)(H)]^+$ (R´= H, Me and M= Co, Rh) ethylene minima complexes (B3LYP/SDD).

Table 23: Relevant distances (Å) and angles (°) of the $[C_5R'_5(L)M(H)(C_2H_4)]^+$ (M=Co, Rh; L=PF_3,PH_3; R'=H, Me) ethylene minima complexes (B3LYP/SDD).

	Co	*L=PF_3*		*L=PH_3*[a]	*Rh*	*L=PF_3*		*L=PH_3*[a]
		R'=H	*R'=Me*	*R'=H*		*R'=H*	*R'=Me*	*R'=H*
d(M-C2)		2.170	2.157	2.13		2.288	2.289	2.25
d(C2-H1)		2.005	2.075	2.08		2.263	2.289	2.31
d(M-H1)		1.468	1.471	1.46		1.565	1.572	1.56
d(C1-C2)		1.404	1.403	1.40		1.405	1.404	1.41
α(M-C1-C2)		72.17	71.51	70.0		72.15	72.32	72.00
β(H-M-C2)		63.48	66.70	67.0		69.05	69.93	72.00

[a] from ref. [72]

Views of the *β*-agostic interaction are presented in figure 52.

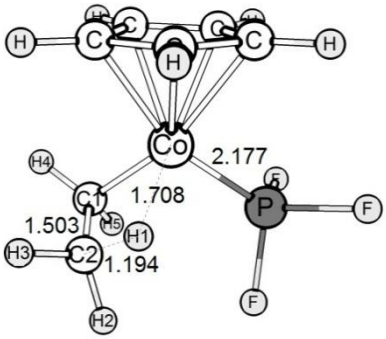

R´=H, M=Co

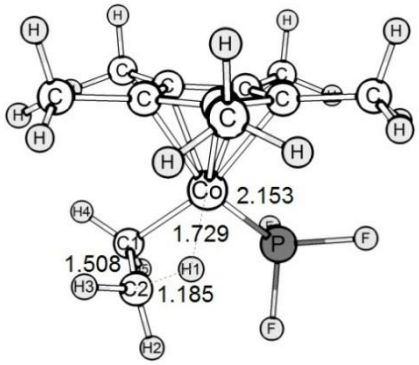

R´=Me, M=Co

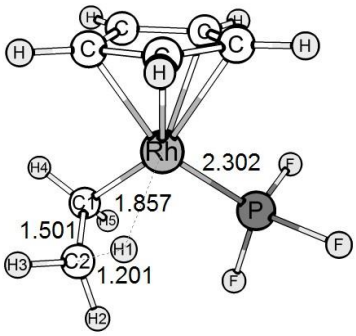

R´=H, M=Rh

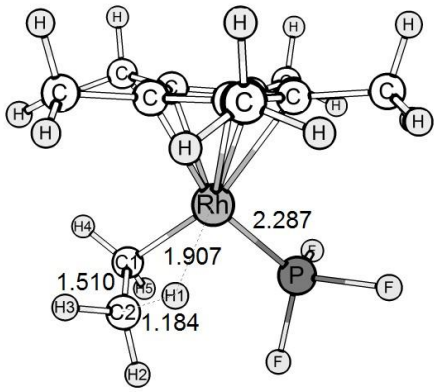

R´=Me, M=Rh

Figure 52: Optimized structures of the $[C_5R'_5(PF_3)M(C_2H_4)(H)]^+$ (R´=H, Me and M=Co, Rh) β-agostic minima (B3LYP/SDD).

The *β*-agostic interaction for the three-center two-electron M···H-C bond in the η^2-agostic ethyl products is marked visibly by elongated C-H distances of 1.19Å and 1.20Å, for Co and Rh respectively, and with the presence of partially stretched C-C double bonds with distances of 1.50Å (Co and Rh). The d(M-H1) and d(C2-H1) geometrical parameters alter by replacing C_5H_5 with C_5Me_5, d(M-H1) becomes longer and d(C2-H1) decreases its size (see table 24). The M-C1 distance is the shortest for L=PH_3.

Table 24: Relevant distances [Å] and angles [°] of $[C_5R'_5(L)M(H)(C_2H_4)]^+$ (M=Co, Rh and L=PF_3, PH_3 [a], R=H, Me) β-agostic minima.

	Co	*L=PF_3*		*L=PH_3* [a]	*Rh*	*L=PF_3*		*L=PH_3* [a]
		R'=H	*R'=Me*	*R'=H*		*R'=H*	*R'=Me*	*R'=H*
d(M-C2)		2.181	2.196	1.95		2.360	2.391	2.09
d(C2-H1)		1.194	1.185	1.18		1.201	1.184	1.19
d(M-H1)		1.708	1.729	1.73		1.857	1.907	1.87
d(C1-C2)		1.503	1.508	1.51		1.501	1.510	1.51
α(M-C1-C2)		76.51	77.10	77.0		79.71	81.04	80.00
β(H-M-C2)		32.99	32.45	33.0		30.21	29.31	30.00

[a] from ref. [72]

Views of the 16-electron ethyl are presented in figure 53.

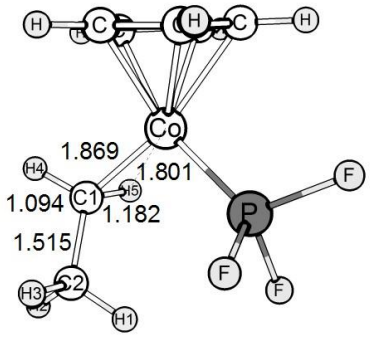

R´=H, M=Co

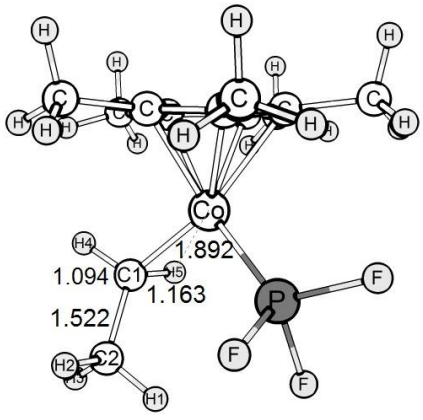

R´=Me, M=Co

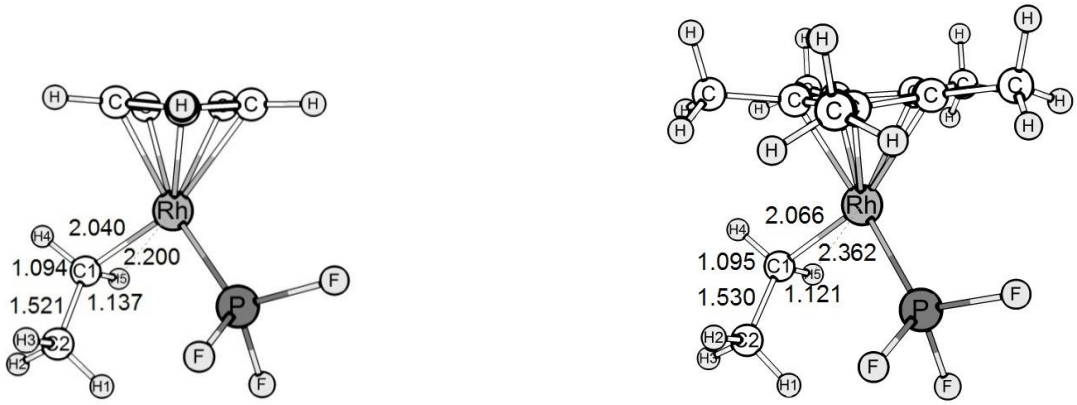

R´=H, M=Rh R´=Me, M=Rh

Figure 53: Optimized structures of the $[C_5R'_5(PF_3)M(C_2H_4)(H)]^+$ (R´= H, Me and M= Co, Rh) 16e-ethyl minima (B3LYP/SDD).

A close inspection of the geometric data in table 25 reveals an α-agostic C1-H5···Co interaction for the Co complex. However, an α-agostic interaction of the η^1-ethyl is not present in the rhodium analogs. This finding was confirmed by additional calculations with different methods, B3LYP and BP86, and basis sets, SDD and split.

The α-agostic interaction is indicated by a stretching of the d(C1-H5) by 8.26% for Co. For $[C_5R'_5(PF_3)Rh(H)(C_2H_4)]^+$, the d(C1-H5) stretches ca. 3.9 and 2.4%, for R'=H and Me respectively.

Table 25: Relevant distances [Å] and angles [°] of $[C_5R'_5(L)M(H)(C_2H_4)]^+$ (M=Co, Rh; L=PF_3, PH_3; R'=H, Me) 16e-ethyl minima.

	L=PF_3		*L=PH_3[a]*	*Rh*	*L=PF_3*		*L=PH_3[a]*
	R'=H	*R'=Me*	*R'=H*		*R'=H*	*R'=Me*	*R'=H*
d(M-C1)	1.869	1.886	1.88		2.040	2.066	2.05
d(M-H5)	1.801	1.892	-[c]		2.200	2.362	-[b]
d(C1-H4/5)	1.093, 1.182	1.094, 1.163	-[c]		1.094, 1.137	1.095, 1.121	-[b]
d(C2-H1/2/3)	1.099, 1.094, 1.101	1.095, 1.098, 1.100	1.10		1.096, 1.097, 1.101	1.097, 1.097, 1.100	1.10
d(C1-C2)	1.515	1.522	1.52		1.521	1.530	1.53
α(M-C1-C2)	131.94	132.39	130.0		127.02	125.26	125.00

[a] from ref. [72]

[b] not available in ref. [72]

4.2.2 Kinetics

The energy profile of the olefin insertion/*β*-elimination reaction for the $[(\eta^5\text{-}C_5H_5)M(PF_3)(H)(C_2H_4)]^+$, (M=Co, Rh) is presented und discussed next. The hydride *β*-migratory insertion process in $[(\eta^5\text{-}C_5Me_5)M(PF_3)(H)(C_2H_4)]^+$, (M=Co, Rh) have been studied. The calculations of the transition states, TS1 and TS2, were not successful and the energy profile for the reaction could not be built for this complex.

The reaction pathway of the olefin insertion/migration runs as described in figure 15 (Chapter 2). The hydride migratory insertion reaction to the olefin isomer leads to a structure with a pronounced M···H-C elongation, the η^2-agostic. These two isomers are connected through a transition state (TS1). The isomerisation of the η^2-agostic structure gives rise to the 16-electron ethyl complex, through TS2. The transition states are calculated through optimizations of the geometries of the maxima located in the reaction pathway.

The energy of the stationary- and the tied saddle points are then depicted graphically and evaluated.

$[CpCo(PF_3)(H)(C_2H_4)]^+$

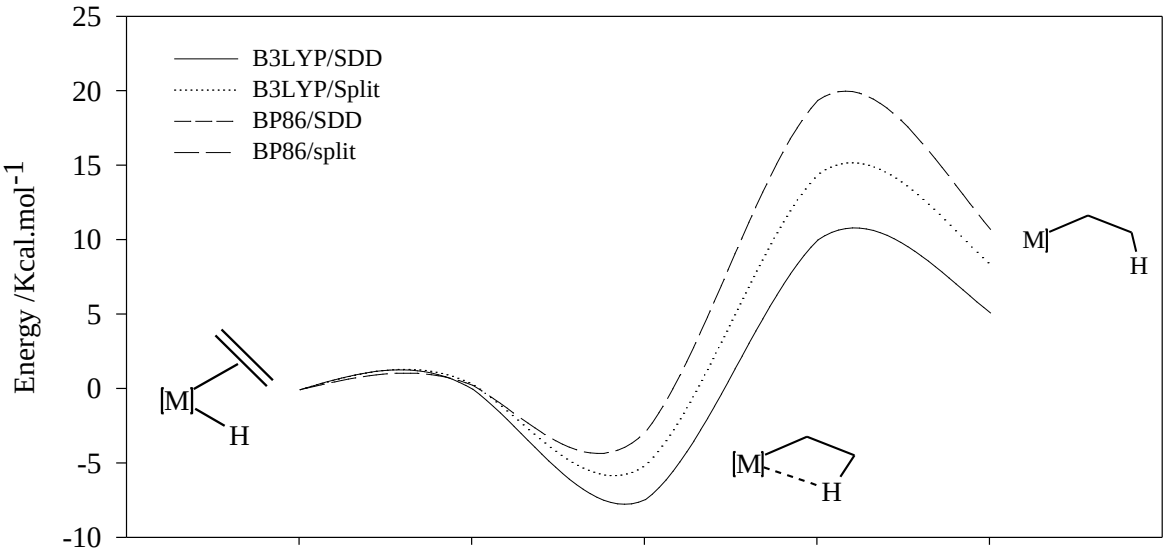

Figure 54: Energy of the stationary points of $[CpCo(PF_3)(H)(C_2H_4)]^+$, estimated with several Methods/basis set (in kcal.mol^{-1}). BP86/SDD is not depicted in the energy diagram (see table 26).

The energy of the stationary and saddle points, TS1 and TS2, is depicted graphically in figure 54. The energy profile of the reaction clearly indicates the *β*-agostic isomer to be the global minimum, being 7.39 kcal/mol more stable than the corresponding ethylene complex.

The relative energy barrier $\Delta E_{ins}^{\neq}$ for the migratory insertion reaction lies 0.03 kcal/mol above the ethylene minimum (B3LYP/SDD). The relative energy barrier of insertion $\Delta E_{ins}^{\neq}$ is +0.34 kcal/mol for B3LYP/split and 0.28 kcal/mol for BP86/split (see table 26). For the $[CpCo(PH_3)(H)(C_2H_4)]^+$ [72] this barrier was estimated in 0.37 kcal/mol (B3LYP/SDD). Calculations carried out by Ziegler *et al.* show for the same complex $[CpCo(PH_3)(H)(C_2H_4)]^+$ an electronic barrier of 0.3 kcal/mol (ADF) [91].

Table 26: Relative energy (in kcal/mol) of the stationary points of $[CpCo(PF_3)(H)(C_2H_4)]^+$ complex, calculated with different methods and basis sets.

	B3LYP/SDD	*B3LYP/Split*	*BP86/SDD*	*BP86/split*
Ethylene	0	0	[a]	0
TS1	0.03	0.34		0.28
β-agostic	-7.39	-5.08	0	-2.85
TS2	10.06	14.47	valor estim	19.43
16e-ethyl	5.14	8.35	13.42	10.76

[a] not obtained

The *β*-agostic structure is the global minimum of the hydride insertion reaction, being -7.39 kcal/mol relative to the ethylene isomer (B3LYP/SDD). This result is backed up by all Methods/basis set, being -5.08 kcal/mol for B3LYP/split and -2.85 kcal/mol for BP86/split. For $[CpCo(PH_3)(H)(C_2H_4)]^+$ this structure is 7.46 kcal/mol (B3LYP/SDD) [72] and 3.4 kcal/mol (ADF) [91] more stable than the corresponding ethylene minima.

The transition states for the hydrogen migratory insertion were fully optimized. The optimized structure of TS1 was confirmed to have a single imaginary frequency.

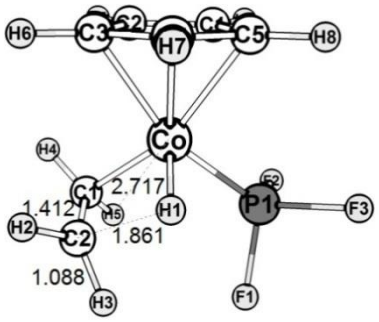

+0.03

Figure 55: Optimized structure and relative energy (kcal/mol) of the TS1 (B3LYP/SDD).

The transition state 1 corresponds to the migration/insertion of hydrogen to the olefin. TS1 is a reactant-like with M-H bond distance close to that found in the terminal hydride complex (see figure 46).

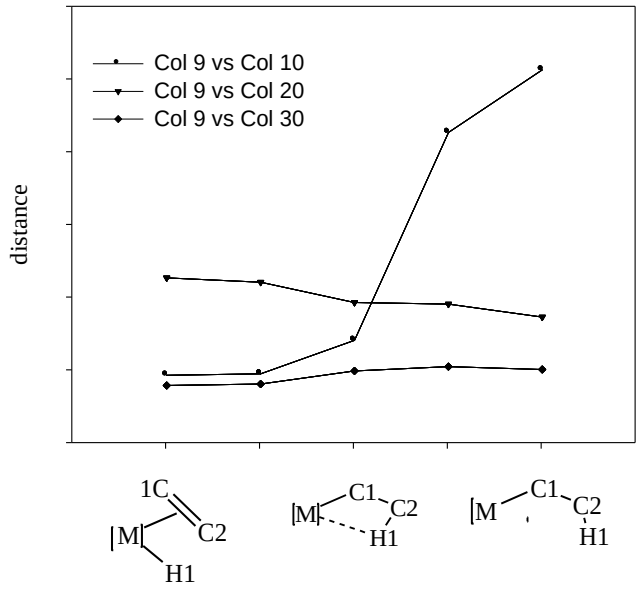

Figure 56: Variation of the coordinates of the stationary points of $[CpCo(PF_3)(H)(C_2H_4)]^+$ (d [Å]).

The reacting *β*-agostic isomer can rearrange to a 16-electron ethyl species, which is stabilized by an α-H agostic interaction. The activation energies (TS2-*β*-agostic) calculated for the cobalt complex with L=PF_3 are +17.45 for B3LYP/SDD, +19.55 for B3LYP/split and +22.28 kcal/mol for BP86/split methods and basis sets. The value found experimentally for the activation energy of the homologous complex $[Cp^*Co(P(OMe)_3)(H)(C_2H_4)]^+$ was +11.1 kcal/mol [58]. Besides the different electronic environment, these values are surprisingly different from the ones obtained experimentally. The activation energies (TS2-*β*-agostic) calculated for the homologous L=PH_3 are +8.68 kcal/mol for B3LYP/SDD and +11.48 kcal/mol for BP86/split2 [72]. These values lie in a closer range to the estimations obtained experimentally.

The unsaturated 16e-ethyl complexe is destabilized. The energy lies +5.14 kcal/mol (Co) above the corresponding ethylene minima (B3LYP/SDD).

$[CpRh(PF_3)(H)(C_2H_4)]^+$

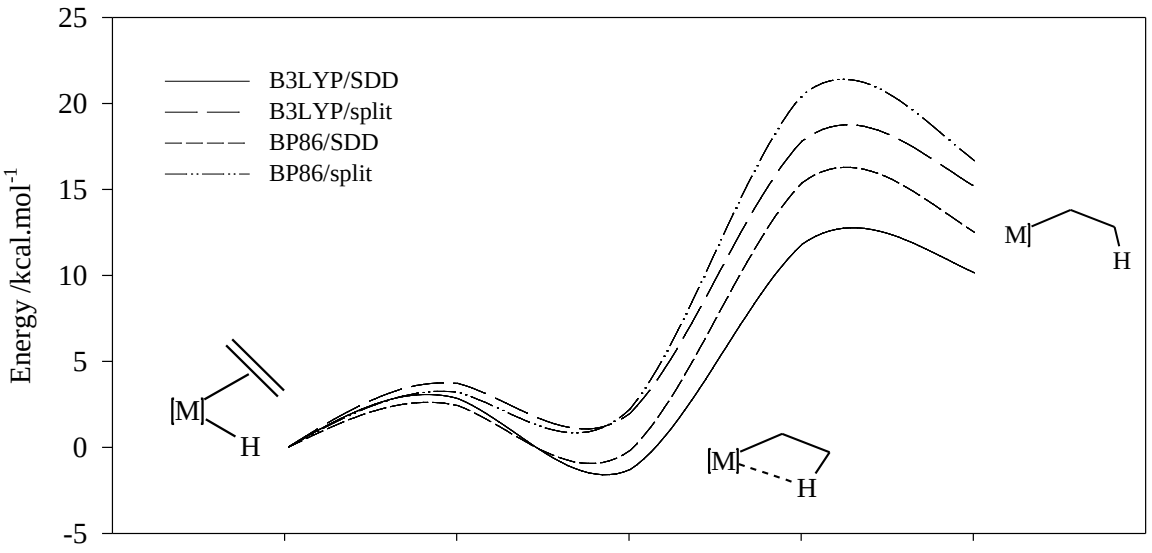

Figure 57: Energy of the stationary points of [η^5-$C_5H_5Rh(PF_3)(H)(C_2H_4)]^+$, estimated with several methods/basis set (in kcal.mol^{-1}).

The energy profile for the Rh complex is depicted graphically in figure 57. The global minimum corresponds to the *β*-agostic isomer, being -1.22 kcal/mol relative to the corresponding ethylene complex (B3LYP/SDD). The calculated energy for L=PH_3 is +0.50 kcal/mol (B3LYP/SDD) [72] and -1.0 kcal/mol (ADF) [91], relative to the corresponding ethylene isomer.

The relative energy barrier $\Delta E_{ins}^{\neq}$ for the migratory insertion reaction lays 2.91 kcal/mol above the ethylene minimum (B3LYP/SDD). The relative energy barrier of insertion $\Delta E_{ins}^{\neq}$ is +3.78 kcal/mol for B3LYP/split, +2.49 kcal/mol for BP86/SDD and 3.27 kcal/mol for BP86/split (see table 26). For the $[[\eta^5\text{-}C_5H_5Rh(PH_3)(H)(C_2H_4)]^+$ this barrier was estimated in +2.70 kcal/mol (ADF) [91]. Calculations carried out by Bittner *et al.* show for the same complex $[[\eta^5\text{-}C_5H_5Rh(PH_3)(H)(C_2H_4)]^+$ an electronic barrier of +4.70 kcal/mol (ADF) [72].

Table 27: Energy (in kcal/mol) of the stationary points of $[CpRh(PF_3)(H)(C_2H_4)]^+$ complex, calculated with different methods and basis sets.

	B3LYP/SDD	*B3LYP/Split*	*BP86/SDD*	*BP86/split*
Ethylene	0	0	0	0
TS1	2.91	3.78	2.49	3.27
β-agostic	-1.22	2.06	-0.11	2.31
TS2	11.89	17.88	15.46	20.54
16e-ethyl	10.22	15.24	12.57	16.73

TS1 is a reactant-like considering the M-H1 and C1-C2 distances do not alter much in this step of the reaction (figure 58).

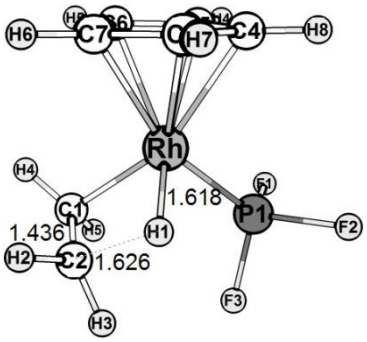

-1.22

Figure 58: Optimized structure and relative energy (kcal/mol) of the TS1 (B3LYP/SDD).

The TS1 is a reactant-like, taking into consideration that the M-H and C1-C2 distances preserve relative invariable in this step of the reaction (see figure 58 and 59).

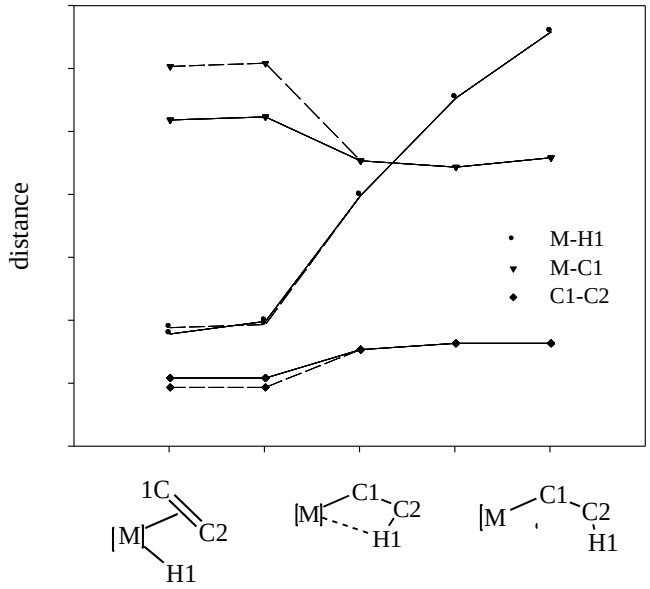

Figure 59: Variation of the coordinates of the stationary points of $[CpRh(PF_3)(H)(C_2H_4)]^+$ (d [Å]).

The *β*-agostic M···H-C isomer rearranges to an unsaturated ethyl species. The activation energies (TS2-Ethylene) calculated for the rhodium complex are +11.89 for B3LYP/SDD, +17.88 for B3LYP/split, +15.46 for BP86/SDD and +20.54 kcal/mol for BP86/split methods and basis sets. The energy barriers obtained fluctuate from the results obtained experimentally in a few kcal/mol. The estimates obtained with experimental values are +15.0 kcal/mol for L=PMe_3 and L=$P(OMe)_3$ [58]. Systems with different ligands η^5-C_5H_5 *vs.* η^5-C_5Me_5 and PMe_3/$P(OMe)_3$ *vs.* PF_3 are expected to differ in a few kcal/mol. For $[CpRh(PH_3)(H)(C_2H_4)]^+$ the activation barrier lies +10.69 kcal/mol above the corresponding ethylene isomer (B3LYP/SDD) [72].

The unsaturated 16e-ethyl complexe is destabilized. The energy lays +10.22 kcal/mol (Rh) above the corresponding ethylene minima (B3LYP/SDD).

4.2.3 Summary

The migratory insertion reaction of the hydride to the olefin complexes $[CpM(PF_3)(C_2H_4)(H)]^+$, M=Co and Rh, have electronic reaction barriers of 0.03 (Co) and 2.91 kcal/mol (Rh), respectively (B3LYP/SDD). For the hydride migration, the transition states are close to the hydrido olefin systems.

The calculations reveal that the *β*-agostic ethyl product is more stable than the hydrido olefin reactant by 7.39 and 1.22 kcal/mol (B3LYP/SDD) for cobalt and rhodium, respectively. Brookhart *et al*. [57] found experimentally in $Cp^*M(P(OMe)_3)(H)(C_2H_4)^+$ that the *β*-agostic ethyl product is favoured over the hydrido olefin reactant by 3-5 kcal/mol in the case of cobalt. The estimates obtained by the B3LYP/split (-5.08 kcal/mol) and BP86/split (-2.85 kcal/mol) are in good agreement with the experimental value. The same authors observe that this energy difference is reduced further (<3 kcal/mol) in the case of rhodium. The values obtained in this theoretical work lay -1.22 kcal/mol for B3LYP/SDD, +2.06 kcal/mol for B3LYP/split, -0.11 kcal/mol for BP86/SDD and +2.31 kcal/mol for BP86/split.

Data reported by Werner and Feser [68] suggest that second row rhodium compound is ethylene-hydride. Only the cationic cobalt complex is *β*-agostic. This series supports the previously made observations and further suggestions that first-row systems will favour *β*-agostic structures relative to their second and third-row analogues. Theoretical calculations made by Bittner *et al.* [72] by way of a model for phosphines, L= PH_3, $[CpM(L)(C_2H_4)(H)]^+$ (M=Co, Rh) divulge a 7.46 kcal/mol stabilization for Co whereas +0,50 kcal/mol for rhodium (B3LYP/SDD) and 12.19 kcal/mol for iridium [66]. These results provide quantitative support for the generally notion that hydrido olefin complexes are stabilized compared to the *β*-agostic alkyl isomers toward the heavier congeners in a triad of late transition metals. The strength of this interaction decreases down the cobalt triad.

The unsaturated 16e-ethyl complexes are destabilized. Their energy lay +5.14 kcal/mol (Co) and +10.22 kcal/mol (Rh) above the corresponding ethylene minima (B3LYP/SDD). The existence α-agostic C1-H5···Co interaction for the Co complex is backed up by key parameters. An α-agostic interaction of the η^1-ethyl is not present in the rhodium analogs.

Chapter 5 Theoretical Investigation of the energy of the Sila-olefin insertion/β-H elimination. Silyl and Silylene ligands – DFT calculations

Theoretical investigation of the energy of the Sila-olefin insertion/β-H-elimination. Silyl and Silylene ligands – DFT calculations

5.1 Introduction

Migratory insertion/*β*-H elimination involving olefins is a very important and well-studied topic. *β*-H elimination from silyl ligands is a more unusual but known reaction. Transition metal-olefin complexes have been the focus of intense research attention in the last years. This interest is largely derived from the fact that transition metal-olefin complexes take part in a wide range of polymerization transformations.

An increased attention in silenes has been encouraged by synthesis of isolable examples that are stabilized by steric protection of the Si=C double bond [115, 116].

It seemed reasonable to believe that stable transition-metal silene complexes $L_nM(\eta^2\text{-}R_2CSiR'_2)$ (figure 60) could be isolated and studied, given the well known capability of transition metals to stabilize reactive species (e.g., carbenes, carbines, cyclobutadienes, ketenes, and thiocarbonyl) by ligation.

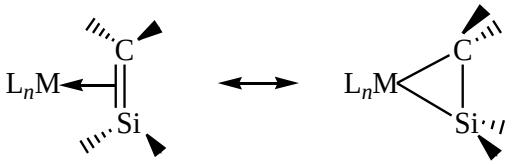

Figure 60: Transition-metal silene complexes $L_nM(\eta^2\text{-}R_2CSiR'_2)$.

Silene complexes have been suggested as intermediates in various metal-mediated rearrangements of organosilicon ligands [117]. Intermediates created by the *β*-hydrogen transfer reaction illustrated in figure 61 were initially proposed by Pannell [117a] and have been detected spectroscopically at low temperature by Wrighton [118].

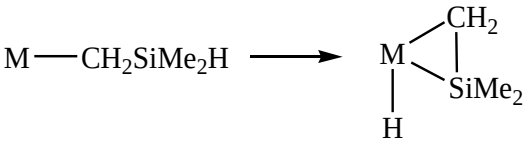

Figure 61: Sila-olefin intermediates generated by the β-hydrogen transfer reaction.

An experimental approach reported by Tilley *et al.* [119] on the sila-olefin insertion/*β*-H elimination involves the use of the hydrogen-transfer process of the figure 62 and stabilization of the more oxidized metal center with a noble metal (ruthenium) and electron-donating ligands (Cp* and trialkylphosphines).

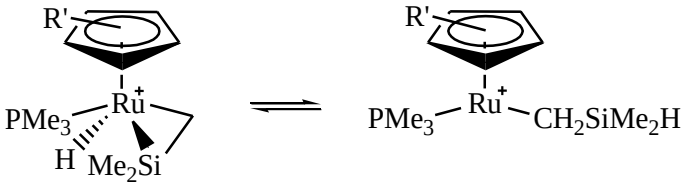

Figure 62: Transition-metal η^2-silene (η^5-C_5Me_5)(PR_3)Ru(H)(η^2-CH_2SiMe_2) (R=i-Pr, Cy) complex [119].

This compound is thermally unstable and decomposes in solution. More stable silene complexes are obtained from diphenylsilylmethyl group, -CH_2SiPh_2H. Both thermally stable η^2-silene complexes, Cp*(PR_3)Ru(H)(η^2-CH_2SiPh_2) were characterized by NMR and infrared spectroscopy. These reactions appear to proceed via intermediate 16-electron ruthenium alkyls Cp*(PR_3)Ru(η^2-CH_2SiPh_2H), which go through *β*-elimination to afford the observed silene complexes. Compared to -CH_2SiMe_2H, complex -CH_2SiPh_2H reveals increased thermal stability, decomposing in solution at room temperature over several days.

The occurrence of substituent metathesis, or redistribution, such as 1,2-migration reaction (figure 63), has been detected for many main-group and transition-metal systems [120]. Redistribution at silicon centers take place more easily than in carbon, yet not as readily as in tin, and can be catalyzed by acids, bases, and metals [121].

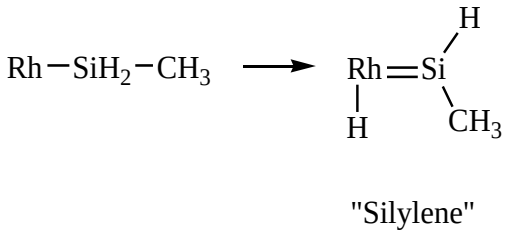

Figure 63: 1,2-Migration reaction.

Silicon redistribution reactions are utilized industrially to convert unwanted byproducts from the synthesis of functionalized silanes into useful materials [120]. The transition-metal-catalyzed pathway is believed to involve 1,2-shifts of groups between the metal and silicon and 1,3-shifts between metal –bound silicon centers. Evidence for intramolecular 1,3-shifts between silicon atoms [122-124], and for an intermolecular exchange between transition-metal silylene and silyl complexes, has been documented [125]. It was recently reported that a silylene complex can be accessed by the 1,2-migration of hydrogen from silicon to platinum [126].

Although a number of base-stabilized silylene complexes are known [127-129], base-free silylene complexes are rare [126, 129-133].

Tilley *et al.* reported in preliminary form the isolation of a rare iridium-silylene complex kinetically stabilized by incorporation of bulky groups on the silicon center [134] (figure 64).

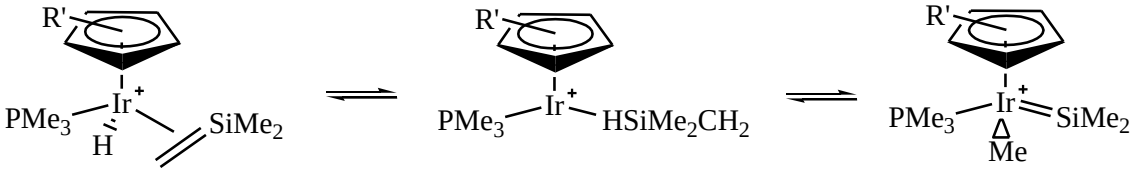

Figure 64: Reactions of Cp(PMe$_3$)Ir(H)(η^2-Me$_2$SiCH$_2$)$^+$. Role of base-free silylene complexes in rearrangements of the resulting silicon-based ligands.*

Although H_2SiMes_2 underwent Si-H activation and migration of a substituent from silicon to iridium, their inability to access similar silylene complexes from anion

metathesis reactions of Cp*(PMe_3)Ir($SiPh_2OTf$)(Ph) and Cp*(PMe_3)Ir($SiPh_2OTf$)(Me) [135] made them suspicious of the generalization that silylene complexes were intermediates in reactions of less hindered silanes. After exploring the reaction scope of Cp*(PMe_3)Ir(Me)OTf with silanes, it is apparent that a rich variety of migration types are possible within this system. These include 1,3-migration in the case of -$(SiMe_3)_3$ and silane redistribution in the case of $HSi(OEt)_3$. Additionally, two reaction pathways that appear to be of comparable in energy for 16-electron silyliridium (III) complexes are metalation to give Ir(V) products and 1,2-migration to afford silylene complexes. Base-free silylene complexes have been generated and characterized, and their data support a 1,2-migration mechanism that proceeds via these species as reactive intermediates [136]. Slow hydride migration to produce a silylene complex from either Cp*(PMe_3)Ir(Me)OTf or Cp*(PMe_3)Ir(Me)(CH_2Cl_2)][$B(C_4F_5)_4$] is observed for large substituents on silicon . However, production of the sterically less crowded complex Cp*(PMe_3)Ir($SiPh_2$)(H)][$B(C_4F_5)_4$] is extremely rapid upon reaction of Cp*(PMe_3)Ir(Me)(CH_2Cl_2)][$B(C_4F_5)_4$] with H_2SiPh_2. This argues for the intermediacy of a three-coordinate silicon species.

Known factors on olefin insertion/β-H elimination have already been reported in the literature and investigated in this work (see figure 65). Important predictions stated on ethylene complexes might assist the investigation of the „sila-olefin" insertion/β-H elimination. This search suggests an increase of the barrier of migratory insertion with increasing electron richness of the metal center, which destabilizes species with β-agostic metal-H-C interactions. It is proposed that there may even be cases where a β-agostic structure is not an intermediate. The insertion barrier is higher for rhodium- than for cobalt complexes. It confirms the evidence of increasing $\Delta E_{ins}^{\ddagger}$ down a group in the periodic table.

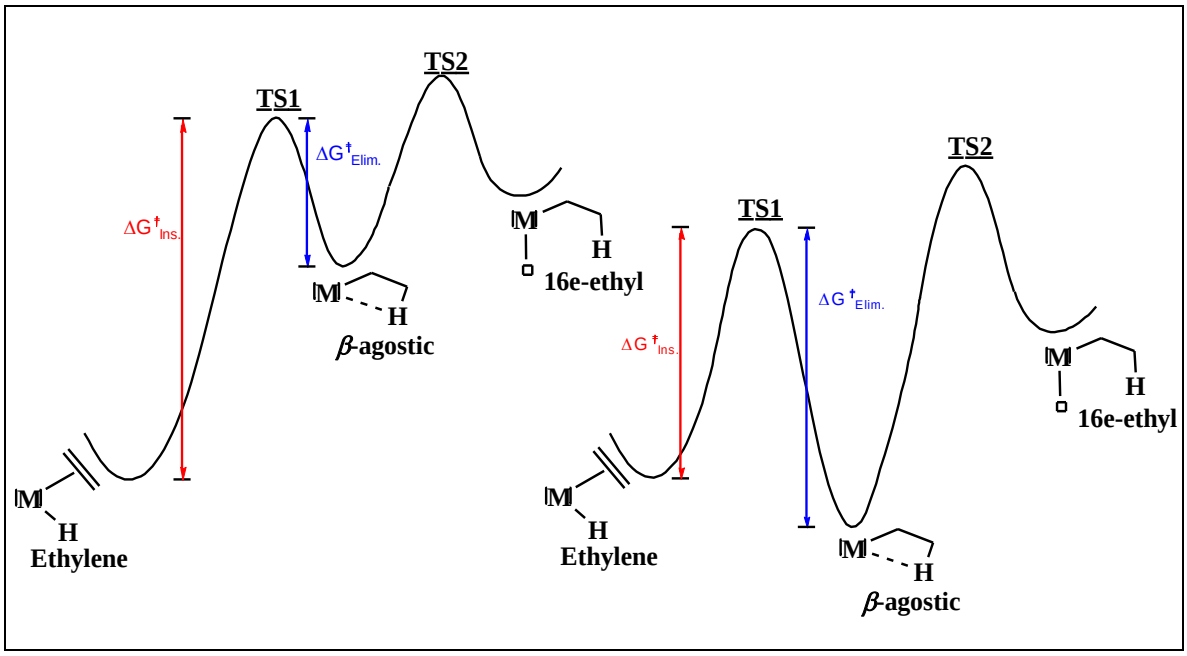

Figure 65: A- Ethylene hydride is the ground state; B - β-agostic ethyl is the ground state.

The model examined in chapters 3 and 4 for the olefin insertion/*β*-H elimination reaction is depicted in figure 66. The study aimed at finding local minima and transition states to delineate an energy profile for the reaction.

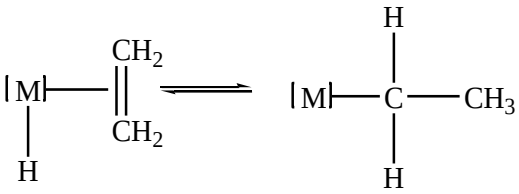

Figure 66: Examined model of the olefin insertion/β-H elimination, reaction with M-ethyl (Chapters 3 and 4).

The investigation of the olefin insertion/*β*-H elimination reaction in chapter 4 involves the rhodium $[(C_5R'_5)M(L)H(CH_2{=}CH_2)]^+$ (R'=H, CH_3) ethylene systems (see figure 67).

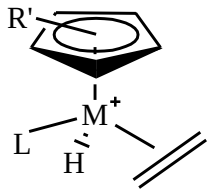

Figure 67: The olefin insertion/β-H-elimination of $[(C_5R'_5)M(L)H(CH_2=CH_2)]^+$ (R', R=H, CH_3 and M=Co, Rh and L=PF_3) ethylene systems studied (see Chapter 4).

The reaction mechanism proposed for the olefin insertion/*β*-elimination reaction is depicted below (figure 68).

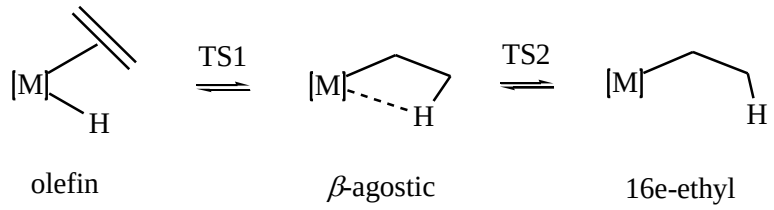

Figure 68: Reaction profile for the olefin insertion/β-elimination reaction.

The purpose of the work developed in this chapter is the search for a trend in the olefin insertion/*β*-elimination reaction by replacing Si by C in the olefin ligand. The $[C_5R'_5Rh(L)(SiR_2CH_2)(H)]^+$ complex has a less complicated geometry than $L_3MH(C_2H_4)$, and can easily be adressed by theoretical and experimental investigations that have been carried out for Cp-systems. The selection of a range of three ligands L and $C_5R'_5$ (R'=H, Me) helps to outline the impact of steric and electronic properties of the reaction.

The model of the "sila-olefin" insertion/*β*-H elimination reaction that is going to be examined in this chapter is depicted in figure 69.

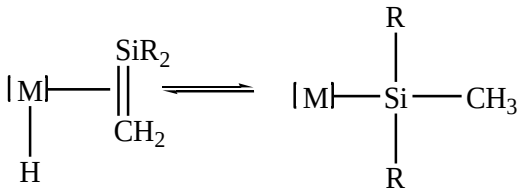

Figure 69: Examined model of the sila-olefin insertion/β-H elimination reaction.

Two reaction channels are going to be created starting from complex I and complex II rhodium $[(C_5R'_5)Rh(L)H(SiR_2{=}CH_2)]^+$ R', R=H, Me; L= PH_3, PF_3, PMe_3 (see figure 70).

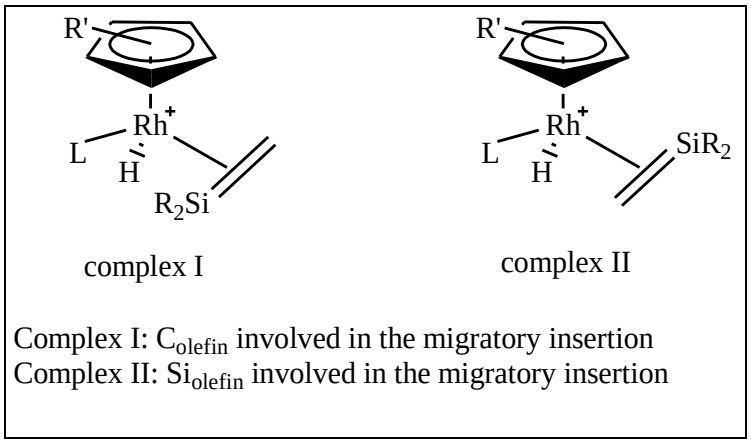

Figure 70: Complexes $[C_5R'_5Rh(L)(SiR_2{=}CH_2)(H)]^+$ (R', R=H, Me and L=PH_3, PF_3, PMe_3) analysed in this study.

Two different structures differing in the orientation of Si relative to the hydrogen atom involved in the migration are expected. These structures will have either the C atom (complex I) or the Si atom of the "sila-olefin" group (complex II) involved on the hydrogen migration. Consequently, the reaction path of the sila-olefin migratory insertion leads to a "silyl" or an "ethyl" complex (figure 71).

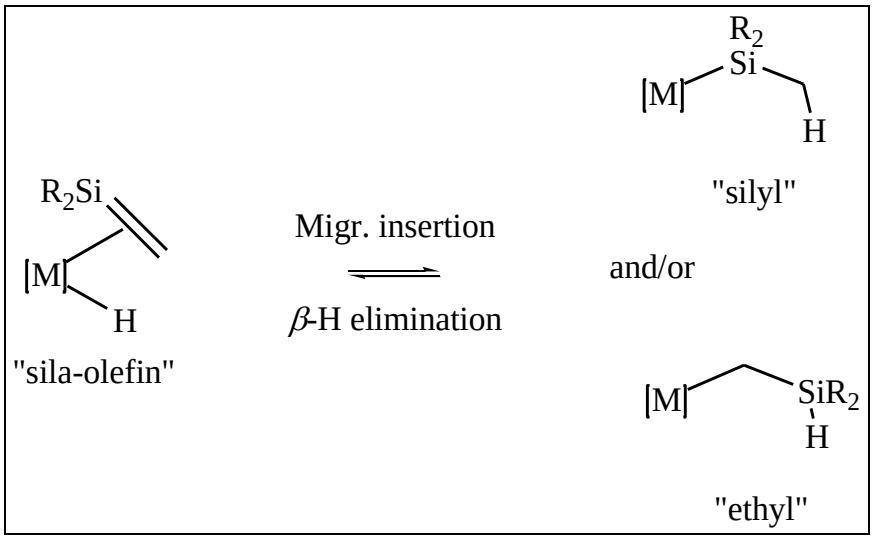

Figure 71: Sila-olefin insertion for rhodium [$C_5R'_5Rh(L)(SiR_2CH_2)(H)]^+$, R', R=H, Me and L=$PH_3$, PF_3, PMe_3 complexes.

Beginning with the sila-olefin "starting structures" and the *β*-agostic optimized geometries, the two angles chosen in the previous chapters as reaction coordinates to localize saddle points and possible intermediates are going to be employed (see figure 15, Chapter 2).

After locating both "sila-olefin" minima (complex I and II), a "scan" get going from the sila-olefin-"starting geometries", throughout delineated coordinates (figure 15, Chapter 2), gave rise to an energy profile capable of locating two more minima and the transition states in-between, for all $[C_5R'_5Rh(L)(SiR_2CH_2)(H)]+$, R', R=H, Me and L=$PH_3$, PF_3, PMe_3 complexes (figure 72).

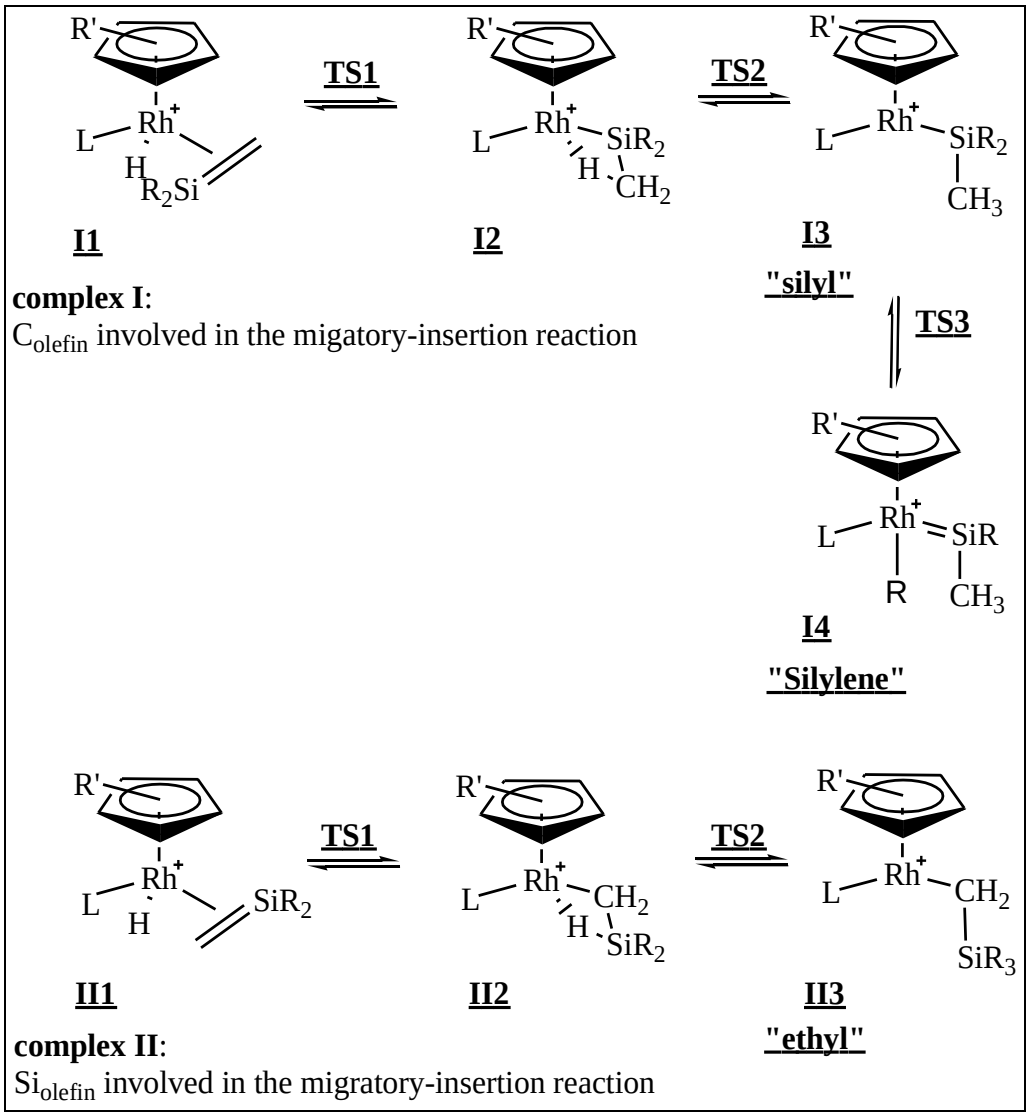

Figure 72: Reaction path of the "sila-olefin" insertion/β-H-elimination with both "sila-olefin"-"starting structures", complex I- (above) and complex II-isomer (below), intermediates and transition states.

It is established that experimental quantities, such as bond lengths or dipole moments, are reproduced better if d-functions are included in the Si basis set [104]. However, the same is also true for the analogous carbon compounds. To maintain consistency, DFT calculations will be further carried out with the B3LYP method and the SDD basis set. This method/basis set proved to be reliable for similar systems by means of calculations accomplished in chapter 4.

5.2 Structural parameters of the stationary points

For the $[C_5R'_5Rh(L)(SiR_2{=}CH_2)(H)]^+$ complexes I and II studied in this chapter (see figure 72), attention will be given to the electronic and steric properties of the ligands implicated in this study (R´, R=H, Me and L=PH_3, PF_3, PMe_3) and their influence on the structural parameters and geometries of the compounds involved. The η^5-$C_5R'_5$ and R`=Me exert higher steric and electron-donating influence on the metal, as compared to R=H. The steric and electron-donating properties of the ligands L increase as follows $PF_3$<$PH_3$<$PMe_3$. For the $[C_5R'_5Rh(L)(CH_2{=}CH_2)(H)]^+$ analogous studied in chapter 4, $\eta^5$-$C_5R'_5$ (R`=H, Me) plays a more determinant role in the structural parameters of the stationary points and transition states than the ligand L.

5.2.1 Complex I (C_{olefin} involved in the migratory-insertion reaction)

Complex I is the first complex elected as a "sila-olefin" "starting structures" (I1). For complex I1 it is the C of the "sila-olefin" $SiR_2{=}CH_2$ ligand that is going to be involved in the "sila-olefin" insertion/*β*-H elimination reaction, in contrast to Complex II, in which the Si atom is involved in the hydrogen migration. Along with the reaction coordinates described in figure 15 (Technical Details, Chapter 2), the hydrogen migrates to C of the "sila-olefin" $SiR_2{=}CH_2$ ligand in the first step of the reaction pathway of the "sila-olefin" insertion (see figure 72). The reaction coordinate α(H1-M-C2) angle decreases and H1 stepwise migrates to the C atom of the "sila-olefin" ligand giving rise to the I2 "silyl-agostic" ligand. Figure 73 depicts the "sila-olefin" geometries of complex I1.

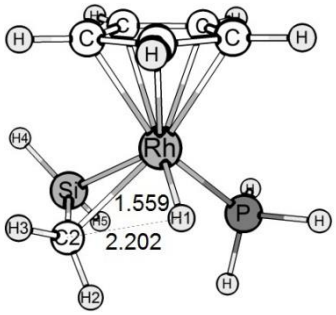

R’, R=H; L=PH_3

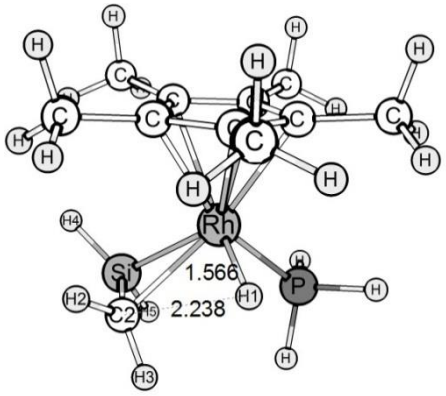

R’=Me; R=H; L=PH_3

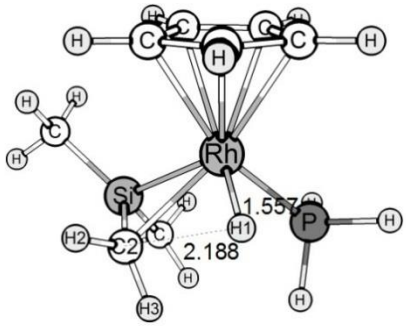

R’=H; R=Me; L=PH_3

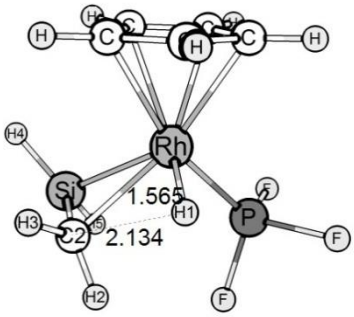

R’, R=H; L=PF_3

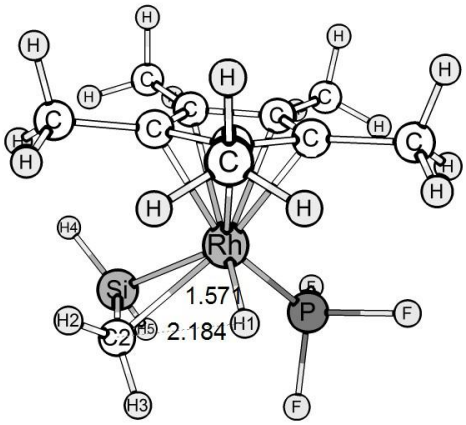

R’=Me; R=H; L=PF_3

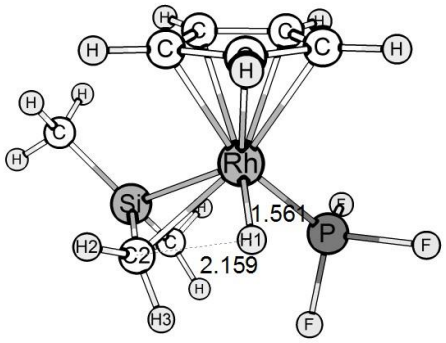

R’=H; R=Me; L=PF_3

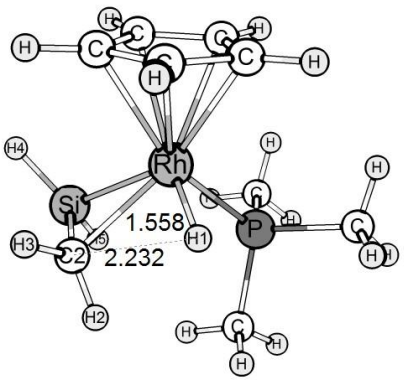

R', R=H; L=PMe_3

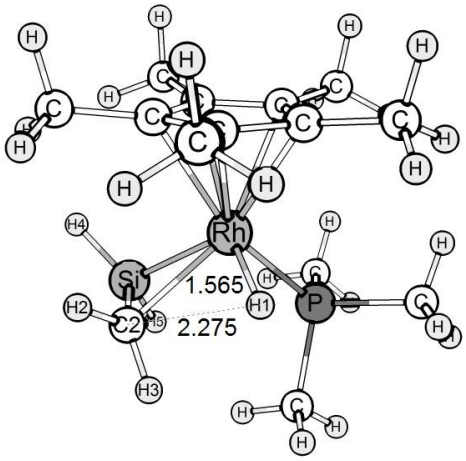

R'=Me; R=H; L=PMe_3

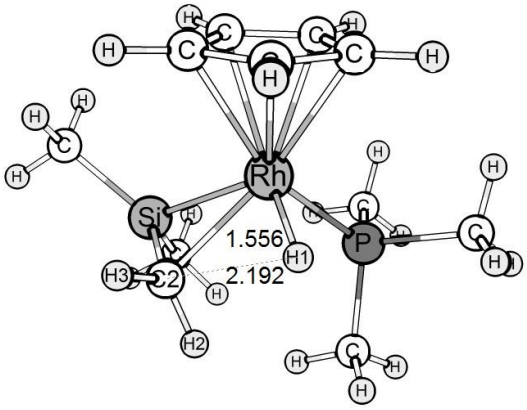

R'=H; R=Me; L=PMe_3

Figure 73: Optimized structures of „sila-olefin" complexes (I1). E(kcal.mol^{-1})=0.

Table 28: Relevant distances [Å] and angles [°] of "sila-olefin" complexes (I1).

		L=PH3	*L=PF3*	*L=PMe3*
d(Rh-Si)	R', R=H	2.521	2.583	2.496
	R'=Me, R=H	2.501	2.553	2.482
	R'=H, R=Me	2.580	2.678	2.567
d(C2-H1)	R', R=H	2.202	2.134	2.232
	R'=Me, R=H	2.238	2.184	2.275
	R'=H, R=Me	2.187	2.159	2.192
d(Rh-H1)	R', R=H	1.559	1.566	1.558
	R'=Me, R=H	1.566	1.571	1.565
	R'=H, R=Me	1.557	1.561	1.556
d(Rh-L)	R', R=H	2.363	2.268	2.373
	R'=Me, R=H	2.369	2.258	2.387
	R'=H, R=Me	2.355	2.254	2.366
d(Si-C2)	R', R=H	1.810	1.810	1.811
	R'=Me, R=H	1.809	1.808	1.812
	R'=H, R=Me	1.813	1.814	1.813
β(H1-M-C2)	R', R=H	68.52	65.13	69.94
	R'=Me, R=H	69.44	66.77	71.32
	R'=H, R=Me	68.02	66.56	68.29

Structural parameters of $[C_5R'_5Rh(L)(SiH_2CH_2)(H)]^+$ R'=H, Me are given in table 28. The Rh-Si distance is the shortest for R'=Me and L=PMe_3, where the larger π-backbonding is expected due to a richer electronic environment around Rh. On the other hand, this distance is the longest for R'=H and L=PF_3. The M-Si distance for $Cp_2W(\eta^2\text{-}Me_2Si{=}CH_2)$ is 2.53Å [137], for $Cp^*(PMe_3)Ir(\eta^2\text{-}SiMe_2CH_2)$ 2.44Å [138], for $Cp^*[P(i\text{-}Pr)_3]Ru(H)(\eta^2\text{-}CH_2SiPh_2)$ 2.35Å [139] and for $Cp^*(PMe_3)Ir(\eta^2\text{-}CH_2SiPh_2)$ is 2.38Å [138], which follows the same trend. The "sila-olefin" Si-C2 bond length of 1.81 Å lies between typical Si-C2 single bond (1.87-1.91Å) and Si-C2 double bond (1.70-1.76Å) distances, which can be attributed to partial Si-C2 double bond character. For example, the Si-C2 bond length of 1.81 Å observed for iridium $Cp^*(PMe_3)Ir(\eta^2\text{-}CH_2SiPh_2)$ [138] is close to the analogous distance of 1.79 Å for rutenium $Cp^*P(i\text{-}Pr)_3Ru(H)(\eta^2\text{-}CH_2SiPh_2)$ [139] and shorter than a normal Si-C2 single bond, despite the different coordination environments at the metals and substituents at silicon in the three compounds. These distances are somewhat longer than Si=C2 double bond distances observed for isolated silenes, due to the

backdonation role. The heteroatom-substituted silene $(Me_3Si)_2Si=C(OSiMe_3)$(1-adamantyl) has a Si=C2 double bond distance of 1.76 Å, which is longer than values observed for $Me_2Si=C(SiMe_3)(SiMe^tBu_2)$ (1.70 Å). The d(Rh-L) decreases in the following order PMe_3> PH_3>PF_3, as the electron acceptor ability of L.

The migration of a hydrogen atom to C of the "sila-olefin" $SiR_2=CH_2$ ligand leads to a complex with a *β*-agostic bond. Following the reaction coordinates defined in figure 15 (Technical Details, Chapter 2) and after a stepwise decrease of the reaction coordinate α(H1-M-C2), d(M-H1) lengthens, becoming weaker, as H1 approaches C2. H1 is now partially bonded to M and to C2, with a so called *β*-agostic bond. Figure 74 illustrates $[C_5R'_5Rh(L)(SiH_2CH_2)(H)]^+$ R'=H, Me and L=PH_3, PF_3, PMe_3 "silyl-agostic" minima (I2).

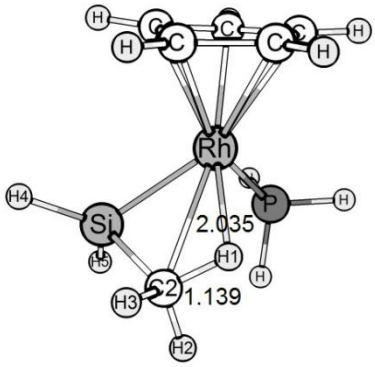

-12.14

R', R=H; L=PH_3

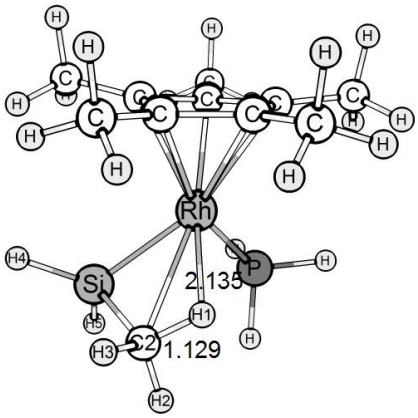

-14.23

R'=Me, R=H; L=PH_3

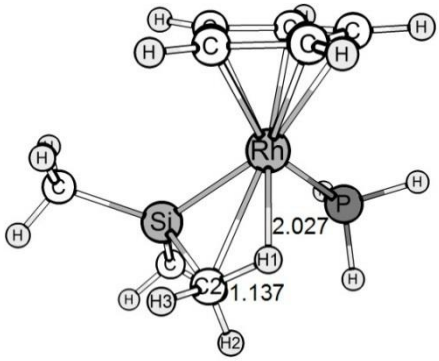

-12.39

R'=H; R=Me; L=PH_3

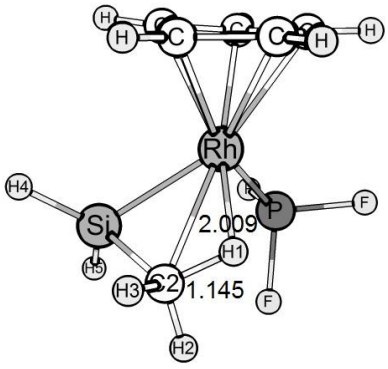

-13.61

R', R=H; L=PF_3

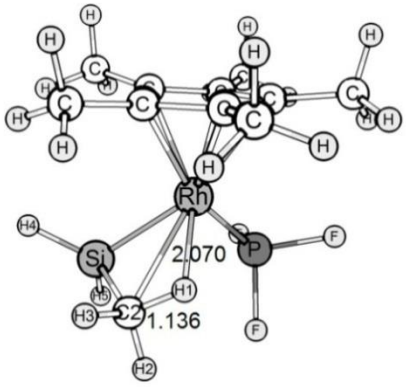

-15.83

R'=Me, R=H; L=PF_3

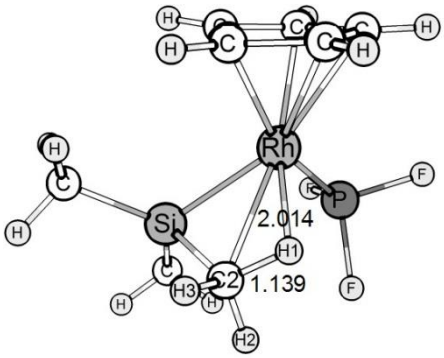

-13.41

R'=H; R=Me; L=PF_3

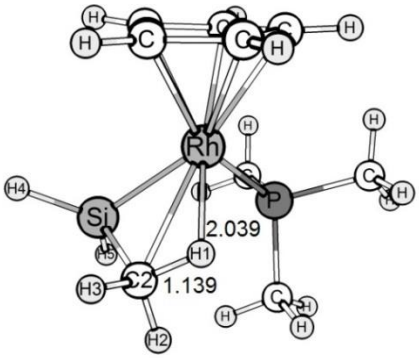

-10.56

R', R=H; L=PMe_3

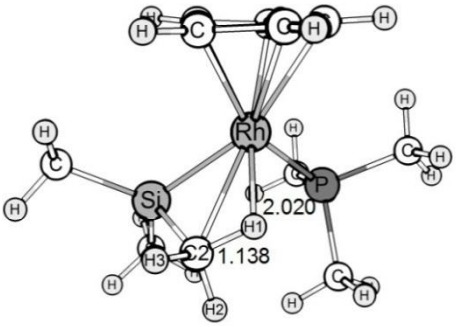

-11.42

R'=H; R=Me; L=PMe_3

Figure 74: Optimized structures and relative energies (kcal/mol) of "silyl-agostic" complexes (I2).ˊThe calculated energies ΔE are relative to each preceding initial "sila-olefin" isomer (I1).

A *β*-agostic minimum was not located for R'=Me and L=PMe_3. This is due to an increased migratory insertion barrier and rising electron richness in the metal center, and species with *β*-agostic metal···H-C interactions will be destabilized. The R', R=H lies 12.14 for L=PH_3, 13.61 for L=PF_3 and 10.56 for L=PMe_3 below the energy of each corresponding "sila-olefin" isomer. Concerning R'=Me and R=H, L=PH_3 lies -14.23, L=PF_3 -15.83 and L=PMe_3 -11.42 relative to the "sila-olefin" isomer. The "silyl-agostic" isomers are stabilized the most for R'=Me and by

increasing electron-acceptor ability of the substituent L, a matter that is going to be discussed later in detail (see Kinetics).

The structural parameters of the *β*-agostic isomers are going to be discussed, based on the individual steric and electronic properties of the substituents. Both d(Rh-Si) and α(H1-Rh-C2) support the formation of a *β*-agostic bond by decreasing its size from, e.g., 2.501 Å and 69.44 Å, to 2.359 Å and 25.53º, respectively, for R'=H and L=PH_3. Additionally, the partially stretched Si-C2 double bond enlarges by 0.12 Å. The Rh-Si bond is the longest for R'=H and L=PF_3 as well as for R'=Me and L=PF_3, and the shortest for R'=H and L=PMe_3. It illustrates the magnitude of the electronic effects of the ligand L in the trans position. The d(Rh-Si) bond increases due to a less π-backdonation aptitude of Rh to Si, when a ligand with a stronger electron-acceptor ability is involved and placed in a trans position (PF_3> PH_3> PMe_3).

The d(C2-H1) shows evidence of an elongation compared to the default value, 1.09Å. This distance decreases from 2.202 Å on the sila-olefin isomer to 1.140 Å (table 29).

Table 29: Relevant distances [Å] and angles [º] of "silyl-agostic" complexes (I2).

Parameter		*L= PH_3*	*L= PF_3*	*L= PMe_3*
d(Rh-Si)	R', R=H	2.359	2.394	2.350
	R'=Me, R=H	2.360	2.387	-
	R'=H, R=Me	2.371	2.412	2.366
d(C2-H1)	R', R=H	1.140	1.145	1.139
	R'=Me, R=H	1.129	1.136	-
	R'=H, R=Me	1.137	1.139	1.138
d(Rh-H1)	R', R=H	2.035	2.009	2.039
	R'=Me, R=H	2.135	2.070	-
	R'=H, R=Me	2.027	2.014	2.020
d(Rh-L)	R', R=H	2.384	2.280	2.387
	R'=Me, R=H	2.390	2.266	-
	R'=H, R=Me	2.378	2.266	2.384
d(Si-C2)	R', R=H	1.929	1.922	1.931
	R'=Me, R=H	1.935	1.928	-
	R'=H, R=Me	1.940	1.937	1.941
β(H1-Rh-C2)	R', R=H	26.53	27.03	26.49
	R'=Me, R=H	25.15	26.04	-
	R'=H, R=Me	26.92	27.36	26.92

The reaction path leads to the 16-electron "silyl" isomers (I3) (see figure 75). These structures were calculated as minima, confirmed by frequency calculations. These I3 unsaturated isomers were obtained for the complexes with an electron richer environment around the metal center (see table 30), either due to the electron donor properties of the ligands as well as from the polarization of the Si^{+}-C^{-} bond. The unsaturated 16-electron "silyl" isomers with an electron poorer environment are destabilized and could not be calculated.

The $Cp^{*}(PMe_3)Rh^{+}$- electron-rich metal center is able to stabilize the electron-deficient 16-electron "silyl" isomer by 14 kcal/mol, relative to the "sila-olefin" isomer. The $L=PMe_3$ (R', R=H) complex lies 8.86 kcal/mol below the "sila-olefin" complex. The donor capacity of the electron rich C_5Me_5 ligand overwhelms the donor capacity of the $L=PMe_3$ ligand trans to Rh and stabilizes the 16e- "silyl" isomer the most. These 16e-electron complexes are stable species even without the formation of an α-bond, as in case of the olefin analogous. The structural parameters of the geometries obtained are shown in table 31.

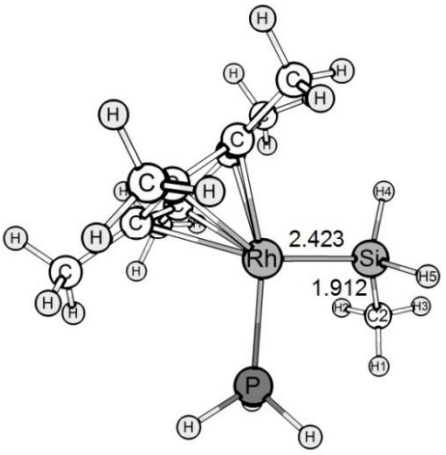

-14.84

R'=Me, R=H; $L=PH_3$

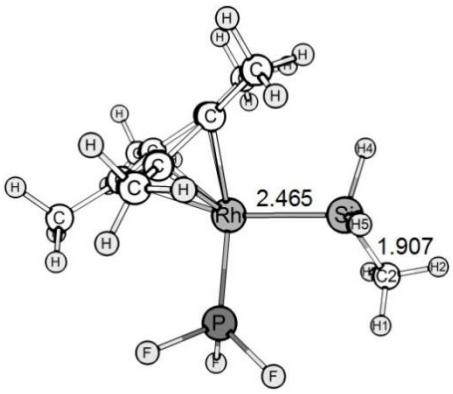

-13.14

R'=Me, R=H; $L=PF_3$

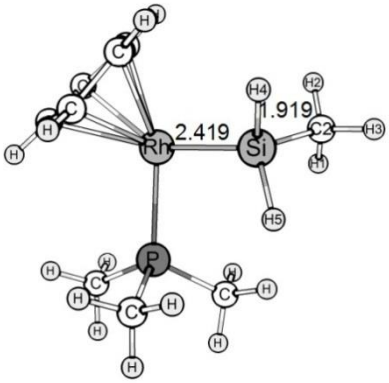

-8.86

R', R=H; L=PMe_3

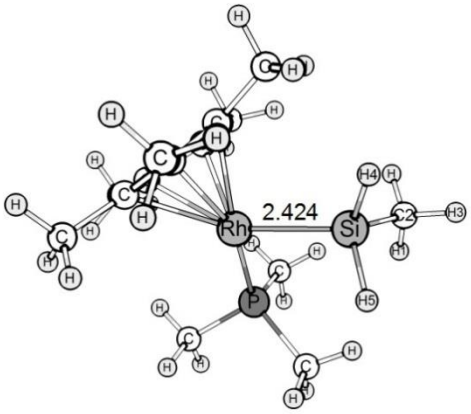

-13.72

R'=Me, R=H; L=PMe_3

Figure 75: Optimized structures and relative energies (kcal/mol) of "silyl" complexes (I3). The calculated energies ΔE are relative to each preceding initial "sila-olefin" isomer (I1).

Table 30: Relative energies (kcal/mol) of the "silyl" minima (I3).

$C_5R'_5$	$L=PH_3$	$L=PF_3$	$L=PMe_3$
R', R=H	-	-	-8.86
R'=Me, R=H	-14.85	-13.14	-13.72
R'=Me, R=H	-	-	-

Table 31: Relevant distances [Å] of 16-"silyl" complexes (I3).

	$C_5R'_5$	$L=PH_3$	$L=PF_3$	$L=PMe_3$
d(Rh-Si)	R'=H	-	-	2.419
	R'=Me	2.423	2.465	2.424
d(Si-C)	R'=H	-	-	1.919
	R'=Me	1.912	1.907	1.916
d(Rh-L)	R'=H	-	-	2.389
	R'=Me	2.397	2.277	2.418

The d(Rh-L) distance decreases in the following order L=PH_3, PMe_3> L=PF_3 by ca. 1 Å.

Attempts to calculate the 16e-"silyl" isomers (I3), see table 30, resulted in a facile 1,2-group migration from silicon to rhodium to give "silylene" isomers (I4) (figure 76).

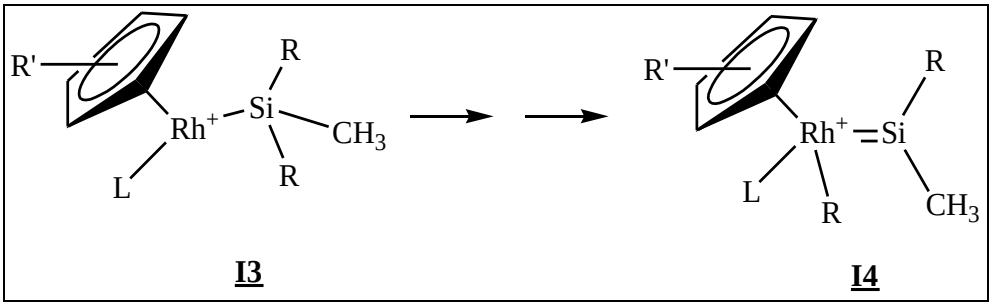

Figure 76: 1,2-group migration of R from silicon to rhodium in $[C_5R'_5Rh(L)(SiRCH_2)(H)]^+$, R', R=H, Me and L= PH_3, PF_3, PMe_3 complexes.

Reactivity studies in an iridium system described by Tilley *et al.* provide evidence for a third type of isomerization, involving sila-olefin and silylene ligands [126]. Tilley *et al.* have shown that observable base-free silylene ligands may be derived from a silyl ligand by α-migration. Silylenes, the silicon analogous for carbenes, are highly reactive divalent species. The trend down the Group 14 column of the periodic table is increased stabilization. Thus silylenes are more stable, relative to silyl radicals, than in the case between carbenes and carbon-centered radicals [139]. A theoretical study on the formation of silacyclopropene from acylsilane and acetylene via silene- to silylene rearrangement carried out by Tanaka *et al.* showed an activation energy in this of 29 kcal/mol in this pathway [140].

These complexes derive, in this study, directly from the "silyl-agostic" isomer, as suggested by Berry and Tilley [137,138]. Their energy is very low comparing to the the "silyl-agostic" isomer, which explains why the 16e-"silyl" isomer is more difficult to obtain.

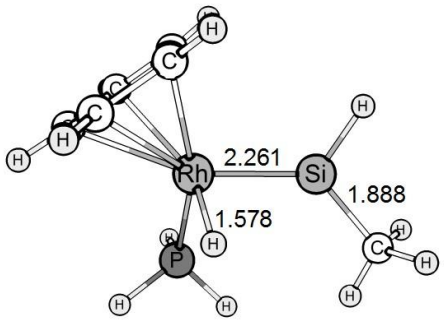

-22.80

R’, R=H; L=PH_3

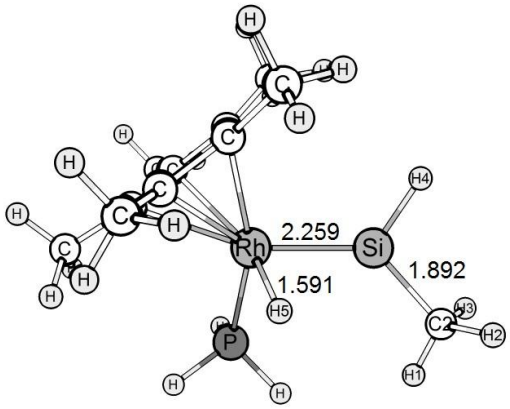

-21.87

R’=Me, R=H; L=PH_3

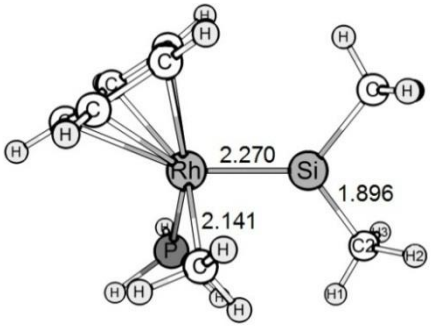

-5.77

R’=H, R=Me; L=PH_3

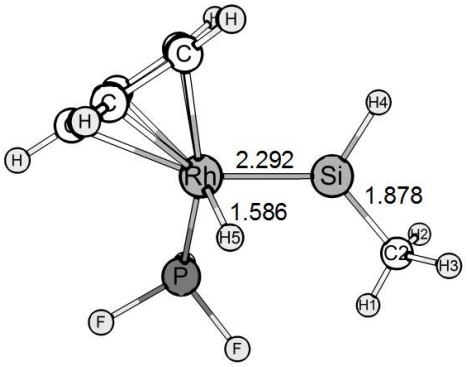

-25.65

R’, R=H; L=PF_3

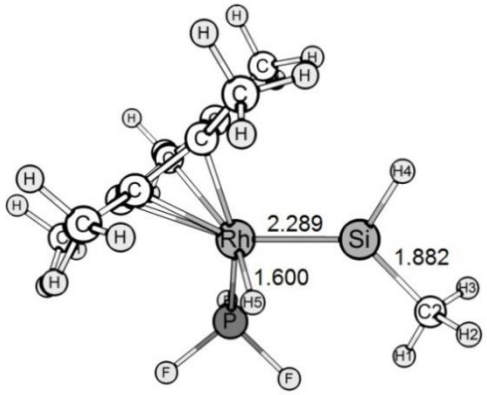

-24.69

R’=Me, R=H; L=PF_3

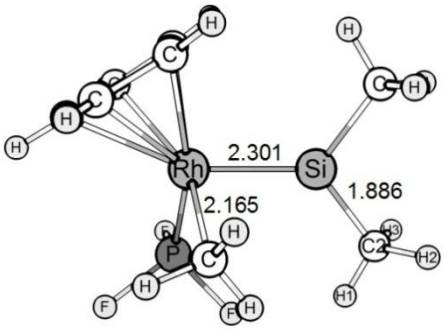

-7.64

R’=H; R=Me; L=PF_3

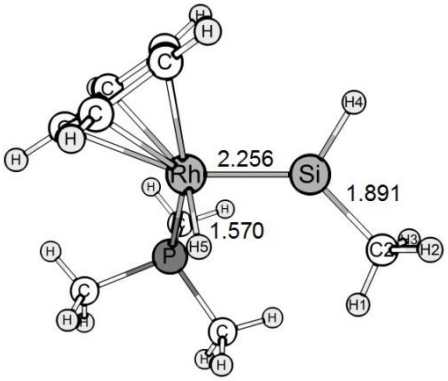

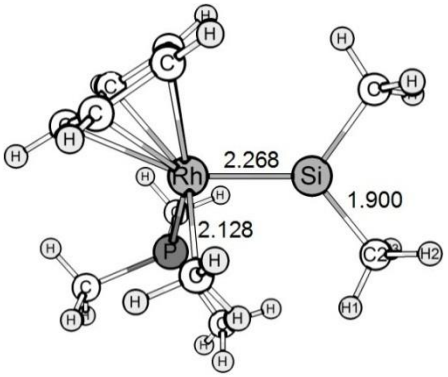

-21.20

R', R=H; L=PMe_3

-4.99

R'=H, R=Me; L=PMe_3

Figure 77: Optimized structures and relative energies (kcal/mol) of "silylene" complexes (I4). The energies ΔE are calculated relative to each preceding initial "sila-olefin" isomer (I1).

The "silylene" structures (I4) are ca. 20-25 kcal/mol more stable relative to the corresponding "sila-olefin" structures (I1). For R'=H and R=Me complexes their energy are ca. -5 kcal/mol (figure 78 and table 32). This can be attributed to a steric hindrance caused by both methyl groups beared by Si and Rh and the PMe_3 ligand.

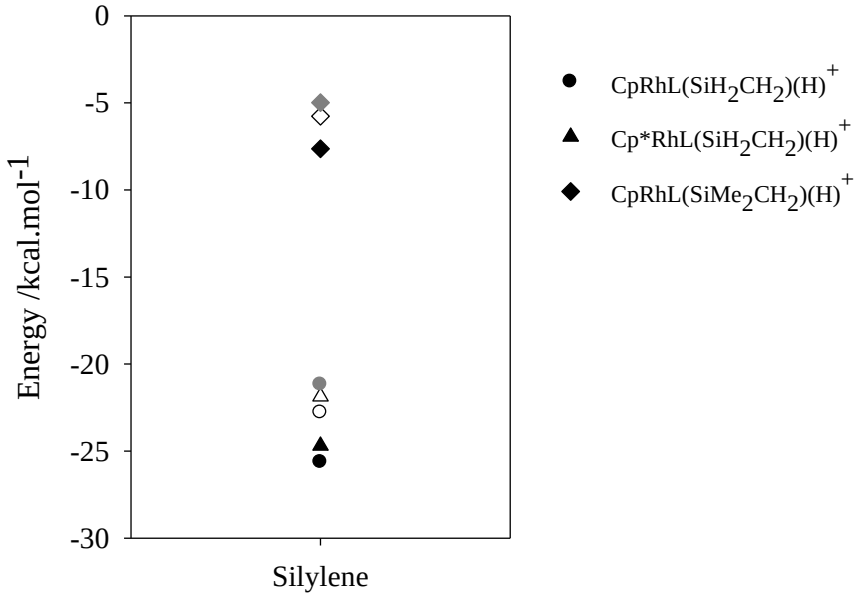

Figure 78: Energy of the silylene isomers (I4), relative to the corresponding sila-olefin structures (I1); (in kcal/mol) (PH_3: white; PF_3=black; PMe_3=dark gray).

Table 32: Relative energies (kcal/mol) of silylene complexes (I4). The energies ΔE are calculated relative to each preceding initial "sila-olefin" isomer (I1).

	L=PH_3	*L=PF_3*	*L=PMe_3*
R',R=H	-22.80	-25.65	-21.20
R'=Me; R=H	-21.87	-24.69	-
R'=H; R=Me	-5.77	-7.64	-4.99

Many of the reactions observed for silylene complexes reflect the presence of a highly electrophilic silicon center. It would seem that the electron-rich $C_5R'_5LRh^+$ fragment stabilizes the formally unsaturated and highly electrophilic silylene ligands through the donation of electron density. This fact reveals a less imperative influence of electronic effects to stabilize the Si center than the steric hindrance created by the Me bulky ligands around it.

A useful structural parameter for describing the amount of "silylene" character at a metal-bond silicon atom is the sum of the bond angles about Si, excluding the anionic substituent. This sum approaches the value of 360º associated with a trigonal planar coordination environment as the degree of "silylene" character increases. Evidence for their classification as "silylene-hydrido" or "-methyl" complexes can be found in the sum of the angles around the silicon atom, Rh-Si-H, Rh-Si-C and H-Si-C, that measures 359.5º. This is the value assigned to sp^2 (360º) hybridization, indicating double bond character between silicon and rhodium. The Rh-Si distance (in the range 2.256-2.289Å) is influenced by the electron richness of the ligands, in the subsequent order: R'=Me, R=H< R', R=H<R'=H, R=Me and L=PMe_3< PH_3< PF_3 (table 33).

Table 33: Relevant distances [Å] of complexes [$C_5R'_5Rh(L)(SiR_2CH_2)(H)]^+$ R', R=H, Me and L=PH_3, PF_3, PMe_3 "silylene" minima (I4).

	$C_5R'_5$	$L=PH_3$	$L=PF_3$	$L=PMe_3$
d(Rh-Si)	R', R=H	2.261	2.292	2.256
	R'=Me; R=H	2.259	2.289	-
	R'=H; R=Me	2.270	2.301	2.268
d(Rh-H5/C5)	R', R=H	1.578	1.586	1.570
	R'=Me; R=H	1.591	1.600	-
	R'=H; R=Me	2.141	2.165	2.128
d(Rh-L)	R', R=H	2.365	2.266	2.372
	R'=Me; R=H	2.371	2.260	-
	R'=H; R=Me	2.369	2.263	2.381
d(Si-C2)	R', R=H	1.888	1.878	1.891
	R'=Me; R=H	1.892	1.882	-
	R'=H; R=Me	1.896	1.886	1.900

This value is also an indicator of a double bond character between both atoms. The M-Si bonds are considerably strengthened compared to the "sila-olefin" isomers (I1). A short Rh-Si contact and a planar coordination environment for the silicon atom are clearly evident. The hydrogen atom is bonded to rhodium in a range 1.570 to 1.600 Å, which is a typical value for a single Rh-H5 atom in this environment. The Si-C2 bond (ca. 1.89 Å) reveals a single bond character.

5.2.2 Complex II: (Si_{olefin} involved in the migratory-insertion reaction)

Complex II is the second complex elected as a "sila-olefin" "starting structure" (II1). For complex II it is the Si of the "sila-olefin" $SiR_2=CH_2$ ligand that is going to be involved in the "sila-olefin" insertion/*β*-H elimination reaction, in contrast to Complex I in which the C atom is involved in the hydrogen migration reaction. Following the reaction coordinates described in figure 15 (Technical Details, Chapter 2), the hydrogen migrates to the Si atom of the "sila-olefin" $SiR_2=CH_2$ ligand in the first step of the reaction pathway of the "sila-olefin" insertion. Figure 79 depicts the "sila-olefin" geometries of complex II1.

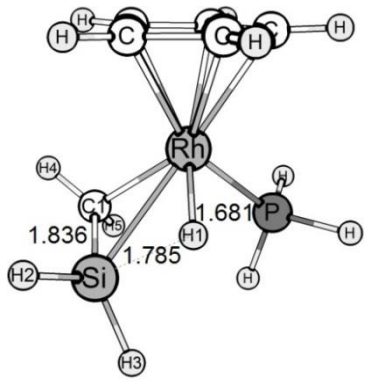

R', R=H; L=PH_3

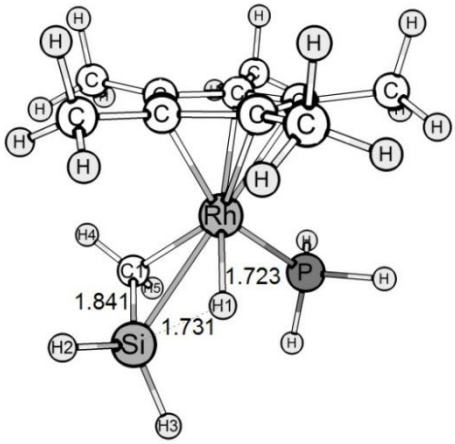

R'=Me, R=H; L=PH_3

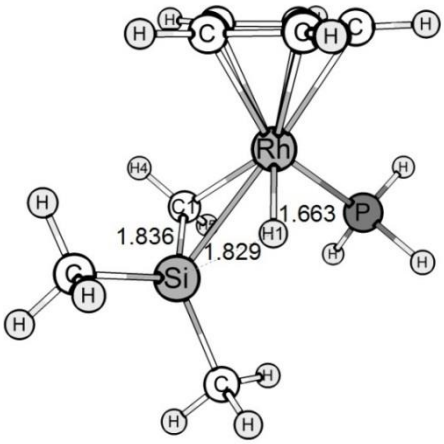

R'=H, R=Me; L=PH_3

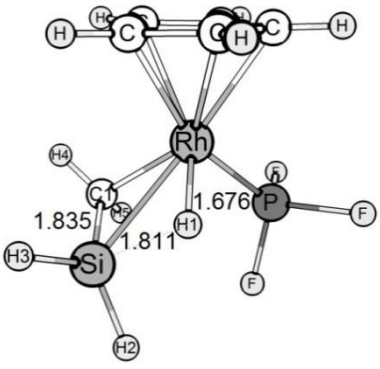

R', R=H; L=PF_3

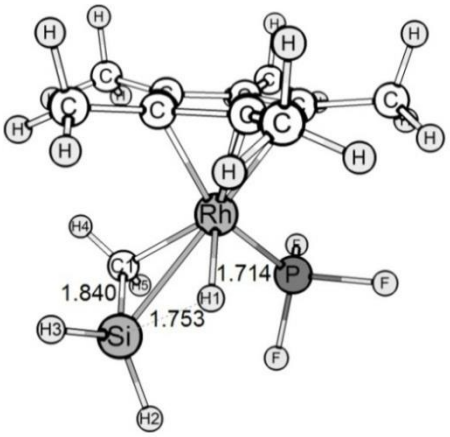

R'=Me, R=H; L=PF_3

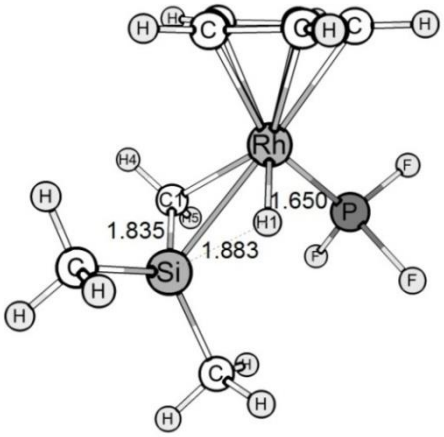

R'=H, R=Me; L=PF_3

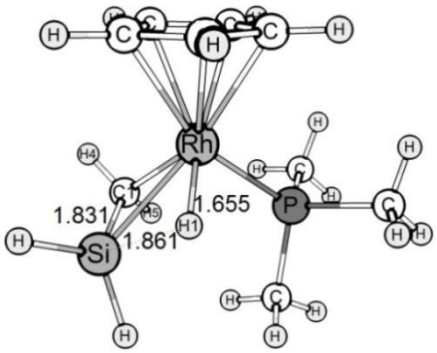

R', R=H; L=PMe_3

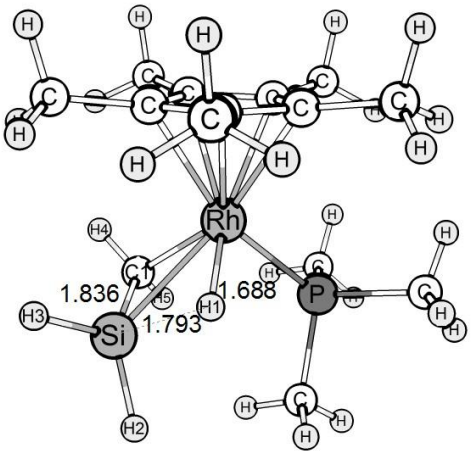

R'=Me, R=H; L=PMe_3

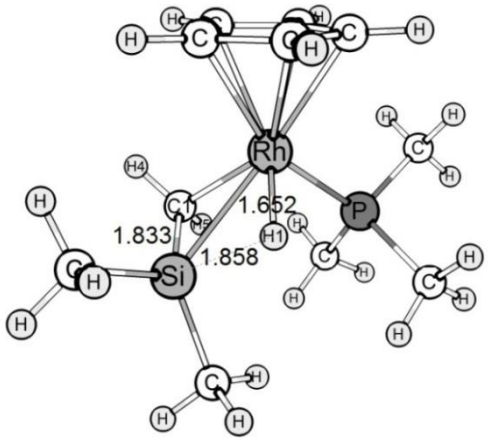

R'=H, R=Me; L=PMe_3

Figure 79: Optimized structures of "sila-olefin" complexes (II1).

The presence of two methyl ligands on Si will protect the Si environment and stabilize it.

The d(Rh-Si) is the longest for L=PF_3 and the shortest for L=PMe_3 (table 34).

Table 34: Relevant distances [Å] and angles [°] of "sila-olefin" complexes (II1).

	L=PH_3: 1.R'=H 2.R'=Me 3.R=Me	*L=PF_3*: 1.R'=H 2.R'=Me 3.R=Me	*L=PMe_3*: 1.R'=H 2.R'=Me 3.R=Me
d(Rh-Si)	2.574, 2.580, 2.621	2.626, 2.624, 2.686	2.537, 2.544, 2.595
d(Si-H1)	1.785, 1.731, 1.829	1.811, 1.753, 1.88	1.861, 1.793, 1.858
d(Rh-H1)	1.681, 1.723, 1.663	1.676, 1.714, 1.650	1.655, 1.688, 1.652
d(Rh-L)	2.384, 2.396, 2.380	2.291, 2.285, 2.281	2.386, 2.408, 2.394
d(Si-C1)	1.836, 1.841, 1.836	1.835, 1.840, 1.835	1.831, 1.836, 1.833
β(H1-M-Si)	43.62, 41.78, 43.80	43.10, 41.36, 43.84	47.15, 44.70, 45.47

The sum of C-Si-C angles for L=PF_3 around the silicon center is 356.3°, which is near the value assigned to sp^2 (360°) hybridization, indicating partial double bond character between silicon and the metalated carbon atom. All other complexes show also a partial double bond character between Si and C1, with a value in a range near 360°. The M-H1 bond distances reveal there is an interaction with a single bond character between the metal and the hydrogen atom, but ca. 10% longer comparing to complex I. The d(Rh-Si) is the longest for L=PF_3 (R', R=H) and L=PF_3 (R'=Me, R=H) and the shortest for L=PMe_3 (R', R=H) and L=PMe_3 (R'=Me, R=H). These bonds are 0.05Å longer comparing to complex I.

Of particular interest are the Si-C1 distances in the silene ligand, ca. 1.84 Å, which seem to reflect partial double bond character since Si-C single bond distances normally range from 1.87 to 1.91 Å [141].

The Si-H···M structural feature of complex II can be attributed to nonclassical interactions. When a hydrosilane reacts with a transition metal complex, there are variations of bonding types in the products formed. A full oxidative addition leads to the formation of 2c-2e bonds between the metal center and Si and the metal center and H. However there are several stages on the way to full oxidative addition that have been identified in isolated complexes (and in calculations). These involve the formation of σ-complexes, complexes with *β*-agostic interactions of a Si-H bond in α-,

β-, and more remote positions with a metal center, and interligand hypervalent interactions (IHI) between an MH bond and an electrophilic silicon center. In addition, there also appear to be interactions between a silicon center and a metal-bond hydrogen that have been identified especially in polyhydride systems (referred to by the term SISHA, or secondary interactions between a silicon and a hydrogen atom. These variations interactions are depicted in Figure 80.

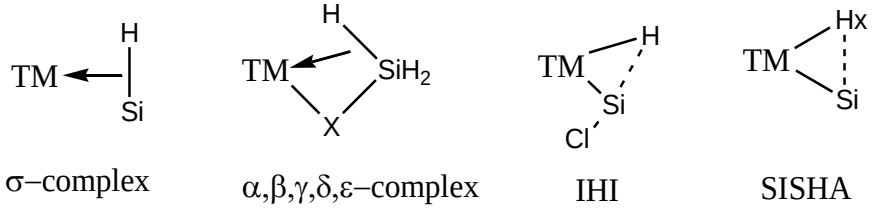

Figure 80: Representations of nonclassical interactions.

There is no uniform agreement as how to distinguish (or if a distinction may actually be realized) between these interactions, although Nikonov *et al.* [142] have attempted to summarize the major differences between σ-, *β*-agostic, and IHI cases in an extensive review. It should be understood at the outset that interactions of Si-H with a metal center form a continuum, thus, boundaries in any classifications are blurred. Furthermore, more than one interpretation has been possible for a given data set.

The IHI type of interaction generally occurs with early transition metals (Ti, Nb, and Ta) but have recently been extended to Fe (in calculations) [143] and experimentally to Ru [144,145]. A common feature of the complexes in this class is a chloride (or halide) substituent on silicon. The structural features that characterize IHI complexes relative to σ-complexes include the following: (a) M-Si bond is shorter than the bond of a σ-complex; (b) Si-X is longer than in averaged values found for tetrahedral silanes; (c) Si···H with longer contacts (in the range 1.8-2.1 Å) than those in σ-complexes (1.7-1.8 Å) (d) M-H elongated bonds. Considering the features reported by Nikonov in his paper review about Si···H interactions [142], the complex II "sila-olefin" Si···H···M interactions form a continuum and is fairly balanced between IHI and an σ-complex. Still, there are monometallic σ-complexes reported in the

literature for the Co triad by Brookhart *et al.* [146,147], but there are no M-H···Si IHI interactions for the Co triad, as stated by Corey in her paper review [148].

Along with the fact that the interactions of Si-H with the rhodium metal center form a continuum, the II1 "sila-olefin" and II2 "silyl-agostic" isomers cannot be isolated as stationary points and the "sila-olefin" insertion/β-migratory elimination reaction could thus not be investigated here. Attempts to approach Si and H, by decreasing the angle H-Rh-Si with fixed coordinates, causes the sila-olefin ligand to rotate, in an attempt to avoid the formation of the bond.

"Ethyl" minima geometries are depicted in figure 81. The Si-C distances confirm a single bond character.

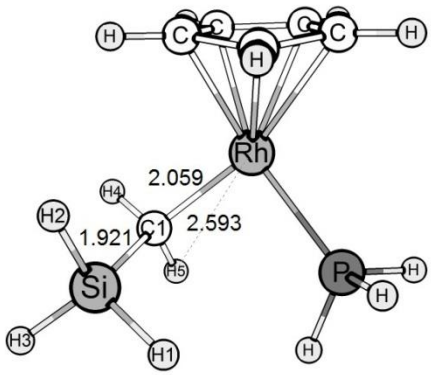

+17.21

R', R=H; L=PH_3

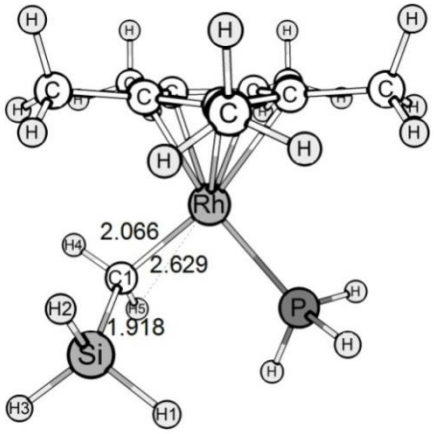

+10.72

R'=Me, R=H; L=PH_3

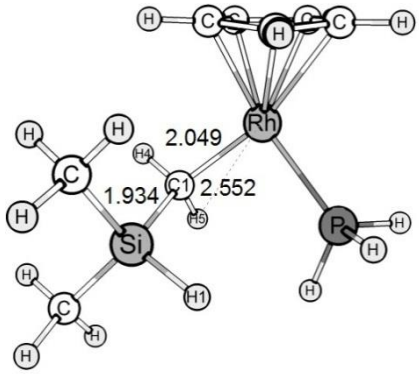

+21.10

R'=H, R=Me; L=PH_3

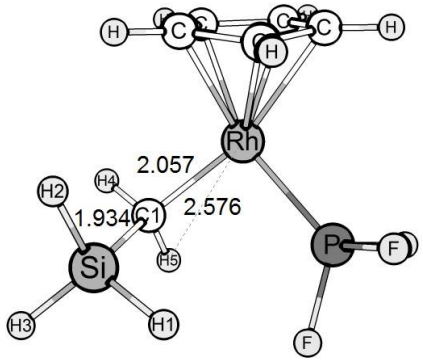

+22.53

R', R=H; L=PF_3

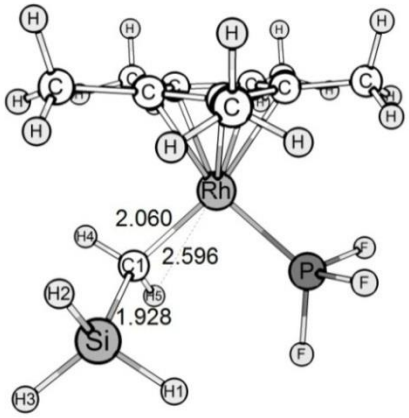

+15.77

R'=Me, R=H; L=PF_3

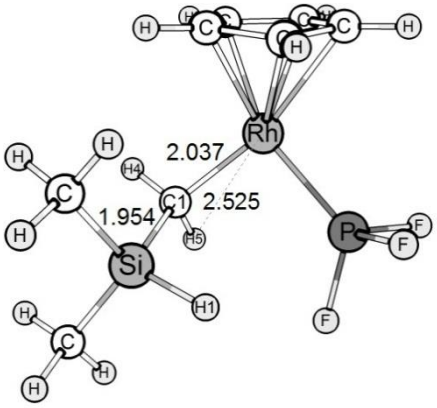

+28.39

R'=H, R=Me; L=PF_3

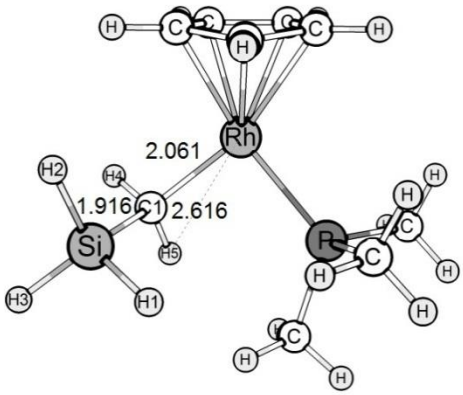

+17.54

R', R=H; L=PMe_3

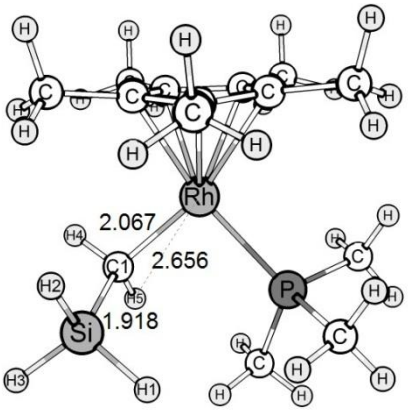

+9.73

R'=Me, R=H; L=PMe_3

Figure 81: Optimized structures and relative energies (kcal/mol) of „ethyl" complexes (II3). The energy ΔE is calculated relative to each preceding initial "sila-olefin" isomer (II1).

The energy of the 16e-"ethyl" (II3) isomers is illustrated in figure 82.

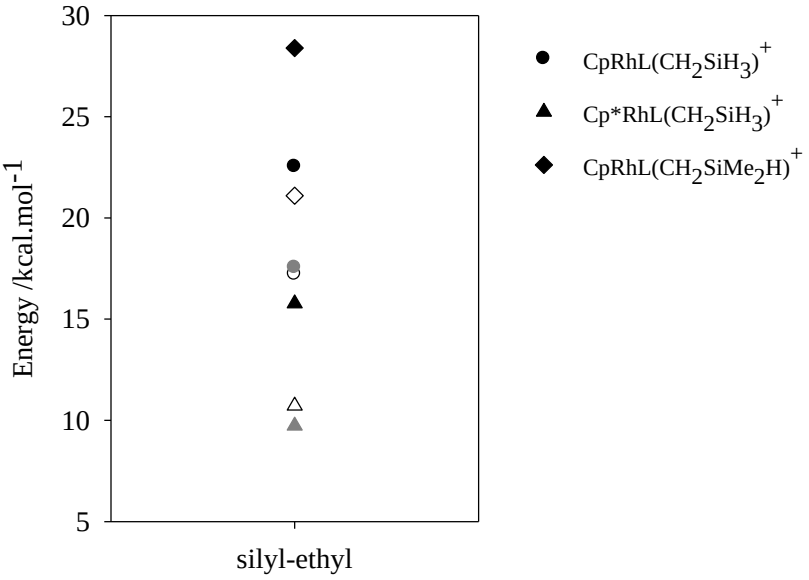

Figure 82: Energy of the "ethyl" isomers (II3), relative to the corresponding "sila-olefin" structures (II1), (in kcal/mol) (PH_3: white, PF_3=black, PMe_3=dark gray).

Table 35: Relative energies (kcal/mol) of the "ethyl"complexes (II3).

$C_5R'_5$	*L=PH_3*	*L=PF_3*	*L=PMe_3*
R', R=H	17.21	22.53	17.54
R'=Me, R=H	10.72	15.77	9.73
R'=H, R=Me	21.10	28.39	-

The energy of these 16-e"ethyl" isomers lies between +10 and +28 kcal/mol (table 35) above the corresponding "sila-olefin" structures. The R'=Me complexes, with the electron donor $C_5Me'_5$, stabilize this structure the most. The structural parameters of the complexes are given in table 36.

Table 36: Relevant distances [Å] of the "ethyl" complexes (II3).

	$C_5R'_5$	$L=PH_3$	$L=PF_3$	$L=PMe_3$
d(Rh-C1)	R', R=H	2.058	2.057	2.060
	R'=Me, R=H	2.066	2.060	2.067
	R'=H, R=Me	2.048	2.037	-
d(Si-C1)	R', R=H	1.921	1.934	1.916
	R'=Me, R=H	1.918	1.928	1.918
	R'=H, R=Me	1.934	1.954	-
d(Rh-L)	R', R=H	2.415	2.336	2.411
	R'=Me, R=H	2.434	2.322	2.442
	R'=H, R=Me	2.418	2.342	-

The electron richness of the environment does not influence the Rh-C1 distance, as it does in case of d(Rh-Si).

Two additional minima were obtained for II3 L=PF_3 (R', R=H) and II3 L=PF_3 (R'=Me, R=H) (figure 83).

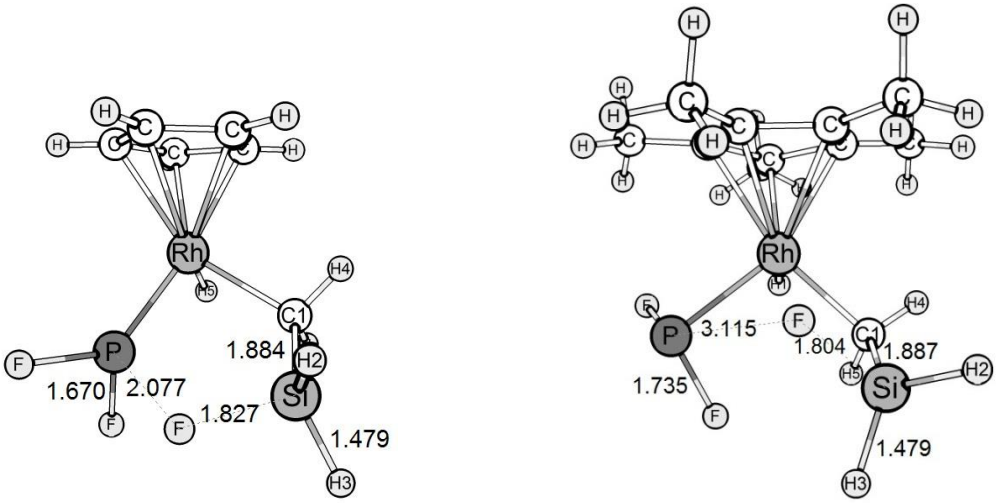

-14.85

(relative to R', R=H; L=PF_3 isomer in figure 81)

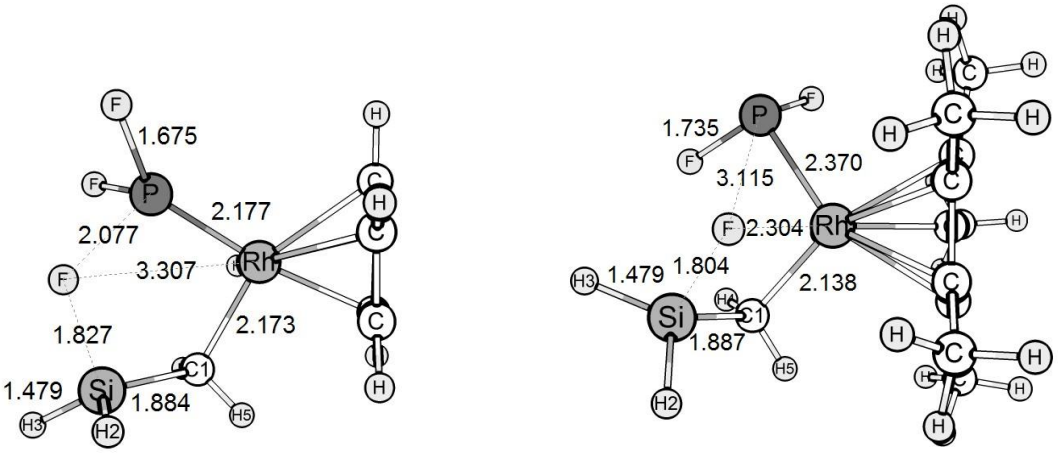

Figure 83: Optimized structures and relative energies of the II3 L=PF_3 (R', R=H) and II3 L=PF_3 (R', R=H) "ethyl" isomers and "best view" of the geometry adopted by these complexes.

The product obtained is indicative of an intramolecular mechanism. This complex lies +7.68 kcal/mol, relative to the II1 L=PF_3 (R', R=H) complex depicted in figure 79. This mechanism implies an oxidative addition of H1 bonded to the metal center via a 1,3-Migration. In an attempt to achieve a tetracoordinate environment, the Si atom interacts with the F atom of the L=PF_3. The "ethyl" complex is then further stabilized by an intramolecular electrodonation from F to Si. The d(P-F) elongates to 2.077 Å (table 37) for R' and R=H complex, and 3.115 Å for R'=Me and R=H complex. The Rh distance to the F atom involved is 3.307 Å for R' and R=H complex, and 2.304 Å for R'=Me and R=H complex.

Table 37: Relevant distances [Å] of the "ethyl" complexes (II3) obtained through a 1,3-migration.

Parameter	*R´, R=H*	*R´=Me, R=H*
d(Rh-C1)	2.173	2.138
d(Si-C1)	1.884	1.887
d(Rh-L)	2.177	2.370
d(P-F)	1.670, 1.675, 2.077	1.735, 3.115
d(Si-F)	1.827	1.804
d(Si-H3)	1.479	1.479

5.3 Kinetics

An energy profile of the "sila-olefin" insertion/*β*-elimination reaction is presented und discussed next. The energy of the stationary and the tied saddle points are then depicted graphically and evaluated. The reaction pathway of the olefin insertion/migration runs as described in figure 15 (Chapter 2). The same reaction coordinates are going to be applyied in this chapter for the "sila-olefin" complex. The hydride migratory insertion reaction to the "sila-olefin" isomer leads to the η^2-agostic isomer. These two isomers are connected through a transition state (TS1). The transition state TS1 is calculated through optimization calculations of the maxima located in the reaction pathway and then checked by frequency calculations. An attempt will be made to determine a trend regarding the influence of the electronic and steric properties of the metal center and the ligands in the energy profile of the reaction.

The first step of the hydrid migratory insertion, concerning the isomeration between the "sila-olefin" and the *β*-silylagostic, will be elected the one relevant to determine the energy barrier of insertion $\Delta Ei_{ns}^{\neq}$ of the reaction. That means that it will be no effort to further calculate the isomerization of the *β*-silylagostic that leads to the 16-electron silyl isomer and englobes the transition state TS2. The facile decomposition of the high destabilized 16-electron silyl isomer leads to a rich variety of migration types within this system and stabilize the system to a greater extend, such as the 1,2 migration to produce a silylene. The step of the hidrid migratory insertion that involves the destabilized silyl complex is, for this reason, considered to confer less reliable results.

Another important aspect has to do with the complex II. The "sila-olefin" conformation in which Si is involved in the hydrogen migratory insertion proved not to be a good candidate for the study of the the "sila-olefin" insertion/*β*-elimination reaction, due to the so-called Si-H···M non classical interactions. Neither "sila-olefin" or the *β*-ethylagostic isomer could be calculated, owing to the fact that the hydrogen atom involved in the migratory reaction cannot be inserted in the "sila-olefin" ligand. The unsaturated "ethyl" isomers ([M]-CH_2-SiH_3) are destabilized. These isomers can be stabilized through a 1,3-migration reaction.

5.3.1 Complex I (L=PH_3): $[C_5R'_5Rh(L)(SiR_2CH_2)(H)]^+$ R', R=H, Me complex

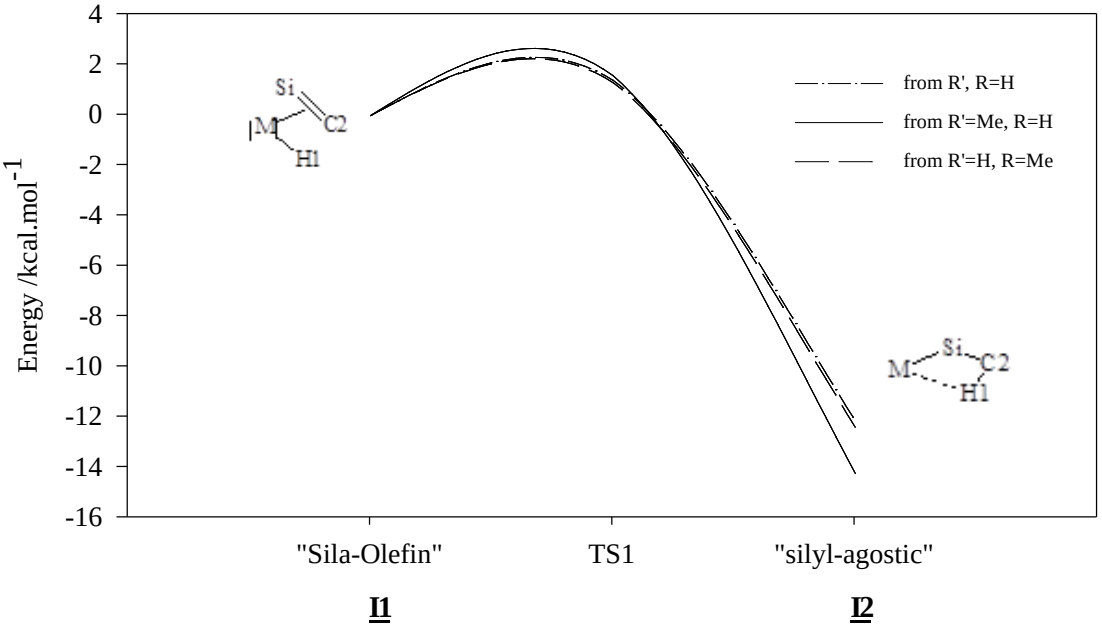

Figure 84: Energy of the stationary points of complex L=PH_3 (in kcal/mol).

The energy of the stationary and the tied saddle point TS1 is depicted graphically in figure 84. The energy scheme of the "sila-olefin" insertion/β-H elimination reaction of L=PH_3 isomers clearly indicates the "silyl-agostic" structure to be the global minimum, being more stable than the correspondent "sila-olefin" structures by 12.14 for R'=H (R=H), 14.23 for R'=Me (R=H) and 12.39 kcal/mol for complex R=Me (R'=H). The electron richer R'=Me (R=H) stabilizes the most upon the formation of the β-agostic bond, being 2 kcal/mol more stable than the other L=PH_3 complexes (table 38).

Table 38: Energy of the stationary points of complex L=PH_3 (in kcal/mol).

		"Sila-olefin"		*TS1*		*„silyl-agostic"*
R', R=H	I1	0	TS1	1.30	I2	-12.14
R'=Me; R=H	I1	0	TS1	1.58	I2	-14.23
R'=H; R=Me	I1	0	TS1	1.30	I2	-12.39

A transition state (TS1) connects the "sila-olefin" with the "silyl-agostic" (figure 85). The achievement of TS1 was confirmed by frequency calculations. An imaginary frequency that matches the scan progress of the reaction coordinate α(H1-M-C2) was obtained.

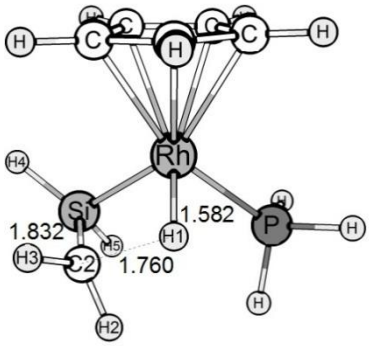

+1.30

R', R=H

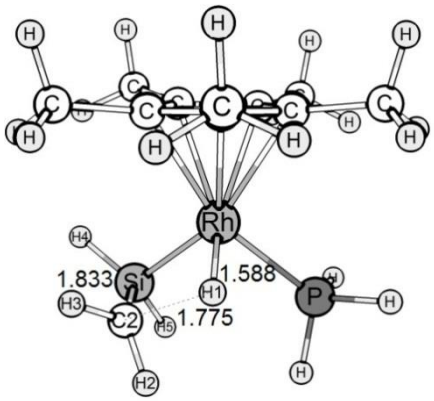

+1.58

R'=Me, R=H

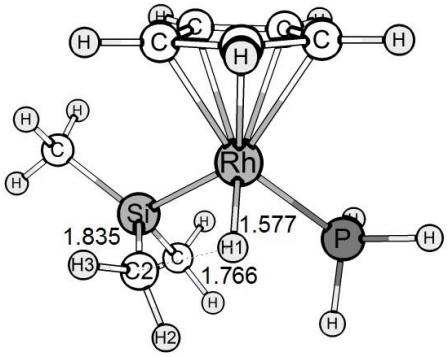

+1.30

R'=H, R=Me

Figure 85: Optimized structures and relative energies (kcal/mol) of TS1 complexes.

Table 39: Relevant distances [Å] and angles [°] of TS1.

	R', R=H	*R'=Me, R=H*	*R'=H, R=Me*
d(M-C2)	2.268	2.278	2.266
d(M-H1)	1.582	1.588	1.577
d(Si-C2)	1.832	1.833	1.835
α(M-Si-C2)	61.77	62.42	60.81
β(H1-M-C2)	50.67	50.94	50.94

The calculated barriers for the "sila-olefin" hydrogen migration are +1.3 kcal mol^{-1} relative to the sila-olefin isomer, for R'=H (R=H) and R=Me (R'=H) complexes. For R'=Me (R=H) this energy barrier is +1.58 kcal/mol. The TS1 is a reactant-like isomer. The M-H1 distance is ca. 1.582 Å for the L=PH_3 complexes and the same distance is ca. 1.56 Å for the "sila-olefin" and ca. 2.0 Å for the "silyl-agostic" isomer. The Si-C2 bond length also shows the same trend and does not alter much in size, from 1.81 Å to 1.83 Å, during the insertion of the hydrogen atom. As expected, this bond reflects partial double bond character since Si-C single bond distances normally range from 1.87 Å to 1.91 Å. This distance stretches ca. 0.1 Å when the reaction lands in the "silyl-agostic" minimum. The M-Si distance decreases progressively during the occurrence of this step of the reaction (figure 86).

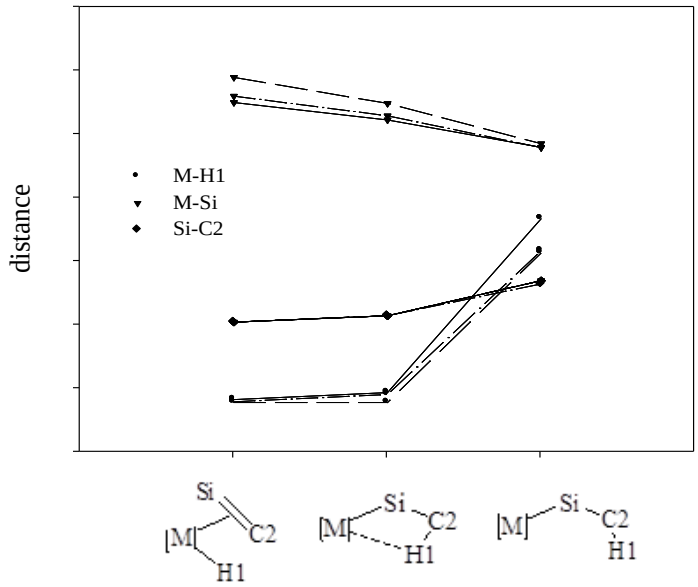

Figure 86: Variation of the coordinates of the stationary points of complexes I1 (d [Å]): from I1 (R', R=H) (line: dash-dot), I1 (R'=Me, R=H) (line: solid), I1 (R'=H, R=Me) (line: long dash).

5.3.2 Complex I (L=PF_3): $[C_5R'_5Rh(L)(SiR_2CH_2)(H)]^+$ R', R'=H, Me complexes.

The energy scheme of the "sila-olefin" insertion/*β*-H elimination reaction of L=PF_3 complex I isomers undoubtedly points out the "silyl-agostic" structure to be the global minimum (figure 87).

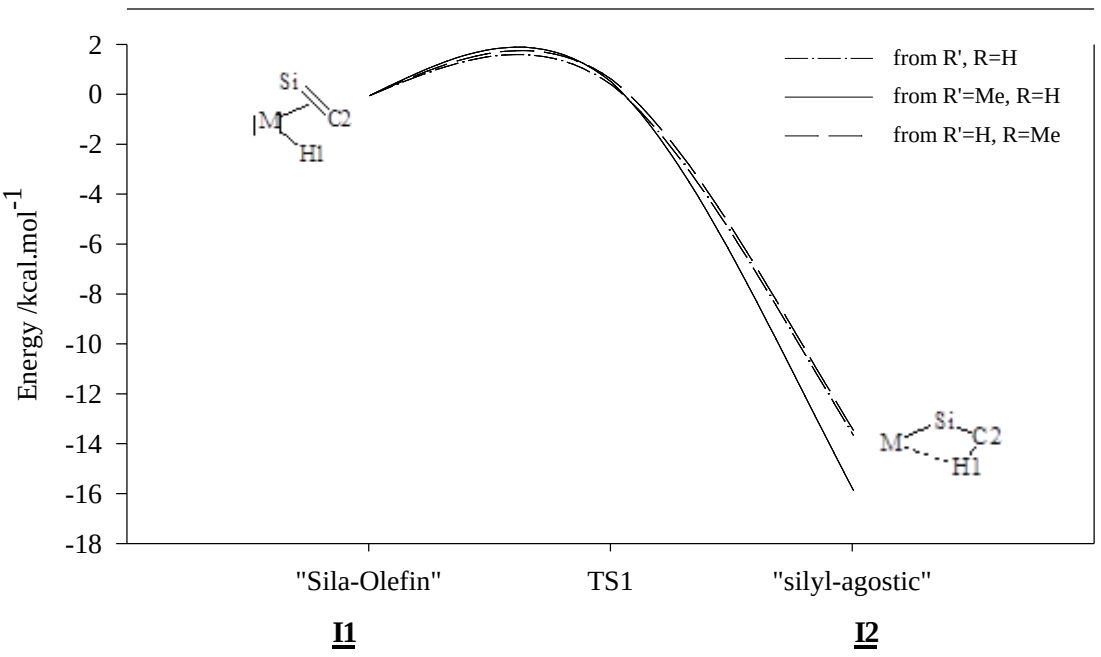

Figure 87: Energy of the stationary points of L=PF_3 complex (in kcal/mol), relative to "sila-olefin".

For L=PF_3 (R', R=H) complex the "sila-olefin" isomer ends in a "silyl" complex with a *β*-agostic interaction, passing through an insertion energy barrier of 0.42 kcal/mol. The "silyl-agostic" structure is 13.61 kcal/mol more stable than the "sila-olefin" isomer and is the global minimum of the reaction The energy barrier of the olefin insertion is very low. The energy of transition state 1 is less than 1 kcal/mol above the sila-olefin isomer. The $\Delta E_{ins}^{\neq}$ barrier for R'=Me (R=H) is 0.53 kcal/mol. The energy sinks by 16.36 kcal/mol upon the formation of the M···H-C bond. For R=Me (R'=H) complex the energy barrier is also very small. The formation of the agostic bond stabilizes the structure by 13.41 kcal/mol, relative to the correspondent "sila-olefin" structure (table 40). The reaching of TS1 (figure 88) was confirmed by frequency calculations. An imaginary frequency that go with the reaction coordinate α(H1-M-C2) was obtained.

Table 40: Energy of the stationary points of L=PF_3 complex (in kcal/mol), relative to "sila-olefin".

		"Sila-olefin"		*TS1*		*"silyl-agostic"*
R', R=H	I1	0	TS1	0.42	I2	-13.61
R'=Me; R=H	I1	0	TS1	0.53	I2	-15.83
R'=H; R=Me	I1	0	TS1	0.64	I2	-13.41

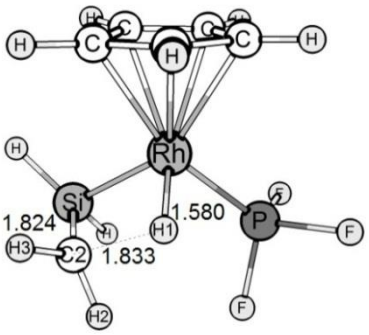

-13.61

R', R=H

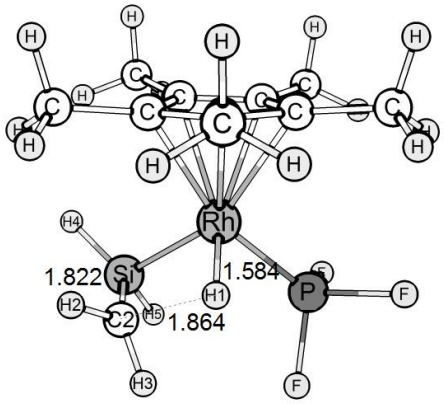

-15.83

R'=Me, R=H

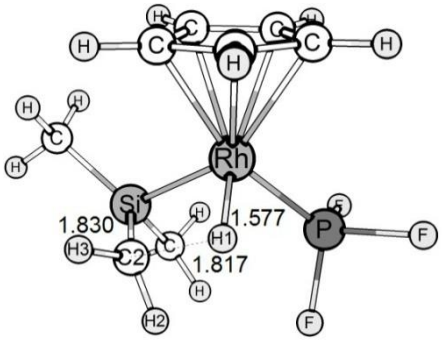

-13.41

R'=H, R=Me

Figure 88: Optimized structures and energies (kcal/mol) of TS1 complexes.

The TS1 is a reactant-like. The M-H1 distance increases only slightly while reaching of the transition state structure. This distance increases to 1.93 Å upon the

formation of the M···H-C *β*-agostic bond and stretches to 2 Å with the formation of the "silyl-agostic" isomer (table 41 and figure 89). Of particular interest are the Si-C2 distances in the transition state 1, ca. 1.83Å, which still reflect partial double bond character since Si-C single bond distances normally range from 1.87 to 1.91 Å.

Table 41: Relevant distances [Å] and angles [°] of TS1.

	R', R=H	*R'=Me, R=H*	*R'=H, R=Me*
d(M-C2)	2.284	2.295	2.279
d(M-H1)	1.580	1.584	1.577
d(Si-C2)	1.824	1.822	1.830
α(M-Si-C2)	60.84	61.68	59.28
β(H1-M-C2)	52.92	53.74	52.46

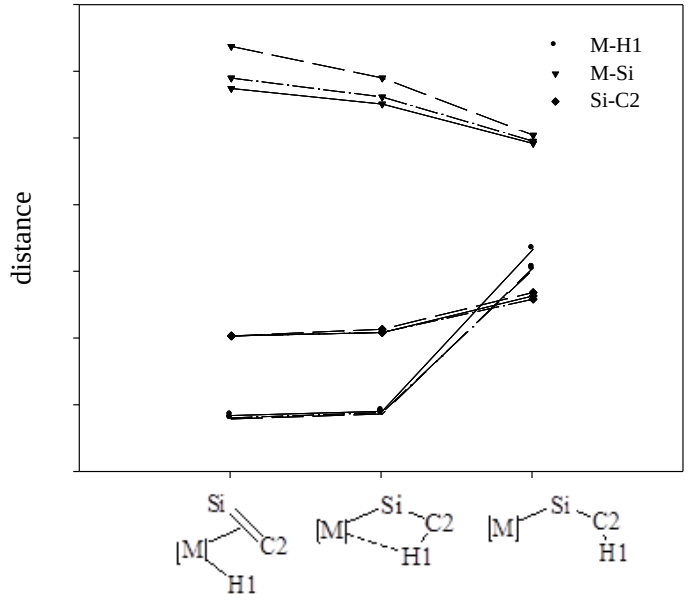

Figure 89: Variation of the coordinates of the stationary points of complexes I2 (d [Å]): from I2 (R', R=H) (line: dash-dot); I2(R'=Me, R=H) (line: solid); I2 (R'=H, R=Me) (line: long dash).

5.3.3 Complex I (L=PMe_3): $[C_5R'_5Rh(L)(SiR_2CH_2)(H)]^+$ R', R=H, Me complexes.

The energy scheme of the "sila-olefin" insertion/*β*-H elimination reaction of L=PMe_3 complex I isomers is depicted in figure 90. The "silyl-agostic" structure is the global minimum of the reaction.

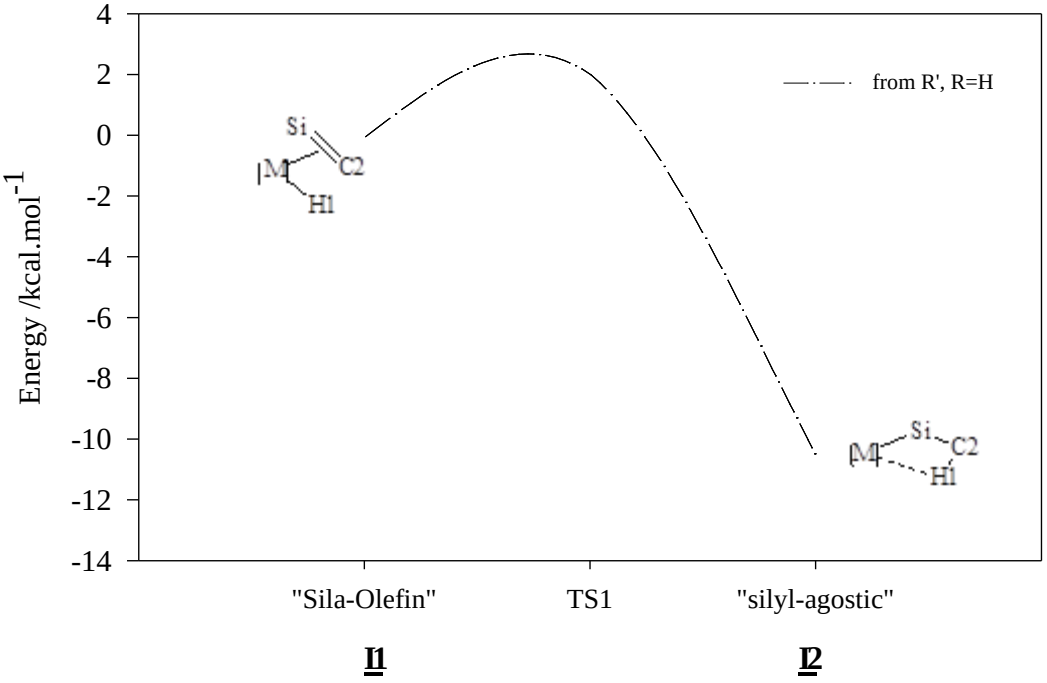

Figure 90: Energy of the stationary points of L=PMe_3 complexes (in kcal/mol), relative to "sila-olefin".

Table 42: Energy of the stationary points of L=PMe_3 complexes (in kcal/mol), relative to "sila-olefin".

		"Sila-olefin"		*TS1*		*"silyl-agostic"*
R', R=H	I1	0	TS1	2.02	I2	-10.56
R'=Me; R=H	I1	0	TS1	2.70	I2	-
R'=H; R=Me	I1	0	TS1	-	I2	-11.42

The "silyl-agostic" structure is again the global minimum of the reaction being 10.56 and 11.42 kcal/mol more stable relative to the correspondent sila-olefin minima, for R'=H (R=H) and R=Me (R'=H) complexes respectively (table 42). The formation of this M···H-C *β*-agostic bond stabilizes complex R=Me (R'=H) the most, although their energy only differs by a minute amount. This stationary point was not found for R'=Me (R=H). The reaction path through the selected coordinates leads to an alkyl structure without a *β*-agostic bond.

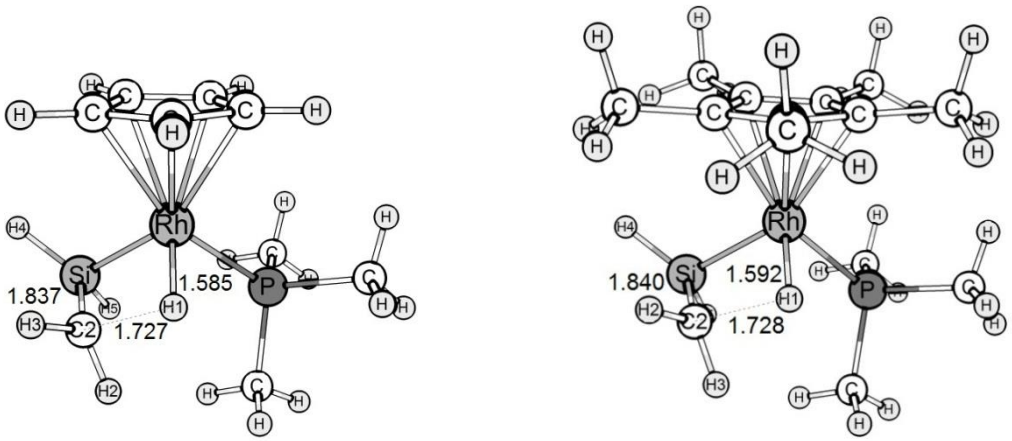

+2.02 R', R=H

+2.70 R'=Me, R=H

Figure 91: Optimized structures and energies (kcal/mol) of TS1 complexes.

The nature of the transition state 1 (figure 91) is confirmed by the existence of an imaginary frequency. $\Delta E_{ins}^{\neq}$ obtained for R'=Me (R=H) transition state, 2.7 kcal.mol^{-1}, only slightly differs from the energy of R'=H (R=H) (2.02 kcal/mol).

Table 43: Relevant distances [Å] and angles [°] of TS1.

	R', R=H	*R'=Me, R=H*
d(M-C2)	2.262	2.273
d(M-H1)	1.585	1.592
d(Si-C2)	1.837	1.840
α(M-Si-C2)	62.07	62.59
β(H1-M-C2)	49.63	49.34

The TS1 is a reactant-like isomer (table 43). The M-H1 distance is ca. 1.59 for both complexes and the same distance is ca. 1.56 for the sila-olefin and ca. 2.0 Å for the *β*-agostic isomer. The Si-C2 bond length makes only a small adjustment, from 1.81 to 1.83 Å, upon the insertion of the hydrogen atom, and still reflects partial double bond character since Si-C2 single bond distances normally range from 1.87 to 1.91 Å. This distance stretches ca. 0.1 Å after the isomerization to the silyl agostic minimum. The M-Si distance decreases progressively during this step of the reaction.

5.4 Summary

The impact of the electronic and geometric properties in the environment of the metal center of the energetic of the Olefin insertion/*β*-H elimination reaction was discussed in chapters 3 and 4.

This chapter refers to the "sila-olefin" insertion/*β*-H elimination reaction. The replacement of either C1 or C2 for Si in the Olefin substituent $H_2C1=C2H_2$ will affect the energy of the hydrogen migratory insertion of the $[C_5R'_5ML(H)(SiR_2=CH_2)]^+$ (M=Co, Rh; L=PH_3, PF_3, PMe_3; R´, R=H, Me) cationic complexes.

For the "sila-olefina" conformation in which C is involved in the hydrogen migratory insertion, the energy barrier $\Delta E_{ins}^{\neq}$ increases with the electron donor strength of the ligands. The $\Delta E_{ins}^{\neq}$ is +2.70 kcal/mol above the "sila-olefin" for L= PMe_3 (R'=Me, R=H) and +0.42 kcal/mol for L= PF_3 (R', R=H) complex. The energy barrier $\Delta E_{ins}^{\neq}$ lies 1.3-1.6 kcal/mol for L=PH_3, 0.4-0.6 kcal/mol for L=PF_3, and 2-3 kcal/mol for L=PMe_3 above each corresponding "sila-olefin" minima. The energy barrier of the hydrogen migratory insertion $\Delta E_{ins}^{\neq}$ will suffer the higher impact by the replacement of an "olefin" with a "sila-olefin" ligand. Comparing to the L=PF_3 "olefin" analogous calculated in chapter 4, the energy barrier of insertion $\Delta E_{ins}^{\neq}$ will decrease from +2.91 kcal/mol to +0.42 kcal/mol, by the substitution of the "olefin" ligand through a "sila-olefin" ligand.

The global minimum of the reaction exhibits a *β*-agostic M···H···C interaction. The "sila-olefin" isomer will be deeply stabilized (12-14 kcal/mol for L=PH_3, 13-16 kcal/mol for L=PF_3, 11 kcal/mol for L=PMe_3) upon the formation of the *β*-agostic

bond, with the electron acceptor strength of the ligands. This energy is -1.22 kcal/mol for the "olefin" isomer calculated in chapter 4.

The theoretical calculations provide quantitative support that -"silyl-agostic" complexes are stabilized compared to "sila-olefin" complex I whilst replacing C1 through Si in the olefin ligand, in rhodium complexes. For the rhodium "olefin" complex in chapter 4, the energy of ethylene is fairly balanced with the energy of the *β*-agostic isomer and the energy barrier of the H1 migratory insertion is positioned 3 kcal/mol above it.

The „silyl" isomer could be isolated for the electron richer complexes of I (R'=Me, R=H; L= PH_3, PF_3, PMe_3). These isomers turned out to be 14 kcal/mol more stable than the correspondent "sila-olefin" isomer, according to the following order of the ligands PH_3<PMe_3<PF_3. For I (R', R=H; L=PMe_3), this isomer lies 8.86 kcal/mol below the "sila-olefin" isomer. This suggests that the C_5Me_5 ligand stabilizes this structure the most.

Following the scan coordinates β(Rh-Si-C2) of the reaction, it lands in a "silylene" complex, in some cases. The "silyl" complex rearranges to the "silylene" isomer via a 1,2-migration. These structures proved to be exceptionally stable, being 20-25 kcal/mol for the less crowded Si atom and 5-8 kcal/mol for the $Si(CH_3)_3$ ligands more stable than the "sila-olefin" minima, respectively. Access to experimental results of similar complexes confirms the generalization that silylene complexes are intermediates in reactions of less hindered silyl. The stabilization of these 16e-"silyl" isomers by way of π-bonding donation involving Rh and Si is believed to have a poor impact. The stability of these isomers is only slightly affected by changes of the ligands accompaniyng the electron acceptor strength of the ligand L. The stabilisation caused by increasing electron acceptor strength of the ligands goes together with higher Rh-Si distances. It pursues that the d(Rh-Si) provides less steric hindrance between the ligands.

The "sila-olefin" conformation in which Si is involved in the hydrogen migratory insertion proved not to be a good candidate for the study of the the "sila-olefin" insertion/*β*-elimination reaction, due to the so-called Si-H···M non classical interactions. Neither "sila-olefin" or the *β*-"ethylagostic" isomer could be calculated, owing to the fact that the hydrogen atom involved in the migratory reaction cannot be inserted in the "sila-olefin" ligand. As H1 approaches Si, by decreasing α, the C1=Si

"sila-olefin" ligand starts to rotate, "avoiding" the insertion of H1 to Si. The unsaturated "ethyl" isomers ([M]-CH_2-SiH_3) are destabilized and show a large range of energies, between +10 and +28 kcal/mol, above the energy of the "sila-olefin" minima. The stability of these structures is going to be affected by the ligands in the order PF_3<PMe_3~PH_3 and C_5H_5<C_5R_5 accompanying the electron donor strength of the ligands. These isomers can be stabilized through a 1,3-migration reaction.

Chapter 6 Conclusions

Conclusions

The energetic of the olefin insertion/ β-H elimination processes was studied using density functional theory. The observed trends based on steric and electronic properties of two late transition metals (Co and Rh) and ligands (L) are reproduced.

The insertion/migration reaction of neutral complexes $[L_3M(C_2H_4)(H)]$ (M=Co, Rh; L=PMe_3, PF_3) with a trigonal bipyramidal geometry was described in chapter 3. The effect of a rich or poor electronic environment around the metal center was evaluated. The barrier of the hydrogen migration insertion reaction $\Delta E_{ins}^{\neq}$ is critically influenced by the electronic character of the ligands L in this complex. The destabilization caused by the increasing electron donor strength of L is accompanied by higher energy barriers in the same series. For both Co and Rh complexes, the relative energy barrier for the hydrogen migratory insertion reaction step increases with the electron donor strength of the ligand. The reaction becomes kinetically less favorable down the triad. The β-agostic interaction decreases from Co to Rh. The theoretical calculations provide quantitative support to the generally held notion that ethylene complexes are stabilized compared to the β-agostic alkyl isomers toward heavier congeners in a triad of late transition metals.

The structural parameters and energies of the unsaturated 16 electron ethyl singlet complexes were weight against complexes in the triplet state. The singlet state with a geometry balanced between a square planar and a tetrahedral is stabilized the most for Rh. The triplet state with a tetrahedral geometry is stabilized the most for Co. This result confirms the trend that electronically unsaturated, open shell configurations tend to be more common for lighter (3d) transition metals. The unsaturated ethyl complexes are stabilized by increasing donor strength of L.

The reactivity of the cationic complexes $[C_5R_5ML(H)(C_2H_4)]^+$ (R=H, CH_3; M=Co, Rh; L=PF_3) is described in chapter 4. The computed energy barriers obtained compare very well with activation energies from the previous NMR studies and confirm that the activation barriers are insensitive towards L, but somewhat higher for R=H than R=Me. The B3LYP method and the SDD basis set proved to be a reliable method/basis set to be applied in this type of cationic complexes.

The Chapter 5 refers to the "sila-olefin" insertion/β-H elimination, by replacing C1 or C2 for a Si in the olefin substituent $H_2C1=C2H_2$. The study deals with

the cationic complexes of the type $[C_5R'_5ML(H)(SiR_2{=}CH_2)]^+$ (M=Co, Rh; L=PH_3, PF_3, PMe_3; R=H, Me), in which either C or Si atoms of the “sila-olefin” are involved in the "sila-olefin" insertion/β-H elimination reaction. To probe the nature of steric and electronic factors on migration the reactivity in a variety of “sila-olefin” complexes was examined.

The "sila-olefin" conformation in which C is involved in the hydrogen migratory insertion is going to be deeply stabilized upon the formation of the "silyl-agostic" bond and the ΔE_{ins} barrier decreases to a greater extent comparing to the olefin isomer. The computed energy barriers confirm that the activation barriers are quite insensitive to L, but somewhat higher for R=H than R=Me.

After exploring the reaction scope of this conformation, it is apparent that a rich variety of migration types are possible within this system and stabilize the system to a greater extent. These include the 1,2-migration reaction. The facile decomposition of the 16-electron silyl isomer resulted in the 1,2 migration to produce a silylene. Access of experimental results of similar complexes confirms the generalization that silylene complexes are intermediates in reactions of less hindered silanes. The facile decomposition of the unsaturated silyl is a result of the large number of different reaction pathways available to them. It makes this system less reliable as a possible catalyst used in the industry.

The "sila-olefin" conformation in which Si is involved in the hydrogen migratory insertion proved not to be a good candidate due to the so-called Si-H···M non classical interactions. The unsaturated “ethyl” isomers ([M]-CH_2-SiH_3) are destabilized. These isomers can be stabilized through a 1,3-migration reaction.

Literature

[1] Natta, G.; Pino, P.; Corradini, P.; Danusso, F.; Mantica, E.; Mazzanti, G.; Moraglio, G. *J. Am. Chem. Soc.* **1955**, *77*, 1708-1710.

[2] Ziegler, K.; Holzkamp, E.; Breil, H.; Martin, H. *Angew. Chem.* **1955**, *67*, 426, 541.

[3] Brookhart, M.; Volpe, A.F., Jr.; Lincoln, D.M.; Horváth, I.T.; Millar, J.M. *J.Am. Chem. Soc.* **1990**, *112*, 5634-5636.

[4] Wu, Z.; Jordan, R.F.; Petersen, J.L. *J. Am. Chem. Soc.* **1995**, *117*, 5867-5868.

[5] Casey, C.P.; Hallenbeck, S.L.; Pollock, D.W.; Landis, C.R. *J. Am. Chem. Soc.* **1995**, *117*, 9770-9771.

[6] Breslow, D.S.; Newburg, N.R. *J. Am. Chem. Soc.* **1959**, *81*, 81-86.

[7] Cossee, P. *Tetrahedron Lett.* **1960**, *No. 17*, 12-16.

[8] Cossee, P. *Tetrahedron Lett.* **1960**, *No. 17*, 17-21.

[9] Cossee, P. *J. Catal.* **1964**, *3*, 80-88.

[10] Arlman, E.J.; Cossee, P. *J. Catal.* **1964**, *3*, 99-104.

[11] Green, M.L.H. *Pure Appl. Chem.* **1978**, *50*, 27-35.

[12] Ivin, K.J.; Rooney, J.J.; Stewart, C.D.; Green, M.L.H.; Mahtab, R. *J. Chem. Soc., Chem. Commun.* **1978**, 604-606.

[13] Dawoodi, Z.; Green, M.L.H.; Mtetva, V.S.B.; Prout, K. *J. Chem. Soc., Chem. Commun.* **1982**, 1410-1411.

[14] Laverty, D.T.; Rooney, J.J. *J. Chem. Soc., Faraday Trans. 1* **1983**, *79*, 869-878.

[15] Brookhart, M.; Green, M.L.H. *J. Organomet. Chem.* **1983**, *250*, 395-408.

[16] Brookhart, M.; Green, M.L.H.; Wong, L.L. *Prog. Inorg. Chem.* **1988**, *36*, 1-124.

[17] Grinzburg, A.G. *Russ. Chem. Rev.* **1988**, *57*, 1175-1193.

[18] Gleiter, R.; Hyla-Kryspin, I.; Niu, S.Q.; Erker, G. *Organometallics* **1993**, *12*, 3828-3836.

[19] Schmidt, G.F.; Brookhart, M. *J. Am .Chem. Soc.* **1985**, *107*, 1443-1444.

[20] Burger, B.J.; Thompson, M.E.; Cotter, W.D.; Bercaw, J.E. *J. Am. Chem. Soc.* **1990**, *112*, 1566-1577.

[21] Resconi, L.; Piemontesi, F.; Franciscono, G.; Abis, L.; Fiorani, T. *J. Am. Chem. Soc.* **1992**, *114*, 1025-1032.

[22] Guo, Z.; Swenson, D.C.; Jordan, R.F. *Organometallics* **1994**, *13*, 1424-1432.

[23] Davies, C.E.; Gardiner, I.M.; Green, J.C.; Green, M.L.H.; Hazel, N.J. *J. Chem. Soc., Dalton Trans.* **1985**, 669.

[24] Dawoodi, Z.; Green, M.L.H.; Mtetwa, V.S.B.; Prout, K.; Schultz, A.J., Williams, J.M.; Koetzle, T.F. *J. Am. Soc., Dalton trans.* **1986**, 1629.

[25] Berry, A.; Dawoodi, Z.; Derome, A.E.; Dickenson, J.M.; Downs, A.J.; Green, J.C.; Green, M.L.H., Hare, P.M. *J. Chem. Soc., Chem. Commun.* **1986**, 520.

[26] Prosenc, M.H.; Janiak, C.; Brintzinger, H.H. *Organometallics* **1992**, *11*, 4036-4041.

[27] Röll, W.; Brintzinger H.H., Rieger, B.; Zolk, R. *Angew. Chem., Int. Ed. Engl*. **1990**, *29*, 279-280.

[28] Lee, I.-M.; Gauthier, W.J.; Ball, J.M.; Iyengar, B.; Collins, S. *Organometallics* **1992**, *11*, 2115-2122.

[29] Burger, B.J; Cotter, W.D.; Coughlin, E.B.; Chacon, S.T.; Hajela, S.; Herzog, T.A., Köhn, R., Bercaw, J.E. In *Ziegler Catalysis*; Fink, G., Mülhaupt, R., Brintzinger, H.H., Eds.; Springer-Verlag: Berlin, 1995; pp 317-331.

[30] Yu, Z.; Chien, J.C.W. *J. Polym. Sci., Part A* **1995**, *33*, 125-135.

[31] Fellmann, J.D.; Schrock, R.R.; Trificante, D.D. *Organometallics* **1982**, *1*, 481.

[32] Thompson, M.E.; Baxter, S.M.; Bulls, A.; Burger, B.J.; Nolan, M.C.; Santarsiero, B.D.; Bercaw, J.E. *J. Am. Chem. Soc.* **1987**, *109*, 203.

[33] Ewen, J.A.; Jones, R.L.; Razavi, A.; Ferrara, J.D. *J. Am. Chem. Soc.* **1988**, *110*, 6255-6256.

[34] Kawamura-Kuribayashi, H.; Koga, N.;Morokuma, K. *J. Am. Chem. Soc.* **1992**, *114*, 8687-8694.

[35] Kawamura-Kuribayashi, H.; Koga, N.;Morokuma, K. *J. Am. Chem. Soc.* **1992**, *114*, 2359-2366.

[36] Alvarez, S.; Aullón, G; *Inorg.Chem.* **1996**, *35*, 3137-3144.

[37] Woo, T.K.; Fan, L.; Ziegler, T. *Organometallics* **1994**, *13*, 2252-2261.

[38] Fan, L.; Harrison, D.; Woo, T.K.; Ziegler, T. *Organomettalics* **1995**, *14*, 2018-2026.

[39] Woo, T.K.; Fan, L.; Ziegler, T In *Ziegler Catalysis*; Fink, G., Mülhaupt, R., Brintzinger, H.H., Eds.; Springer-Verlag: Berlin, 1995; pp 291-315.

[40] See, for example: (a) Collman, J.P.; Hegedus, L.S.; Norton, J.R.; Finke, R.G. *Principles and Applications of Organotransition Metal Chemistry;* University Science Books: Mill Valley, CA, 1987. (b) Parshall, G.W. *Homogeneous Catalysis*; Wiley: New York, 1980. (c) *Transition Metal Catalyzed Polymerization; Ziegler-Natta and Metathesis Polymerization*; Quirk, R.P., Ed.; Cambridge Press: Cambridge 1988

[41] See, for example: (a) Cross, R.J. In The Chemistry of the Metal-Carbon Bond; Hartley, F.R., Partai, S., Eds.; Wiley: New York 1985; Vol. 2, Chapter 8. (b) Bullock, R.M. In *Transition Metal Hydrides*; Dedieu, A., Ed.; VCH: New York, 1992; p 263.

[42] Brookhart, M.; Green, M.L.H.; Parkin, G. *Proc. Natl. Acad. Sci. U.S.A.* **2007**, *104*, 6908.

[43] Steinke, T.; Shaw, B.K.; Jong, H.; Patrick, B.O.; Fryzuk, M.D.; Green, J.C. *J. Am. Chem. Soc.* **2009**, *131*, 10461-10466.

[44] Green, M.L.H.; Sella, A.; Wong, L.-L. *Organometallics* **1992**, *11*, 2650-2659.

[45] (a) Green, M.L.H.; Wong, L.-L J. *Chem. Soc., Chem. Commun*. **1988**, 677-679. (b) Derome, A.E.; Green, M.L.H.; Wong, L.-L. *New J. Chem.* **1989**, *10*, 747-753.

[46] For an earlier investigation of the dynamics of this system, see: (a) Byrne, J.W.; Kress, J.R.M.; Osborn, J.; Richard, L.; Weiss, R.E. J. *Chem. Soc., Chem. Commun.* **1977**, 662-663 (b) Byrne, J.W.; Blaser, H.U.; Osborn, J.A. *J. Am. Chem. Soc.* **1975**, *97*, 3871-3873.

[47] Bercaw, J.E.; Burger, B.J.; Green, M.L.H.; Santarsiero, B.D.; Sella, A.; Trimmer, M.; Wong, L.-L. J. *Chem. Soc., Chem. Commun*. **1989**, 734-736.

[48] Burger, B.J.; Santarsiero, B.D.; Trimmer, M.S.; Bercaw, J.E. *J. Am. Chem. Soc*. **1988**, *110*, 3134-3146 and references therein.

[49] (a) McNally, J.P.; Cooper, N.J. *Organometallics* **1988**, *7*, 1704-1715. (b) Casey, C.P.; Yi, C.S. *Organometallics* **1991**, *10*, 33-35 (c) Tempel, D.J.; Brookhart, M. *Organometallics* **1998**, *17*, 2290-2296.

[50] (a) Xu, R.; Klatt, G.; Wadepohl, H.; Köppel. H. *Inorg. Chem*. **2010**, *49*, 3289-3296. (b) Scherer, W.; Herz, V.; Bruck, A.; Hauf, C.; Reiner, F.; Leusser, D.; Stalke, D. Angew. Chem., *Int. Ed.* **2011**, 50, 1-6. (c) Mitoraj, M.P.; Michalak, A.; Ziegler, T. *Organometallics* **2009**, *28*, 3727-3733 and references therein. (d) Clot, E.; Eisenstein, O. *Struct. Bonding (Berlin)* **2004**, *113*, 1-36.

[51] Brookhart, M.; Lincoln, D.M.; Volpe, A.F., Jr.; Schmidt, G.F. *Organometallics* **1989**, *8*, 1212.

[52] Brookhart, M.; Lincoln, D.M.; Beunett, M.A.; Pelling, S. *J. Am. Chem. Soc.* **1990**, *112*, 2691.

[53] Brookhart, M.; Hauptman, E.; Lincoln, D.M. *J. Am. Chem. Soc.* **1992**, *114*, 10394.

[54] (a) Shiotsuki, M.; White, P.S.; Brookhart, M.; Templeton, J.L. *J. Am. Chem. Soc.* **2007**, *129*, 4058-4067. (b) Tempel, D.J.; Johnson, L.K.; Huff, R.L.; White, P.S.; Brookhart, M. *J. Am. Chem. Soc*. **2000**, *122*, 6686-6700. (c) Killian, C.M.; Johnson, L.K.; Brookhart, M. *Organometallics* **1997**, *16*, 2005-2007. (d) Killian, C.M.; Johnson, L.K.; Brookhart, M. *J. Am. Chem. Soc.* **1999**, *121*, 10634-10635. (e) Rix, F.C.; Brookhart, M. *J. Am. Chem. Soc.* **1995**, *117*, 1137-1138. (f) Killian, C.M.; Johnson, L.K.; Brookhart, M. *J. Am. Chem. Soc.* **1995**, *117*, 6414-6415. (g) Malinoski, J.M.; Brookhart, M. *Organometallics* **2003**, *22*, 5324-5335.

[55] Stromberg, S.; Zetterberg, K.; Siegbahn, P.E.M., *J. Chem. Soc., Dalton Trans*. **1997**, 4147-4152. (b) Musaev, D.G.; Froese, R.D.J., Morokuma, K. *Organometallics* **1998**, *17*, 1850-1860. (c) Musaev, D.G.; Morokuma, K. *Top. Catal.* **1999**, *7*, 107-123. (d) Michalak, A.; Ziegler, T. *Kinet. Catal.*

2006, 47, 310-325 (e) Deubel, D.V.; Ziegler, T. *Organometallics* **2002**, *21*, 1603-1611. (f) Deubel, D.V.; Ziegler, T. *Organometallics* **2002**, *21*, 4432-4441. (g) Michalak, A.; Ziegler, T. *Organometallics* **2003**, *22*, 2660-2669.

[56] Brookhart, M.; Lincoln, D.M.; Schmidt, G.F., Rivers, D.S. „Transition Metal Catalyzed Polymerizations“ R. Quirk, Ed., Cambridge Univ. Press, 1988.

[57] Pavankumar, P.N.V.; Ashok, B.; Jemnis, E.D. *J. Organomet. Chem.* **1986**, *315*, 361.

[58] Brookhart, M.; Lincoln, D.M. *J. Am. Chem. Soc.* **1988**, *110*, 8719-8720.

[59] Parkin, G.; Bunel, E.; Burger, B.J.;Bercaw, J.E. *J. Mol. Cat.* **1987**, *41*, 21.

[60] Hydride migration is observable in numerous terminal ethylene hydride complexes, but none of their alkyl analogous exhibit migration due to much higher activation barriers: see Ref. 5. from [58].

[61] (a) Klazinga, A.; Teuben, J.H. *J. Organomet. Chem.* **1979**, *165*, 31. (b) Klazinga, A.; Teuben, J.H. *J. Organomet. Chem.* **1980**, *192*, 75.

[62] (a) Lamanna, W.; Brookhart, M. *J. Am. Chem. Soc.* **1981**, *103*, 989. (b) Lamanna, W.; Humphrey, M.B. *J. Am. Chem. Soc.* **1982**, *104*, 2117.

[63] 1 do idem aspras aspras

[64] Benfield, F.W.S.; Green, M.L.H. *J. Chem. Soc., Dalton Trans*. **1979**, 1324.

[65] Crackness, R.G.; Orpen, A.G.; Spencer, J.L. *J. Chem. Soc., Chem. Commun.* **1984**, 326.

[66] Green, M.L.H.; Wong, L.-L. *J. Chem. Soc., Dalton trans.*, **1987**, 411.

[67] Green, M.L.H.; Wong, L.-L. *J. Chem. Soc., Chem. Commun.*, **1984**, 1442.

[68] Werner, H.; Feser, R. *Angew. Chem. Int. Ed. Engl.*, **1979**, *18*, 157.

[69] Bennett, M.A.; McMahon, S.; Pelling, S.; Robertson, G.B. *Organometallics*, **1985**, *4*, 754.

[70] Klazinga, A.H.; Teuben, J.H. *J. Organomet. Chem.*, **1978**, *157*, 413.

[71] Tebbe, F.N.; Parshall, G.W. *J. Am. Chem. Soc.*, **1971**, *93*, 3793.

[72] Bittner, M.; Köppel, H. *J. Phys. Chem.* **2004**, *108*, 11116.

[73] Bittner M., Wadepohl H., Kohl U., Köppel H. *Organometallics*, **2005**, *24*, 2097

[74] Sharp, P.R.; Schrock, R.R. *J.Organomet. Chem.* **1979**, *171*, 43.

[75] McGrady, N.D.; McDade, C.; Bercaw, J.E. *Organometallic Compounds*, Shapiro, B.L., Ed., Texas A and M University Press, College Station, Texas, 1983.

[76] Werner, H.; Werner, R. *J. Organomet. Chem.* **1979**, *174*, C63.

[77] Klein, H.-F.; Hammer, R.; Gross, J.; Schubert, U. *Angew. Chem. Int., Ed. Engl.* **1980**, *19*, 809.

[78] Jensen, F. *Introduction to computational chemistry*, Wiley, Chichester, 1999.

[79] Parr, R. G.; Yang, W. *Density fuctional theory of atoms and molecules*, Oxford University Press, Oxford, 1989.

[80] Hohenberg, P.; Kohn, W. *Phys. Rev. B* **1964**, 136, 864.

[81] Kohn, W.; Sham, L. J. *Phys. Rev. A* **1965**, 140, 1133.

[82] Löwdin, P. O. *Adv. Chem. Phys.* **1959**, 2, 1207.

[83] Becke, A. D.; *J. Chem. Phys*. **1993**, 98, 5648.

[84] Perdew, J. P.; *Electronic Structure of Solids '91*, Ziesche, P.; Eschring, H. Eds., Akademie, Berlin, 1991.

[85] Lee, C.; Yang, W.; Parr, R. G. *Phys. Rev. B* **1988**, 37, 785.

[86] (a) Fuckui, K. *Acc. Chem. Res.* **1981**, 14, 363. (b) Gonzalez, C.; Schlegel, H. B. *J. Phys. Chem.* **1990**, 94, 5523.

[87] Dunning, T. H.; Hay, P. J.; In: Schaefer, H. F.: *Modern theoretical chemistry*, Band 3. Plenum, 1976.

[88] Pople, J. A.; Krishnan, R.; Schlegel, H. B.; Binkley, J. S. *Int. J. Quantum Chem*. **1978**, 14, 545.

[89] Bartlett, R. J.; Purvis, G. D. . *Int. J. Quantum Chem*. **1978**, 14, 516.

[90] Frisch, M. J. *et al*.: *Gaussian 03*. Wallingford, **2003**.

[91] Han, Y.; Deng, L.; Ziegler, T. J. Am. Chem. Soc. **1997**, *119*, 5939-5945.

[92] Review articles: (a) Wilke, G. *Angew. Chem.* **1988**, *100*, 189. (b) Keim, W. *Angew. Chem*. **1990**, *102*, 251. (c) Guan, Z.; Cotts, P.M.; McCord, E.F. *Science* **1999**, *283*, 2059. (d) Ittel, S.D.; Johnson, L.K.; Brookhart, M. *Chem. Rev.* **2000**, *100*, 1169. (e) Mecking, S. *Angew. Chem.* **2001**, *113*, 550.

[93] Direct β-hydrogen transfer to the coordinated monomeris also a possibility for chain transfer: (a) Stehling, U.; Diebold, J.; Kirsten, R.; Röll, W.; Brintzinger, H.H. *Organometallics* **1994**, *13*, 964.

[94] Daugulis, O.; Brookhart, M.; White, P.S. *Organometallics* **2003**, *22*, 4699.

[95] Ledford, J.; Shultz, C.S.; Gates, D.P.; White, P.S.; Brookhart, M. *Organometallics* **2001**, *20*, 5266.

[97] Shultz, C.S.; Tempel, D.J.; Brookhart, M. *J.Am. Chem. Soc.* **2001**, 123, 11539.

[98] Leatherman, M.D.; Svejda, S.A.; Johnson, L.K.; Brookhart, M. *J.Am. Chem. Soc.* **2003**, 125, 3068.

[99] Rossi, A.R.; Hoffmann, R. Inorg. Chem. **1975**, *14*, 365.

[100] Klein, H.-F.; Hammer, R.; Gross, J.; Schubert, U. *Angew. Chem. Int., Ed. Engl.* **1980**, *92*, 835.

[101] Klein, H.-F.; Karsch, H.H. *Chem. Ber.* **1975**, *108*, 944.

[102] Albright, T.; Burdett, J.K.; Whangbo, M.-H.; *Orbital Interactions in Chemistry*; Wiley: New York, 1985; Chapter 17.

[103] Berry, R.S. *J. Chem. Phys.* **1960**, *32*, 933.

[104] Tolman, C.A. *Chem. Rev.* **1977**, *77*, 313.

[105] Taken from the Cambridge Crystallographic Database (CCDC), Cambridge, U. K., version 5.25, 2004.

[106] Vigalok, A.; Kraatz, H. –B.; Konstantinovsky, L.; Milstein, D. *Chem. Eur. J.* **1997**, *3*, 253.

[107] Co and Rh complexes: (a) Brookhart, M.; Green, M. L. H.; Pardy, R. B. A. *J. Chem. Soc., Chem. Commun.* **1983**, 691.

[108] Daugulis, O.; Brookhart, M.; White, P. S. *Organometallics* **2003**, 22, 4699.

[109] Lauher, J. W. ; Hoffmann, R.; *J. Am. Chem. Soc.* **1976**, *98*, 1729.

[110] Kazlaukas, R. J.; Wrighton, M. S. *J. Am. Chem. Soc.* **1982**, *104*, 6005

[111] V.C; Spitzmesser, S.K. *Chem. Rev.* **2003**, *103*, 283-316.

[112] Ittel, S.D.; Johnson, L.K.; Brookhart, M. *Chem. Rev.* **2000**, *100*, 1169-1203, and references therein.

[113] Niu, S.; Hall, M.B. *Chem. Rev.* **2000**, *100*, 353-405.

[114] Shultz, L.H.; Brookhart, M. *Organometallics* **2001**, 20, 3975.

[115] Brook, A.G.; Baines, K.M. *Adv. Organomet. Chem.* **1986**, *25*, 1.

[116] (a) Wiberg, N. *Organomet. Chem.* **1984**, *273*, 141. (b) Wiberg, N.; Wagner, G.; Riede, J.; Müller, G. *Organometallics* **1987**, *6*, 32.

[117] (a) Pannel, K.H. *J. Organomet. Chem.* **1970**, *21*, 17. (b) Windus, C.; Sijishi, S.; Giering, W.P. *J. Am. Chem. Soc.* **1974**, *96*, 1951. (c) Cundy, C.S.; Lappert, M.F.; Pearce, R. *J. Organomet. Chem.* **1973**, *59*, 161. (d) Pannel, K.H.; Rice, J.R. *J. Organomet. Chem.* **1974**, *78*, 35. (e) Ishikawa, M.; Ohshita, J.; Ito, Y. *Organometallics* **1986**, *5*, 1518. (f) Tamao, K.; Yoshida, J.; Okasaki, S. *Isr. J. Chem.* **1976**/**77**, *15*, 265.

[118] (a) Lewis, C.; Whrighton, M.S. *J. Am. Chem. Soc.* **1983**, *105*, 7768. (b) Randolph, C.L.; Wrighton, M.S. *Organometallics* **1987**, *6*, 365.

[119] Tilley, T.D.; Heyn, R.H.; Campion, B.K. *J. Am. Chem. Soc.* **1988**, *110*, 7558-7560.

[120] Brook, M.A. Silicon in Organic, Organometallic, and Polymer Chemistry; Wiley-Interscience: New York, 2000.

[121] Curtis, M.D.; Epstein, P.S. *Adv. Organomet. Chem.* **1981**, *19*, 213.

[122] Pannel, K.H.; Cervantes, J.; Hernandez, C.; Vicenti, S. *Organometallics* **1986**, *5*, 1056.

[123] Tobita, H.; Ueno, K.; Ogino, H. *Bull. Chem. Soc. Jpn.* **1988**, *61*, 2797.

[124] Haynes, A.; George, M.W.; Haward, M.T.; Green, M. *J. Am. Chem. Soc.* **1991**, *113*, 2011.

[125] Grumbine, S.D.; Tilley, T.D. *J. Am. Chem. Soc.* **1994**, *116*, 6951.

[126] Mitchell, G.P.; Tilley, T.D. *Angew. Chem., Int. Ed.* **1998**, *37*, 2524.

[127] Tilley, T.D. In *The Silicon-Heteroatom Bond*; Patai, S., Rapport, Z., Eds.; Wiley: New York, 1991; p.309.

[128] Zybill, C. *Top. Curr. Chem.* **1991**, *160*, 1.

[129] Corriu, R.J.P.; Chauhan, B.P.S. *Organometallics* **1995**, *14*, 1646.

[130] Mork, B.V.; Tilley, T.D. *J. Am. Chem. Soc.* **2001**, *123*, 9702.

[131] Peters, J.C.; Feldman, J.D.; Tilley, T.D. *J. Am. Chem. Soc.* **1999**, *121*, 9871.

[132] Feldman, J.D.; Mitchell, G.P.; Tilley, T.D. *J. Am. Chem. Soc.* **1998**, *120*, 11184.

[133] Straus, D.A.; Grumbine, S.D.; Tilley, T.D. *J. Am. Chem. Soc.* **1990**, *112*, 7801.

[134] Klei, S.R.; Tilley, T.D.; Bergman, R.G. *J. Am. Chem. Soc.* **2000**, *122*, 1816.

[135] Klei, S.R.; Tilley, T.D.; Bergman, R.G. *Organometallics* **2001**, *20*, 3220.

[136] Klei, S.R.; Tilley, T.D.; Bergman, R.G. *Organometallics* **2002**, *21*, 3376.

[137] Koloski, T. S.; Carroll, P. J.; Berry, D. H. *J. Am. Chem. Soc.* **1990**, *112*, 6405.

[138] Tilley, T.D.; Heyn, R.H.; Campion, B.K. *J. Am. Chem. Soc.* **1990**, *112*, 4079.

[139] Walsh, R. *Acc. Chem. Res.* **1981**, *14*, 246.

[140] Niu, S.; Zaric, S.; Bayse, C.A.; Strout, D.L.; Hall, M.B. *Organometallics* **1998**, *17*, 5139.

[141] See for example: Aylett, B.J. *Organometallic Compounds*; Chapman and Hall: London, 1979; Vol. 1, Part 2, Chapter 2; Bazant, V.; Chvalovsky, V.; Rathousky, J. *Organosilicon Compounds*; Academic: New York, 1965; p. 179.

[142] Nikonov, G. I. *Adv. Organomet. Chem.* **2005**, *53*, 217.

[143] Vyboishchikov, S.F.; Nikonov, G.I. *Chem.-Eur. J.* **2006**, *12*, 8518.

[144] Gutsulyak, D.V.; Osipov, A.L.; Kuzmina, L.G.; Howard, J.A.K.; Nikonov, G.I. *Dalton trans.* **2008**, 6843.

[145] Osipov, A.L; Howard, J.A.K.; Nikonov, G.I. *Organometallics* **2005**, *24*, 587.

[146] Doherty, M.D.; Grant, B.; White, P.S.; Brookhart, M. *Organometallics* **2007**, *26*, 5950.

[147] Taw, F.L.; Bergman, R.G.; Brookhart, M. *Organometallics* **2004**, *23*, 886.

[148] Corey, J.Y. *Chem. Rev.* **2011**, *111*, 863.

[149] Nikonov, G. I. *J. Organomet. Chem.* **2001**, *635*, 24.

[150] Gountchev, T. I.; Tilley, T. D. *J. Am. Chem. Soc.* **1997**, *119*, 12831

[151] see for example: a) Ditchfield, R.; Hehre, W. J.; Pople, J. A. *J. Chem. Phys*. **1971**, 54, 724. b) Hehre, W. J.; Ditchfield, R.; Pople, J. A. *J. Chem. Phys*. **1972**, 56, 2257. c) Hariharan, P. C.; Pople, J. A. *Theor. Chem. Acc.* **1973**, 28, 213. d) Hariharan, P. C.; Pople, J. A. *Mol. Phys.*, **1974**, 27, 209. e) Gordon, M. S.; *Chem. Phys. Lett.*, **1980**, 76, 163. f) Binning, R. C.; Curtiss, L. A. *J. Comput. Chem*., **1990**, 11, 1206.